

UNIVERSIDADE DE LISBOA
INSTITUTO SUPERIOR TÉCNICO

**DESIGN AND FABRICATION OF FULL-THICKNESS VASCULARIZED HUMAN
SKIN WITH 3D BIOPRINTING TECHNOLOGY**

Tânia Daniela Calaveiras Baltazar

Supervisor: Doctor Pankaj Karande

Co-supervisor: Doctor Frederico Castelo Alves Ferreira

**Thesis approved in public session to obtain the PhD Degree in
Bioengineering**

Jury final classification: Pass with Distinction

UNIVERSIDADE DE LISBOA
INSTITUTO SUPERIOR TÉCNICO

**DESIGN AND FABRICATION OF FULL-THICKNESS VASCULARIZED
HUMAN SKIN WITH 3D BIOPRINTING TECHNOLOGY**

Tânia Daniela Calaveiras Baltazar

Supervisor: Doctor Pankaj Karande

Co-supervisor: Doctor Frederico Castelo Alves Ferreira

**Thesis approved in public session to obtain the PhD Degree in
Bioengineering**

Jury

Chairperson: Doctor Joaquim Manuel Sampaio Cabral, Instituto Superior Técnico, Universidade de Lisboa.

Members of the Committee:

Doctor Joaquim Manuel Sampaio Cabral, Instituto Superior Técnico, Universidade de Lisboa.

Doctor Pankaj Karande, School of Engineering, Rensselaer Polytechnic Institute, USA.

Doctor Alexandra Margarida Pinto Marques, Grupo de Investigação 3B's (Instituto de Investigação em Biomateriais, Biodegradáveis e Biomiméticos-I3Bs), Universidade do Minho.

Doctor Jorge Alexandre Monteiro de Carvalho Silva, Faculdade de Ciências e Tecnologia, Universidade Nova de Lisboa.

Doutor Carlos André Vitorino Rodrigues, Instituto Superior Técnico, Universidade de Lisboa.

Funding Institutions

Fundação para a Ciência e Tecnologia

Rensselaer Polytechnic Institute

2019

ABSTRACT

Treatment of chronic skin wounds (e.g. diabetic ulcers and venous ulcers) remains a significant clinical challenge. Autologous split-thickness skin grafts represent the 'gold standard of care' but are limited by the pain and discomfort associated with harvesting skin from donor sites, limited availability of donor sites, and the need for multiple surgeries. To overcome this challenge, many bioengineered skin substitutes using biological and artificial matrices and/or allogeneic cells have been developed and are beneficial in conditions when urgent care is needed. However, the use of foreign or synthetic materials to cover the wounded area is only a temporary solution, and sub-optimal engraftment often leads to unsatisfactory clinical results. When the clinical situation allows for a delayed reconstruction of the defects such as chronic wounds, tissue engineered skin constructs are the ideal choice. Nevertheless, current artificial skin grafts do not include dermal vascular networks important for graft survival and integration with the native tissue. To date, the construction of tissue-engineered skin substitutes for clinical use has involved self-assembly of various constituents, resulting in homogenous or bilayered structures without specific instructions for organization normally provided by the extracellular matrix. Three-dimensional (3D) bioprinting, an adaptation from tools developed for non-living systems, has enabled the precise fabrication of living systems, which can be organized over multiple and relevant length scales. Here, using a 3D bioprinting platform, we have successfully fabricated a multilayered bioengineered skin construct that consists of human keratinocytes in the epidermis and dermal fibroblasts in the dermis to mimic the morphology and function of human skin. Second, we have developed a method to generate functional endothelial networks of physiologically relevant size *in vitro*. Bioprinted vascular endothelial cells and fibroblasts formed dense interconnected capillary networks with open lumens mimicking the dermal microvasculature. Third, we shown successful integration of a vascularized bed in a 3D bioprinted skin model. 3D bioprinted vascularized skin substitutes formulated with human endothelial colony forming cells (HECFC) derived from cord blood were implanted on the dorsal part of immunodeficient mice, showing human vascular structures that were perfused. These data illustrate the feasibility of studying 3D printed skin comprised of human primary cells in immunodeficient mice and the ability of HECFC to produce vasculature in the grafted 3D printed bioengineered skin. These advances will allow the fabrication of more complex skin tissues suitable for clinical translation.

Keywords: Skin; Tissue Engineering; 3D bioprinting; Regenerative Medicine; Microvasculature

RESUMO

O tratamento de feridas crônicas de pele (por exemplo, úlceras diabéticas e úlceras venosas) continua a ser um desafio clínico significativo. Enxertos autólogos de pele de espessura parcial representam o padrão de cuidados, mas são limitados pela dor e desconforto associados à remoção de pele na região doadora, à disponibilidade limitada de doadores e à necessidade de cirurgias múltiplas. Para superar este desafio, muitos substitutos de pele produzidos artificialmente têm sido desenvolvidos usando matrizes extracelulares biológicas e artificiais e/ou células alogênicas, e têm demonstrado benefício em situações de cuidado urgente. No entanto, o uso de materiais sintéticos em feridas de pele representa apenas uma solução temporária e enxertos de pele artificiais geralmente levam a resultados clínicos insatisfatórios. Enxertos de pele artificiais produzidos atualmente não incluem redes vasculares dérmicas importantes para a sobrevivência do enxerto e a integração com o tecido nativo. Até o momento, a produção de substitutos de pele para uso clínico depende da deposição de vários constituintes, que tipicamente resultam em estruturas homogêneas ou em bicamada sem organização da matriz extracelular. A bioimpressão tridimensional (3D), uma adaptação de ferramentas desenvolvidas para sistemas não vivos, permite a fabricação com precisão de sistemas vivos, que podem ser organizados em várias escalas. Através de uma plataforma de bioimpressão 3D, demonstramos a produção de um equivalente de pele constituído de várias camadas (queratinócitos humanos na epiderme e fibroblastos na derme), com o objetivo de mimetizar a morfologia e a função da pele humana. Em segundo lugar, desenvolvemos um método *in vitro* para gerar redes endoteliais funcionais de tamanho fisiologicamente relevante. Células endoteliais e fibroblastos formaram redes capilares interconectadas com lúmen, semelhante à microvasculatura dérmica. Por último, demonstramos a integração do modelo de pele bioimpressa na parte dorsal de ratinho imunodeficientes, formulado com células formadoras de colônias endoteliais derivadas do sangue do cordão umbilical. Estruturas vasculares humanas perfundidas por sangue de ratinho foram observadas. Estes resultados ilustram a potencialidade de produzir pele humana com bioimpressão 3D composta por células primárias humanas e a capacidade de células endoteliais humanas em produzir microvasculatura funcional em pele bioimpressa. Estes avanços permitirão a fabricação de tecidos cutâneos mais complexos e adequados à translação clínica.

Palavras-chave: Pele; Engenharia de Tecidos; Bioimpressão 3D; Medicina Regenerativa, Microvasculatura.

ACKNOWLEDGMENTS

For the past 4 years I had the chance to know, interact and bond with different people and personalities that molded me both professionally and personally. Here I take the chance to acknowledge them.

First of all, I would like to show my most sincere appreciation to my advisor **Dr. Pankaj Karande**. Thank you for guiding me through this amazing and challenging project. Above all, thank you for always taking into consideration my goals and points of view. You gave me the opportunity to work in a field that I always admired, and you always helped me to find new collaborations and opportunities. I am truly grateful for the support, guidance and dedication.

Thank you to my co-advisor **Dr. Frederico Ferreira** for his guidance in planning and structuring this project at its early stages. I'm grateful for all your help and inputs in Lisbon and during all our conference calls.

During 3.5 years of my PhD project I got the chance to work as a Visiting Student at the Rensselaer Polytechnic Institute, in Troy, USA. In RPI, I met amazing and professional people that thought me a lot. My deepest acknowledgement goes to **Dr. Vivian Lee** and **Dr. Guohao Dai** for starting this project with Dr. Karande and for sharing your love and knowledge for 3D bioprinting with me. I'm very grateful for your mentoring during my first year at RPI.

Thank you to **JP, Sriram, Divya C.** and **John** for making me feel welcome when I joined the lab and thank you for all the shared adventures in and outside lab.

A special thanks to **Marta, André** and **João**. More than the best roommates you were my family in USA. Thanks for the friendship, conversations and amazing cookouts.

Also thank you to my dearest friends **Akshat, Ronit, Ronak, Deepika and Alexis**. Thank you for the laughs, jokes and talks about life. You know that these 3.5 years would have been a lot harder if you weren't around.

A huge thanks to **Carolina** for sharing her knowledge and techniques on skin equivalents. Without your help this project wouldn't have been possible.

Also, thanks to **Sergey** and **Brigitte** for helping me in my experiments whenever I needed. I will always remember your guidance and inputs.

A huge thanks to **Jonathan Merola**, for helping me push this project forwards and for doing the *in vivo* imaging and sample collections at Yale University. More than that, thank you for your support and contribution in making my new adventure at Yale happen.

I am also very grateful to **Dr. Jordan Pober** for his guidance and input throughout this entire project. It is an honor to be now part of your lab and be your mentee for the next years to come.

I am also grateful for the opportunity to pursue my studies through the **PhD Program in Bioengineering – Cell Therapies and Regenerative Medicine**. During the first year of the program I met amazing people with a lot of different backgrounds and ambitions. Even if we end up pursuing different careers, we will always be connected through this amazing journey we have lived together.

A very special acknowledgement goes to **Professor Joaquim Sampaio Cabral** for believing in me. This would not have been possible without your support.

I would also like to acknowledge **Fundação para a Ciência e Tecnologia (FCT)** and **RPI** for funding my research.

I want to show my gratitude for having the chance to share these last years with my best friend and partner in life. **Ignacio**, you will always be my inspiration in life and I am grateful for your love, dedication and positivity, especially in the worst moments.

At last, I want to give an enormous thanks to my **family**. Thank you for calling me every single day and for showing your unconditional love and support. We know that these last years have been the hardest. I promise it will all be worth it. For this, I dedicate this PhD Thesis to you.

TABLE OF CONTENTS

ABSTRACT	1
TABLE OF CONTENTS	xi
LIST OF FIGURES	xv
LIST OF TABLES	xix
ABBREVIATIONS	xxiii
THESIS MOTIVATION.....	xxv
References.....	xxvii
CHAPTER I – INTRODUCTION	1
I.1. Cutaneous wound healing: an unmet clinical need	1
I.2. The Structure of Human Skin.....	3
I.2.1. The Epidermis.....	3
I.2.2 The Papillary Dermis.....	3
I.2.3 The Reticular Dermis	5
I.3. Current Human Skin Equivalents.....	5
I.3.1 Natural and Synthetic ECM.....	7
I.3.1 Source of Skin Cells.....	8
I.3.2. The Need for Blood Supply	9
I.4. Developing Disease Skin Models.....	10
I.4.1. <i>In Vitro</i> Skin Model of Psoriasis.....	11
I.4.2 <i>In Vitro</i> Skin Model of Melanoma	12
I.5. Efficacy Models for Drug and Formulation Screening	13
I.6. 3D Bioprinting.....	13
I.6.1 3D Bioprinting Modalities	13
I.6.2 3D Bioprinting of Human Skin	15
I.6.3 Incorporating 3D bioprinted vasculature in human skin equivalents	18
I.6.1. Incorporating adnexal structures in human skin equivalents	19

I.7.	References	20
CHAPTER II: 3D bioprinting of non-vascularized human skin.....		27
II.1.	Introduction.....	28
II.2.	Materials and Methods	31
II.2.1.	3D bioprinter.....	31
II.2.2.	Cell isolation	32
II.2.3.	Cell culture	33
II.2.4.	Dermal and epidermal bioinks	33
II.2.5.	3D bioprinting of dermal and epidermal compartments.....	33
II.2.6.	Bioprinted skin maturation	36
II.2.7.	Viability analysis	36
II.2.8.	3D projection of skin constructs	37
II.2.9.	Histological and immunofluorescence analysis of skin constructs.....	38
II.2.10.	Barrier Function	39
II.2.11.	Determination of steady state flux and permeability coefficient.....	39
II.2.12.	Statistical analysis	40
II.3.	Results	41
II.3.1.	Resolution and Pressure	41
II.3.2.	Cell viability	42
II.3.3.	3D Bioprinting of the Dermal Compartment	43
II.3.4.	3D Bioprinting of the Epidermal Compartment.....	44
II.3.5.	Epidermal and Dermal Bioink Optimization.....	46
II.3.6.	Skin maturation/ ALI culture.....	51
II.3.7.	Barrier Function.....	53
II.4.	Discussion	55
II.5.	Conclusions	61
II.6.	References	62

CHAPTER III: Microvascular network development in vitro.....	67
III.1. Introduction.....	69
III.2. Materials and methods.....	71
III.2.1. Cell culture	71
III.2.2. Preparation of telo- and atelo-collagen type I gels	71
III.2.3. Analysis of RFP-expressing HUVEC area coverage.....	71
III.2.4. Confocal fluorescence and reflectance microscopy of collagen gels.....	72
III.2.5. Statistical analysis	72
III.3. Results	73
III.3.1. The effect of collagen type I concentration in vessel formation and gel contraction <i>in vitro</i>	73
III.3.2. The effect of collagen source and extraction method on vessel formation <i>in vitro</i>	75
III.3.3. The effect of endothelial cells to fibroblasts ratio and total cell number in endothelial network formation <i>in vitro</i>	77
III.3.4. The effect of vascular endothelial growth factor media supplementation in the absence of dermal fibroblasts in endothelial network formation <i>in vitro</i>	79
III.3.5. The effect of fetal bovine serum in endothelial network formation <i>in vitro</i>	79
III.3.6. 3D organization of endothelial cell networks <i>in vitro</i>	82
III.4. Discussion	85
III.5. Conclusions	89
III.6. References	90
CHAPTER IV: 3D Bioprinting of vascularized human skin.....	93
IV.1. Introduction.....	95
IV.2. Materials and methods.....	97
IV.2.1. Cell culture	97
IV.2.2. Microvasculature and epidermal bioinks.....	97
IV.2.3. 3D bioprinting of vascularized skin – Protocol 1	97
IV.2.4. 3D bioprinting of vascularized skin – Protocol 2	99

IV.2.5. Histological and immunofluorescence analysis of skin constructs	100
IV.2.6. Engraftment of bioprinted vascularized skin in SCID/bg mice.....	100
IV.2.7. Two-Photon Laser Scanning Microscopy	101
IV.2.8. Histochemical analysis of bioprinted skin tissues	101
IV.2.9. Statistical analysis.....	101
IV.3. Results	103
IV.3.1. Part A: Fabrication of bioprinted vascularized skin constructs with Protocol 1.....	103
IV.3.2. Part B: Generation of bioprinted vascularized skin constructs with Protocol 2.....	105
IV.3.3. Part C: Characterization of 3D bioprinted skin transplanted to immunodeficient mice.....	106
IV.3.4. Part D: Incorporation of human pericytes in bioprinted endothelial networks .	109
IV.4. Discussion	113
IV.5. Conclusions	117
IV.6. References	118
NEW DIRECTIONS AND FUTURE ADVANCES	121
- Incorporation of adnexa in bioprinted human skin.....	121
- Development of bio-inks specific for tissue engineering of human skin.....	122
- Isolation and culture of cell types free of animal proteins for 3D printing.....	123
- Fabrication of “immuno-evasive” human skin graft.....	124
References.....	126
LIST OF PUBLICATIONS.....	129

LIST OF FIGURES

Figure I.1.1 - Immune mechanisms in acute and chronic wound healing	2
Figure I.2.1 – Schematic of human skin.....	4
Figure I.6.1 - Components of inkjet, microextrusion and laser-assisted bioprinting.....	14
Figure I.6.2 - 3D bioprinting of human skin with HaCaT cells.....	16
Figure I.6.3 – 3D bioprinting of human skin	17
Figure I.6.4 - Development of vascularized human skin equivalents.....	18
Figure II.2.1 - Modular tissue printing platform.....	31
Figure II.2.2 - Microvalve components and operating modes.....	32
Figure II.2.3 – Layer-by-layer printing of human skin equivalents.	35
Figure II.2.4 - Representative images of LIVE/Dead staining of printed human keratinocytes at day 1	37
Figure II.3.1 - Droplet-based bioprinting. Bright field images of collagen type I droplets printed at 2.5, 5.5 and 7 psi at resolution of 800 and 300 μm	41
Figure II.3.2 - Cell viability of manually deposited and printed cells.	42
Figure II.3.3 – Evaluation of collagen cross-linking method on dermal fibroblasts distribution and epidermal differentiation in 3D printed constructs.....	44
Figure II.3.4 - Evaluation of dermal compartment incubation time on the spatial distribution of printed keratinocytes and its effects on epidermal differentiation.....	45
Figure II.3.5 – Thickness of suprabasal (CK10+) and basal (CK14+) layers of 3D bioprinted constructs and native human foreskin	47
Figure II.3.6 – H&E and immunofluorescence staining of bioprinted constructs generated with varying numbers of dermal fibroblasts and keratinocytes.	49

Figure II.3.7 – Thickness of printed skin tissues over the course of 4 weeks. Bioprinted constructs were cultured under submerged culture for 4 days and lifted to the air-liquid interface from day 4 until day 30 of <i>in vitro</i> maturation.	51
Figure II.3.8 - H&E and immunofluorescence staining of bioprinted constructs at different stages of <i>in vitro</i> maturation.	52
Figure II.3.9 - Cumulative permeation profile of fluorescein dextran-10 kDa (FD-10) and fluorescein dextran-20 kDa (FD-20) molecules in 3D bioprinted constructs cultured <i>in vitro</i> for 30 days	53
Figure III.2.1 – Representative image of endothelial cell networks in 3 mg/mL collagen type I gel at day 10	72
Figure III.3.1 - Live epifluorescence imaging of 2 and 3 mg/mL collagen type I gels at day 5 with varying number of endothelial cells and fibroblasts ($\times 10^5$ cells)	73
Figure III.3.2 – Area covered at day 5 by RFP-expressing HUVEC in 2 and 3 mg/mL collagen type I gels at varying number of endothelial cell and fibroblasts ($\times 10^5$ cells).....	74
Figure III.3.3 - Percentage of gel contraction observed at day 5 at varying number of endothelial cells and fibroblasts ($\times 10^5$ cells).....	75
Figure III.3.4 - Live epifluorescence imaging of Telo and Atelo-collagen type I gels at day 5 with varying number of endothelial cells and fibroblasts ($\times 10^5$ cells)	76
Figure III.3.5 - Percentage of gel contraction observed at day 15 at varying number of endothelial cells and fibroblasts ($\times 10^5$ cells)	77
Figure III.3.6 - Live epifluorescence imaging of 3 mg/mL collagen type I gels at day 5 with varying number of endothelial cells and fibroblasts ($\times 10^5$ cells).....	78
Figure III.3.7 - Area covered at day 5 by RFP-expressing HUVEC in 3 mg/mL collagen type I gels at varying number of endothelial cell and fibroblasts ($\times 10^5$ cells)..	78
Figure III.3.8 – Collagen gels containing RFP-expressing HUVEC in the presence of dermal fibroblasts or with VEGF media supplementation in the absence of fibroblasts..	80
Figure III.3.9 - Collagen gels containing RFP-expressing HUVEC in the presence of 2% or 2 % supplemented with 10% Fetal Bovine Serum.	81

Figure III.3.10 – 3D dimensional reconstruction of self-assembled endothelial networks in vitro. Z-stack images of 3 mg/mL collagen gels containing RFP-expressing HUVEC and dermal fibroblasts at 15 days.	82
Figure III.3.11 – Confocal reflectance and fluorescence microscopy of 3 mg/mL collagen gels seeded with 5 EC: 10 FB ($\times 10^5$). Unlabeled HUVEC and dermal fibroblasts were co-cultured in 3 mg/mL collagen for 15 days.	83
Figure IV.2.1 – Protocol 1 for bioprinting and maturation of vascularized human skin equivalents.....	98
Figure IV.2.2 - Protocol 2 for bioprinting and maturation of vascularized human skin equivalents.....	99
Figure IV.3.1 - Live cell fluorescence microscopy of RFP-expressing ECFC co-cultured with dermal fibroblast in bioprinted constructs.	103
Figure IV.3.2 - Live cell fluorescence microscopy of RFP-expressing ECFC co-cultured with dermal fibroblast in bioprinted constructs..	104
Figure IV.3.3 - Characterization of 3D bioprinted vascularized skin equivalents before engraftment.....	105
Figure IV.3.4 - Characterization of 3D bioprinted skin equivalents after engraftment.....	106
Figure IV.3.5 – Stratified epidermis in 3D bioprinted vascularized skin equivalents after engraftment is of human origin.....	107
Figure IV.3.6 - 3D bioprinted human skin substitutes support perfusable micro vessels in vivo.	107
Figure IV.3.7 – Vascularized bioprinted human skin substitutes form anastomoses with mouse vessels. Whole-mount epifluorescence imaging of human skin and bioprinted grafts with and without ECFC, 6 weeks following engraftment on SCID/bg mouse.	108
Figure IV.3.8 – Characterization of bioprinted endothelial networks with Incorporated human placental pericytes <i>in vitro</i>	110
Figure IV.3.9 - Characterization of 3D bioprinted vascularized skin equivalents with human placental pericytes.	111

LIST OF TABLES

Table I.3.1 – FDA approved human skin equivalents.....	6
Table II.3.1 - Summary of printing parameters used to generate bioprinted skin constructs.	46
Table II.3.2 - Summary of the thickness mean and SEM values of suprabasal (CK10+) and basal (CK14+) layers of 3D bioprinted constructs and native foreskin.....	48
Table II.3.3 – Summary of calculated steady state flux, lag-time and permeability coefficients of FD-10 and FD-20 molecules in bioprinted constructs cultured in vitro for 30 days.....	54
Table II.3.4 – Summary of reported permeability coefficient values for FD-10 and FD-20 molecules in different skin models.....	54
Table IV.3.1 - Summary of observations on gel contraction of the co-culture of human dermal fibroblasts, endothelial cells and human pericytes in vitro at different ratios in collagen type I gels for 15 days.....	109

LIST OF EQUATIONS

Equation II.2.1- Fick's first law	39
---	----

ABBREVIATIONS

A

α -SMA – Alpha smooth muscle actin
ALI – Air-liquid interface

B

bFGF – Basic Fibroblast Growth Factor
BSA – Bovine Serum Albumin

C

CD – Cluster of differentiation
CK – Cytokeratin
CM – Conditioned Media
Col I – Collagen type I
Col IV – Collagen type IV
CS – Chondroitin Sulfate

D

DMEM – Dulbecco's Modified Eagle's Medium
DVP – Deep Vascular Plexus

E

EC – Endothelial Cells
ECFC – Endothelial Colony Forming Cells
ECM – Extracellular Matrix
EDTA - Ethylenediamine Tetraacetic Acid
EGM-2 – Endothelial Growth Medium-2
EPCs – Endothelial Progenitor Cells

F

FBS – Fetal Bovine Serum
FDA – Food and Drug Administration
FGF – Fibroblast Growth Factor
FITC – Fluorescein Isothiocyanate

G

GAG – Glycosaminoglycans
GFP – Green Fluorescent Protein

H

H&E – Hematoxylin and Eosin
HCL – Hydrochloric Acid
hbFGF – Human Basic FGF
HECFC – Human endothelial colony forming cells
hEGF – Human Epidermal Growth Factor
HUVEC – Human Umbilical Vein Endothelial Cell

I

IGF – Insulin Growth Factor
IL – Interleukin
ILC – innate-like lymphocytes
iPSC – Induced Pluripotent Stem Cell
IST – Instituto Superior Técnico

K

KC - Keratinocyte
KGF - Keratinocyte growth factor;
KGM – keratinocyte growth medium

M

MEM – Minimal Essential Medium
MHC – Major Histocompatibility Complex
MMP – Matrix Metalloproteinase

N

NaOH – Sodium Hydroxide
NaHCO₃ – Sodium Bicarbonate
NBF – Neutral-Buffered Formalin
NGS – Normal Goat Serum
NSCs – Neural Stem Cells

O

OCT – Optimal Cutting Temperature

P

PBS – Phosphate Buffered Saline
PC - pericytes
PDGF – Platelet Derived Growth Factor
PFA – Paraformaldehyde
PGA – Polyglycolic Acid
PGE₂ – Prostaglandin 2
PLA – Polylactic Acid
PLGA – Poly(lactic-co-glycolic) Acid
P/S – Penicillin-Streptomycin

R

RFP – Red Fluorescent Protein
RGP – Radial Growth Phase
ROS – Reactive Oxygen Species
RPI – Rensselaer Polytechnic Institute
RT – Room Temperature

S

SDS – Sodium Dodecyl Sulfate
SEM – Standard Error of the Mean
SVP – Superficial Vascular Plexus

T

TGF- β – Transforming Growth Factor β
TIMP – Tissue Inhibitor of Metalloproteinase.
TNF - Tumor Necrosis Factor

U

U.S.A – United States of America

V

VEGF – Vascular Endothelial Growth Factor
VGP – Vertical Growth Phase
VSMC – Vascular Smooth Muscle Cells

THESIS MOTIVATION

Tissue engineering, as a field, has matured significantly in the last 2-3 decades providing substantial clinical benefits for patients. Relentless innovations in basic and applied research have opened new avenues for furthering developments in transplantation science. It would, however, be compromising and naïve to assume that clinical solutions satisfy all patient needs. Several gaps still remain in clinical translation, and provide tremendous opportunities for scientific enquiries and engineering innovations. Our efforts, both engineering and translational, are geared towards mitigating this gap for the patient. To motivate our efforts, we pose the following questions:

1. What are the limitations of current clinical therapies?

Many skin substitutes and grafts are available on the market for clinical use (Augustine, Kalarikkal, & Thomas, 2014). They include epidermal replacements (e.g., EpiCel™, Myskin™, etc.), dermal replacements (e.g., Permacol™, Dermagraft™, Transyte™, Integra™, etc.), and full-thickness replacements (e.g., Apligraf™, Permaderm™, Orcell™, etc.). All provide some clinical benefits but none is ideal, irrespective of the therapeutic context. Firstly, these involve some animal-derived matrix components that exclude recipients susceptible to contraindications. For example, Apligraf™ cannot be applied on infected wounds, or be used on patients with known allergies to bovine collagen (Zaulyanov & Kirsner, 2007). Dermagraft™ cannot be applied in ulcers that have sinus tracts or on patients with known allergies to bovine products (Organogenesis, 2018). EpiCel™ also cannot not be used in patients with sensitivities to materials of bovine or murine origin (Vericel, 2016). Further, receiving grafts constructed from animal sources may limit individuals from becoming viable donors for others in need in future. Secondly, these solutions fail to meet critical endpoints (Chua et al., 2016). Skin grafts are produced in specific sizes that are then stitched together as needed. This approach may increase scar and contraction events between the skin edges leading to poor aesthetic results, but also poor mobility especially when the grafts are transplanted on joints. And finally, but most importantly, current grafts are inherently a temporary solution that eventually slough off the wound site because they cannot completely integrate with the host (Kirsner et al., 2015). The very fact that there is no vasculature incorporated in any of these substitutes amplifies their prospects to fail in patients where they can provide the most benefit – deep wounds (Haller & Billingham, 1967). We argue that clinical modalities are limited by their failure to incorporate relevant biological materials and functional attributes.

2. What are the limitations of current engineering platforms?

Biological systems are characteristically complex in their length scales, and capturing this complexity at the cellular and sub-cellular length scales is a significant challenge. Unambiguously, one of the most significant advancements in tissue engineering over the last decade has been the advent of new platforms that employ a radically new approach for fabricating tissues that address this challenge (Huang, Yao, Xie, & Fu, 2016; H. Lee & Cho, 2016; Munoz-Abraham et al., 2016). 3D bioprinting, an adaptation from tools developed for non-living systems, has enabled the precise fabrication of living systems over multiple and relevant length scales. Previous work in Dr. Karande's lab at the Rensselaer Polytechnic Institute (RPI) has demonstrated the feasibility of using this platform to fabricate skin tissue with desired spatial complexity that also provide improved mechanical attributes (V. Lee et al., 2014). To date, however, such efforts have focused on technological improvements to the fabrication platforms with little attention to translational needs.

The main motivation of this thesis is to develop of protocols for the production of a full-thickness, bioengineered skin equivalent by means of 3D printing that will contain a perfusable microvascular system suitable for clinical use. This will serve as the basis for developing an "off-the-shelf" product or one potentially made to order using pre-sourced materials comparable to Apligraf™ but superior in performance.

References

- Augustine, R., Kalarikkal, N., & Thomas, S. (2014). Advancement of wound care from grafts to bioengineered smart skin substitutes. *Progress in Biomaterials*, 3(2–4), 103–113. <https://doi.org/10.1007/s40204-014-0030-y>
- Chua, A. W. C., Khoo, Y. C., Tan, B. K., Tan, K. C., Foo, C. L., & Chong, S. J. (2016). Skin tissue engineering advances in severe burns: review and therapeutic applications. *Burns & Trauma*, 4(1), 3. <https://doi.org/10.1186/s41038-016-0027-y>
- Haller, J. A., & Billingham, R. E. (1967). Studies of the origin of the vasculature in free skin grafts. *Annals of Surgery*, 166(6), 896–901. Retrieved from <http://www.pubmedcentral.nih.gov/articlerender.fcgi?artid=1477517&tool=pmcentrez&rendertype=abstract>
- Huang, S., Yao, B., Xie, J., & Fu, X. (2016). 3D bioprinted extracellular matrix mimics facilitate directed differentiation of epithelial progenitors for sweat gland regeneration. *Acta Biomaterialia*, 32, 170–177. <https://doi.org/10.1016/j.actbio.2015.12.039>
- Kirsner, R. S., Bernstein, B., Bhatia, A., Lantis, J., Le, L., Lincoln, K., Liu, P., Rodgers, L., Shaw, M., & Young, D. (2015). Clinical Experience and Best Practices Using Epidermal Skin Grafts on Wounds. *Wounds: A Compendium of Clinical Research and Practice*, 27(11), 282–292.
- Lee, H., & Cho, D.-W. (2016). One-step fabrication of an organ-on-a-chip with spatial heterogeneity using a 3D bioprinting technology. *Lab Chip*, 16, 2618–2625. <https://doi.org/10.1039/C6LC00450D>
- Lee, V., Singh, G., Trasatti, J. P., Bjornsson, C., Xu, X. W., Tran, T. N., Yoo, S.-S. S., Dai, G. H., & Karande, P. (2014). Design and fabrication of human skin by three-dimensional bioprinting. *Tissue Engineering. Part C, Methods*, 20(6), 473–484. <https://doi.org/10.1089/ten.TEC.2013.0335>
- Munoz-Abraham, A. S., Rodriguez-Davalos, M. I., Bertacco, A., Wengerter, B., Geibel, J. P., & Mulligan, D. C. (2016). 3D Printing of Organs for Transplantation: Where Are We and Where Are We Heading? *Current Transplantation Reports*, 3(1), 93–99. <https://doi.org/10.1007/s40472-016-0089-6>
- Organogenesis. (2018). Dermagraft Patient Guide - Treating Your Diabetic Foot Ulcer. Retrieved April 5, 2018, from <http://www.dermagraft.com//patient>
- Vericel. (2016). Epicel (cultured epidermal autografts). Retrieved from www.fda.gov
- Zaulyanov, L., & Kirsner, R. S. (2007). A review of a bi-layered living cell treatment (Apligraf) in the treatment of venous leg ulcers and diabetic foot ulcers. *Clinical Interventions in Aging*. <https://doi.org/10.2147/cia.2007.2.1.93>

CHAPTER I – INTRODUCTION

I.1 Cutaneous wound healing: an unmet clinical need

In a review published in the *New England Journal of Medicine* in 1999, the combined annual incidence of skin ulcers in the U.S.A due to venous stasis, diabetes or pressure was estimated as 7 million individuals (Singer & Clark, 1999). Although current figures are not readily available, this incidence has and will undoubtedly continue to increase with population growth, population aging, and increased prevalence of diabetes. Susceptible patients often have impaired wound healing, and cutaneous wounds that do not heal may directly cause disability and are portals for local and systemic infectious complications (Han & Ceilley, 2017).

Normal healing in acute wounds is achieved through four phases: *homeostasis*, *inflammation*, *proliferation* and *remodeling* (Figure I.1.1). During the *homeostasis* phase, which initiates immediately after injury, blood loss is prevented through vasoconstriction and blood clotting. The resulting fibrin plug serves as a lattice for platelet aggregation. Platelets secrete cytokines such as Transforming Growth Factor- β (TGF- β) and Platelet Derived Growth Factor (PDGF) to attract fibroblasts and immune cells to the wound site to initiate the healing process (P Martin, 1997). Within hours after injury, the *inflammation* stage initiates and neutrophils and macrophages infiltrate the injury site to kill bacteria, remove debris and secrete growth factors and chemokines to induce cell migration and proliferation (Paul Martin & Leibovich, 2005). The *proliferative* phase is initiated when fibroblasts migrate inwards from the wound margins to begin the production of glycosaminoglycans, proteoglycans and collagen. Keratinocytes and endothelial cells also proliferate during this period to restore the skin barrier and blood supply to the tissue (Landén, Li, & Ståhle, 2016). Finally, as the wound matures, randomly deposited collagen type I and type III fibers are *remodeled* to form a more organized structure in order to achieve higher tensile tissue strength (Robson, Steed, & Franz, 2001).

In chronic wounds, many physiological and mechanical factors can impair the healing process, resulting in a wound that often stalls in the *inflammation* phase (Eming, Krieg, & Davidson, 2007). During this phase, constant influx of immune cells and secretion of pro-inflammatory cytokines continue to amplify the inflammation cycle. In addition, non-healing wounds fail to achieve complete re-epithelization increasing the chance of bacterial biofilm formation and infection that prolong the inflammatory response at the wound site.

Current chronic wound treatments range from topical wound therapies/dressings to more advanced therapies such as skin grafts (Chakrabarti, Bhattacharya, & Deb, 2016; Mustoe, O'Shaughnessy, & Kloeters, 2006; Sun, Siprashvili, & Khavari, 2014). A common treatment is a process known as debridement in which the dead or inflamed tissue is removed. This

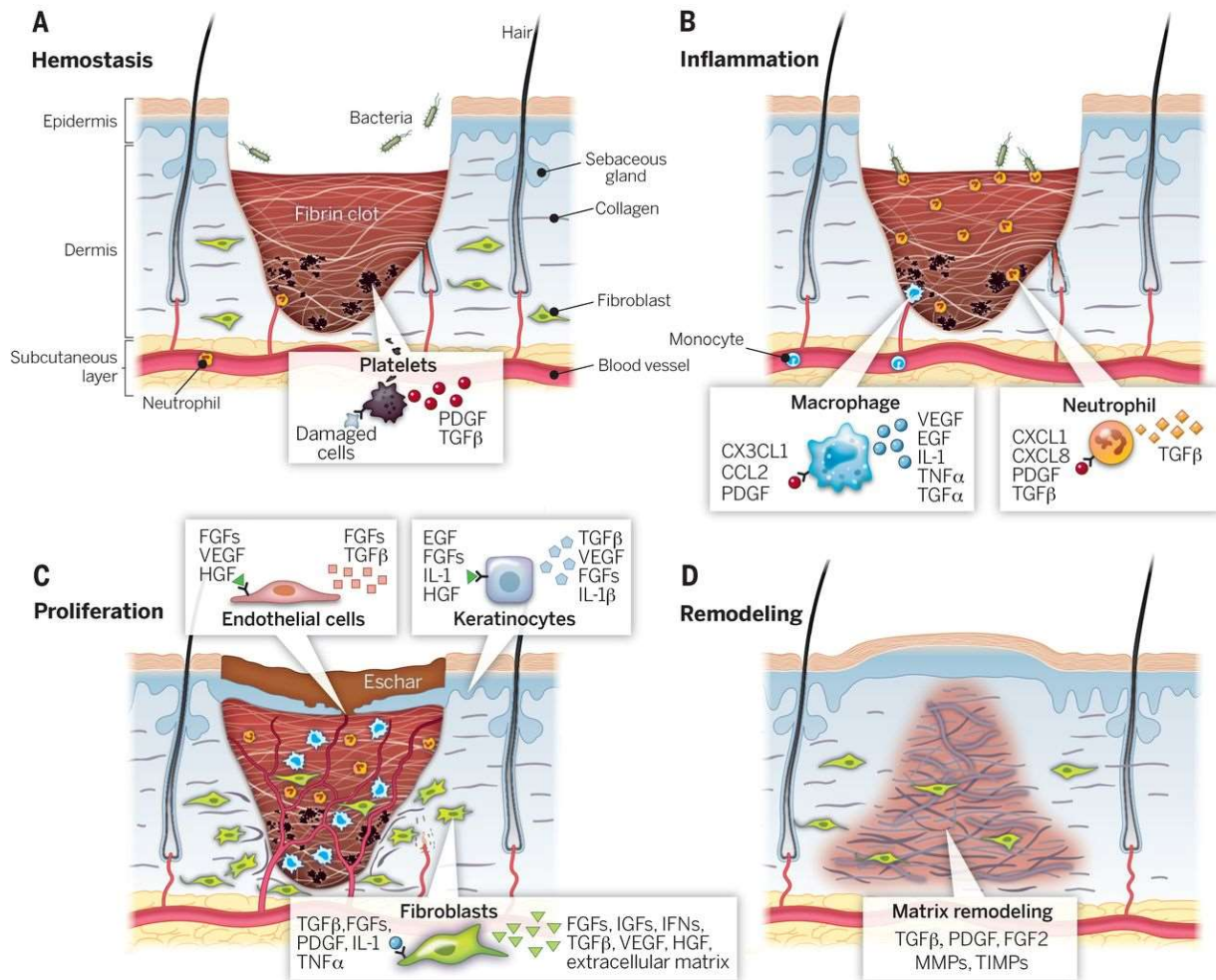


Figure I.1.1 - Immune mechanisms in acute and chronic wound healing. Acute wound healing can be divided into four overlapping phases: (A) homeostasis, (B) inflammation, (C) proliferation/matrix deposition, and (D) tissue remodeling. High numbers of inflammatory cells and the formation of a biofilm prevent the restoration of tissue homeostasis in chronic wounds. Excess secretion of inflammatory mediators leads to growth factor and ECM degradation which prevents wound healing. From (Sun et al., 2014). Reprinted with permission from AAAS.

process is often painful and larger wounds are sometimes cleaned under general anesthetic (Atkin, 2014). In addition, as an alternative to traditional dry gauze wound dressings that often cause further injury when removed, low adhesion hydrogel-based dressings are now available as these can simultaneously keep a moist environment, act as a barrier to microbial penetration and be easily replaced (Kamoun, Kenawy, & Chen, 2017). Moreover, several recent advancements in wound dressings have been focusing on the inclusion of antimicrobial molecules, such as iodine, honey and silver, to protect the wound from infection (Bradshaw, 2011; Halstead et al., 2015). Although these treatments help control the level of inflammation at the wound site, these do not constitute a permanent solution for the treatment of chronic wounds. Alternatively, autologous skin grafting is an effective treatment for wound closure, but

it creates a new wound at the harvest site that heals poorly, especially in individuals with compromised healing capacity. Allogeneic sources of skin can provide wound closure without the creation of a new wound but can be vigorously rejected by the patient's immune system (Benichou et al., 2011). Treatment for these patients is an unmet need and tissue engineering of skin resistant to rejection for grafting is a potential solution.

I.2 The Structure of Human Skin

I.2.1 The Epidermis

The skin is divided into three main structural layers: the epidermis, the dermis and the subcutis (Figure I.2.1) (McGrath, Eady, & Pope, 2004). The outermost layer, epidermis, is exposed to the environment and creates a water impermeant barrier while preventing microbial invasion. It is subdivided into five separate layers: *stratum basale*, *stratum spinosum*, *stratum granulosum*, *stratum lucidum* and *stratum corneum* (Eckert, 1989). The *stratum basale*, located at the base of the epidermis, is comprised of proliferating basal keratinocytes, a committed and self-renewing stem cell population attached to the underlying basement membrane. These cells undergo continuous mitosis to yield non-dividing progeny that undergo autophagy as they are displaced progressively upwards into the *stratum spinosum* (Crompton, Dexter, Wright, & Watt, 1998). This layer is composed of polyhedral keratinocytes that initiate the production of keratin, a process known as keratinization. As keratinocytes move upwards to the next layer, the *stratum granulosum*, a waterproof barrier forms due to the production of keratohyalin granules (Matoltsy & Matoltsy, 1970). Once these cells leave the *stratum granulosum*, they die and form the *stratum lucidum* layer as they can no longer be supported by nutrient diffusion from the basal layers. The last layer, *the stratum corneum*, is comprised of terminally differentiated keratinocytes, also known as corneocytes. These are flattened dead cells that slough as they are replaced by newly formed corneocytes. Due to the high content of keratin and water repellent lipids in corneocytes, the *stratum corneum* functions as a hard-protective barrier against the environment (Sheu, Chao, Wong, Lee, & Tsai, 1999). In addition to keratinocytes, the epidermis also contains melanocytes and leukocytes, notably Langerhans cells, a type of dendritic cell, and resident memory T cells (Salmon, Armstrong, & Ansel, 1994).

I.2.2 The Papillary Dermis

At the epidermal-dermal junction, a basement membrane undulates forming rete ridges that extend downward, away from the relatively flat outer skin surface. The region immediately

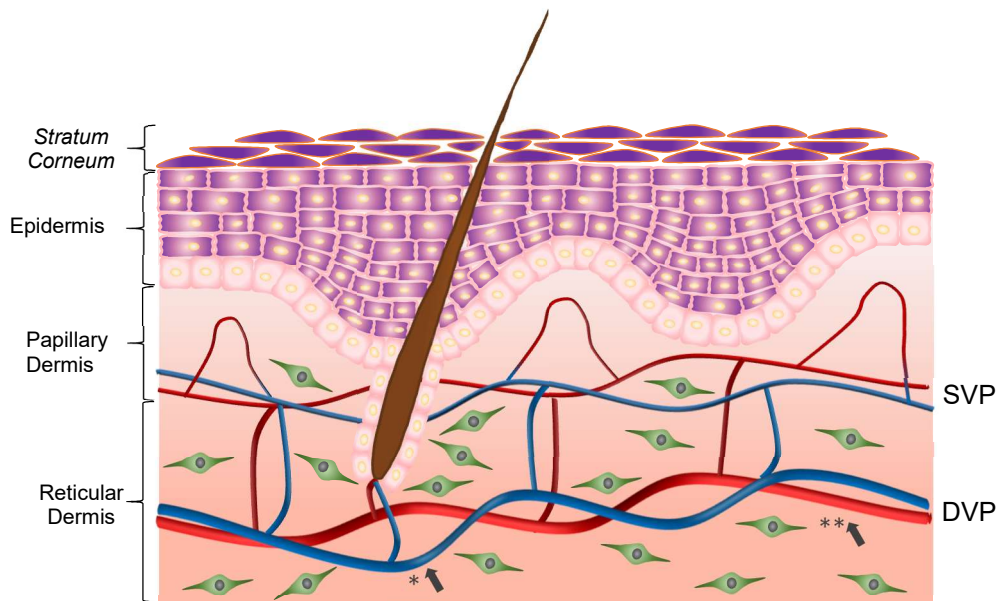


Figure I.2.1 – Schematic of human skin. Human skin is a layered organ consisting of epidermis, dermis and subcutis (the latter is not shown here). The epidermis, subdivided in 5 different layers, is comprised of keratinocytes at different stages of differentiation. The dermis is divided into two functional layers, the papillary dermis and reticular dermis. These two layers are separated by the superficial vascular plexus, which is fed by the deep vascular plexus (DVP) located at the base of the reticular dermis. Fibroblasts are the main cells in the dermis and are found throughout the papillary layer and reticular dermis. The dermis also contains hair follicles. The base of the hair follicle is located in the reticular dermis and is fed by the DVP. Other skin adnexa such as sweat glands and sebaceous glands are also located in the dermis (not shown here). *venule (blue); **arteriole (red).

beneath the epidermal basement membrane is called the papillary dermis, consisting of relatively loose connective tissue that contains a few scattered fibroblasts as well as the superficial vascular plexus (SVP) (Wong, Geyer, Weninger, Guimberteau, & Wong, 2016).

The architecture of the SVP consists of paired arterioles and venules that run parallel to the skin surface below the level of the rete and capillary arcades, arising from the arteriole and emptying into the venule, that arc upward into the dermal papillae, where they nourish the living keratinocytes of the basal layer and the still living keratinocytes in the several cell layers immediately above the basal cells (Sorrell & Caplan, 2004).

The microvessels of the SVP are continuously lined by endothelial cells and supported by pericytes (Braverman & Yen, 1977). Resident leukocytes of the papillary dermis include macrophages, dermal dendritic cells, resident memory T cells, innate-like lymphocytes (ILC, especially type 2) and mast cells. Lymphatic capillaries, nerve endings and portions of adnexa (e.g. hair follicles, sweat glands, etc.) are also present within the papillary dermis (Lu & Fuchs, 2014; Salmon et al., 1994).

I.2.3 The Reticular Dermis

The thickest layer of the skin, located deep to the papillary dermis and extending to the underlying subcutis, is the reticular dermis. It is composed of a denser, more collagenous extracellular matrix than the papillary dermis and contains scattered fibroblasts, which appear to be embryologically distinct from those of the papillary dermis, as well as the comparatively larger microvessels of the deep vascular plexus (DVP) (Driskell et al., 2013; Meigel, Gay, & Weber, 1977).

Arterioles of the DVP course upwards to perfuse the arterioles of the SVP, as well as capillaries that nourish the skin adnexa, such as hair follicles (Mecklenburg et al., 2000). DVP venules drain the venules of the SVP via straight connecting venules, and also drain the capillaries that nourish the various adnexa. The DVP itself is perfused and drained by larger vessels arising from the underlying subcutis. Lymphatic capillaries both course downward from the papillary dermis and arise in the reticular dermis, serving to drain excess interstitial fluid from the skin and as a conduit for leukocyte migration to draining lymph nodes (Swartz & Lund, 2012).

It also in the reticular dermis that the pilosebaceous units are located, comprising hair follicles and sebaceous glands, which are complex structures formed by about 15 types of cells of epithelial and mesenchymal origins (Niemann & Horsley, 2012; Schmidt-Ullrich & Paus, 2005). The pilosebaceous unit is connected to the apocrine sweat gland, the arrector pili muscle, the underlying skin vasculature, and nerve cells (Bernard, 2017; Velasquillo, Galue, Rodriguez, Ibarra, & Ibarra-Ibarra, 2013; Yano, Brown, & Detmar, 2001). While the apocrine sweat gland, has openings directly into the hair follicle (Lu & Fuchs, 2014; Velasquillo et al., 2013), the eccrine sweat glands present ducts opening to the outside surface of the skin. These are the primary functional units responsible for physical thermoregulation and hydration through the release of water and salt-based solutions (sweat) across the skin (Lu & Fuchs, 2014).

I.3 Current Human Skin Equivalent

In the last four decades, a variety of acellular and cellular matrices have been developed to promote skin wound healing, such as Alloderm™, Biobrane™, Dermagraft™ and Apligraf™, and these can be subdivided into epidermal, dermal and bilayer constructs (summary in Table I.3.1; please see reviews by Lazic and Falanga 2011 and Brohem et al. 2011 for further details).

Table I.3.1 – FDA approved human skin equivalents.

	Product	Company	Characteristics	Advantages/Limitations
Epidermal constructs	Bioseed-S®	BioTissue Technologies	Cultured autologous keratinocytes suspended in a fibrin glue	Simple handling; the gel-like construct is applied to the wound with a syringe
	ReCell®	Avita Medical	Keratinocytes are harvested in their proliferating state and then applied to the wound bed by spraying	Convenient way of delivery at earlier stages after wounding; recently launched
	Epicel®	Vericel Corp.	Cultured autograft composed of living keratinocytes cultured for 3 weeks; no dermal component; delivered on a petrolatum gauze backing	Variable take rate; 1-day shelf life; requires dermal support and a 3-wk cultivation period
Dermal constructs	AlloDerm®	Allergan	Cadaveric freeze-dried acellular dermal matrix	2-year shelf life; minimal wound contracture and scarring; safety concerns of allogeneic disease transfer
	Biobrane®	Smith & Nephew	Porcine collagen chemically bound to nylon/silicone membrane	3-year shelf life; good barrier function; decreased wound contracture; temporary dressing, needs removal 7–14 days after application
	Dermagraft®	Organogenesis	Living allogeneic fibroblasts from neonatal skin on a biodegradable polyglactin mesh; fibroblasts remain viable after implantation, continuing to secrete matrix proteins and growth factors	6-month shelf life; requires rapid time-sensitive thawing, and needs to be applied within 30 min after thawing; requires multiple applications
	Integra®	Integra LifeSciences	Temporary acellular silicone layer over a dermal scaffold consisting of collagen and chondroitin-6-sulfate	Good barrier function; long shelf life; used in over 10,000 patients; operative removal of silicone layer required
	Oasis®	Smith & Nephew Inc.	Porcine small intestine submucosa provides scaffold for growth of new tissue; acellular, but contains collagen and growth factors	1.5-year shelf life; requires multiple applications; potential host immune response
	TransCyte®	Organogenesis, Inc	Nylon mesh seeded with allogeneic human dermal fibroblasts; cryopreserved matrix contains high levels of proteins and growth factors with no viable cells	1.5-year life frozen; because nylon is not biodegradable, it serves as a temporary wound cover; must be removed after 7-14 days
Bilayered constructs	Apligraf®	Organogenesis, Inc	Composed of bovine collagen and living human keratinocytes and fibroblasts, derived from human neonatal foreskin;	Provides living cells to the wound, with potential for temporary stimulation; shelf-life of 5 days; risk of disease transfer
	OrCel®	Ortec International	Allogeneic neonatal fibroblasts and keratinocytes cultured in bovine collagen sponge; matrix contains viable cells that secrete growth factors and cytokines to promote healing	9-month shelf life if cryopreserved; secretion of cytokines and growth factors; immediate availability

Reconstructed skin models typically contain fibroblasts embedded in a collagenous matrix to simulate the dermis, and augmented with a layer of keratinocytes atop the dermis to simulate the epidermis. Nonetheless, this structure recreated *in vitro* does not recapitulate the complexity of the skin. *In vivo*, skin presents a diverse population of cells, and a complex and heterogenous distribution of proteins and growth factors that cannot be adequately represented in the simplified models fabricated in the laboratory (Panteleyev, Jahoda, & Christiano, 2001). Furthermore, many of these cells are organized and compartmentalized in distinct structures within the skin, such as vasculature, and adnexal structures (for e.g., hair follicles, sweat glands, and sebaceous glands), which confers an even higher level of complexity to this organ. The creation of more complex skin models, containing multiple cell types, vasculature, hair follicles, and sweat and sebaceous glands is significant for different applications.

In regenerative medicine, there is a critical need for skin grafts that present better aesthetic and functional recapitulation of native skin aiming at complete integration of the graft onto, and into, the wounded tissue. This also applies to grafts developed as a clinically superior alternative for the treatment of skin diseases (Moulin, Mayrand, Laforce-Lavoie, Larochelle, & Genest, 2011; Velasquillo et al., 2013). In the field of drug and cosmetic screening, the motivation lies in the need for skin models that can result in better translation between the *in vitro* and *in vivo* responses (Vijayavenkataraman, Lu, & Fuh, 2016).

I.3.1 Natural and Synthetic ECM

Biomaterial components used in skin substitutes range from synthetic to natural materials and provide a scaffold for skin cells to grow. Synthetic materials include poly-ethylene-glycol (PEG), poly-lactic-co-glycolic acid (PLGA) and poly-caprolactone (PCL) (please see review by BaoLin & Ma, 2014). These scaffolds are often designed to provide a porous 3D structure to permit sufficient transport of nutrients and growth factors to cells. As skin cells produce new ECM components and rearrange the newly formed tissue, some scaffolds are designed to undergo controlled biodegradation overtime (Yannas & Burke, 1980). Natural materials include collagen, fibronectin, chitosan and several glycosaminoglycans, such as hyaluronic acid. Collagen Type I, in particular, has been the most commonly used biomaterial in the generation of skin equivalents as it is a major component of the extracellular matrix of human skin (Glowacki & Mizuno, 2008; MacNeil, 2008).

I.3.2 Source of Skin Cells

Besides the choice of material to generate 3D skin scaffolds, the source of epithelial cells to reconstruct the skin tissue in cellular matrices is of special importance. Soon after keratinocytes were successfully cultured in a laboratory for the first time in 1977 (Rheinwald & Green, 1977), the first autologous skin equivalent was reported (Bell, Ehrlich, Buttle, & Nakatsuji, 1981). Autologous keratinocytes can be easily obtained through a small biopsy of healthy skin, expanded *in vitro* and grafted back onto the patient wound. Despite their clinical benefit, the generation of autologous skin equivalents requires long periods of *in vitro* culture to produce a skin construct large enough to fit the wound site. Moreover, keratinocytes cannot be expanded indefinitely as these senesce in culture overtime (Gilchrest, 1983). These factors can be limiting steps to the application of autologous skin equivalents, particularly in cases when immediate care is critical.

Alternatively, induced pluripotent stem cells (iPSCs) have the potential of self-renewal and to differentiate into any cell type of the human body. Through a process known as “reprogramming”, terminally differentiated cells isolated from a biopsy can return to a state of pluripotency *in vitro* (Chen et al., 2011). Treatment of iPSCs with retinoic acid and BMP4 in cell culture has shown to induce differentiation of these stem cells into keratinocytes (Itoh et al., 2013). Itoh *et al.* have shown that iPSCs-derived keratinocytes can successfully form a multilayered epidermis and cornified layer. Moreover, Sebastiano *et al.* have generated iPSCs from keratinocytes and fibroblasts isolated from skin biopsies of adult patients with recessive dystrophic epidermolysis bullosa (RDEB), a disease characterized by a mutation in the *COL7A1* gene which encodes the alpha-1 chain of type VII collagen, which results in severe blistering and skin fragility (Sebastiano et al., 2014). Using an adeno-associated virus, the authors demonstrated correction of the *COL7A1* mutation in patient-derived iPSCs. These cells were then differentiated in culture into keratinocytes that expressed functional collagen type VII. Both *in vitro* and in a mouse model, the genetically-edited keratinocytes were able to form a stratified skin tissue and secrete functional collagen VII. However, the skin grafts slough off after 3 weeks, an indication of lack of blood supply within the graft.

In the last 3 decades, cultured allografts have been most commonly used in skin replacement due to their immediate availability. However, it is now known that these do not integrate efficiently with the host skin. Instead, these artificial grafts act as pharmacological agents that stimulate wound healing by inducing re-epithelization from the dormant wound edges, a process known as the edge effect (Kirsner, Falanga, Kerdel, Katz, & Eaglstein, 1996). Moreover, cultured allografts work to provide immediate wound coverage from injuries and infections; release of healing growth factors (for e.g., TGF- α and β , GM-CSF, β FGF, PDGF,

TNF- α) and cytokines (for e.g., IL-1, 3, 6, and 8) (Lim, Phan, Lim, & Cao, 2009; Maas-Szabowski, Stärker, & Fusenig, 2003; Uchi, Terao, Koga, & Furue, 2000); and biosynthesis of new matrix components (Boehnke et al., 2007). Phillips *et al.* have shown that allogeneic cells were rarely detected in patients with venous ulcers treated with Apligraf™ at 2 months after grafting (Phillips et al., 2002). In agreement with this observation, Griffiths *et al.* demonstrated that Apligraf™ DNA does not persist beyond 4 weeks in the host skin (Griffiths, Ojeh, Livingstone, Price, & Navsaria, 2004). The relatively short clinical persistence of Apligraf™ and other cultured allografts can be a disadvantage, particularly in the treatment of chronic wounds which require more than 4 weeks to heal. Since these grafts do not integrate with the host skin and are only temporary, patients often need multiple rounds of treatment until re-epithelization is achieved. This makes the use of cultured allografts expensive, time-consuming, and with sub-optimal clinical outcomes.

I.3.3 The Need for Blood Supply

Skin microvasculature not only promotes graft survival by supplying skin cells with oxygen and nutrients but also modulates inflammation and immune cell migration to the wound site (Pasparakis, Haase, & Nestle, 2014). Moreover, the presence of a vascularized bed has been shown to promote skin engraftment through microvascular connections between graft and recipient capillaries that surround the wound region (Gibot, Galbraith, Huot, & Auger, 2010; Tremblay, Hudon, Berthod, Germain, & Auger, 2005).

Since the early studies on the physiology of graft acceptance in the late-19th century by Bert (Bert, 1865) and Thiersch (Thiersch, 1869), there has been an ongoing debate between two opposing theories regarding the origin of skin graft revascularization: is it achieved through graft's vessel growth and connection with the host tissue, or is the new vascular supply originating by capillary invasion from the host bed?

In 1865, pioneering studies by Bert demonstrated direct vascular connections between recipient and graft vessels as early as 18 hours after grafting (Bert, 1865). These findings founded the theory of anastomosis. Observations by Converse *et al.* on vascular changes in skin autografts in mice showed that blood flow was recovered 48 hours after grafting (Converse, Smahel, Ballantyne, & Harper, 1975). This short time interval between grafting and blood perfusion reinforced Bert's anastomosis theory. Supporting the alternative theory, Garré (Garré, 1889) reported evidence that graft vessels degenerated soon after engraftment, and therefore, new vascular ingrowth from the recipient bed had to occur. It was not until recently that it became possible to answer some of these controversial questions on the mechanisms of graft acceptance.

The development of improved imaging techniques and animal models provided researchers with new tools to understand these mechanisms. Using a *tie2/lacZ* transgenic mouse, Capla *et al.* demonstrated that skin graft revascularization occurs through recipient vascular ingrowth and simultaneous donor vascular regression (Capla *et al.*, 2006). Recipient-derived endothelial cells use the donor vascular framework as a guiding conduit for vascular ingrowth. This dynamic process of regression and ingrowth events results in quick connection between the capillaries of the host and the graft. These findings suggest that successful skin revascularization is greatly dependent on a critical and short window of time in which anastomosis needs to occur to reestablish blood flow and oxygenation to the wound site. The presence of a pre-existing vascular network in autologous full-thickness skin grafts accelerates this process facilitating the successful acceptance of the graft. In contrast, non-vascularized grafts rely on a neovascularization process which can take 3 weeks until blood flow is restored (Tsur, Daniller, & Strauch, 1980). Failure in the reestablishment of the supply of oxygen and nutrients to the wound site often causes the graft to slough off.

The development of new strategies to promote *the* graft-host angiogenic cross-talk that allows quick anastomosis and vascular integration of skin grafts is crucial to overcome the current limitations of skin graft acceptance. Approaches such as the *in vitro* generation of capillary-like networks embedded in engineered skin constructs pre-transplantation can not only yield faster integration within the host tissue but can also promote long-term skin homeostasis *in vivo*.

I.4 Developing Disease Skin Models

For many years, researchers have been trying to gain better understanding of the biological mechanisms involved in human skin diseases (please see review by Mathes, Ruffner, and Graf-Hausner 2014). Although significant advances have been made in creating better animal models, many of these still fail in reflecting the human situation. This challenge has boosted efforts among biologists and engineers to create *in vitro* 3D models containing human cells that recapitulate the pathophysiology of the disease-states in skin. Such alternative systems not only provide insights into the origin of the disease and its progression, but can also be used as drug discovery platforms as they allow for high-throughput screening of topical agents and the development of improved diagnostic and prognostic approaches.

I.4.1 *In Vitro* Skin Model of Psoriasis

Psoriasis is a chronic autoimmune disease that causes skin cells to accumulate rapidly on the surface of the skin which creates red and itchy patches that may vary in size and severity. This building up of skin cells results from the interaction between genetic and environmental factors that cause the over-production of cytokines by T cells (Cai, Fleming, & Yan, 2012). This increase in cytokine production stimulates keratinocyte proliferation and the expression of adhesion molecules in the skin microvasculature to facilitate the infiltration of inflammatory cells into psoriatic skin to maintain high levels of cytokine production (Lee, To, Nicholson, & Schrieber, 1994). In addition, the hyperproliferative and parakeratinized epidermis is associated with an increased density of capillaries. The capillary loops which are typically found in normal skin as single and arterial loops change to highly coiled, dilated and venous loops in psoriatic lesions (Braverman, 1989; Braverman & Sibley, 1982). Cutaneous blood flow in patients with active psoriasis has been found to be 10 times higher than in healthy individuals (Klemp, 1987).

Psoriasis was one of the first *in vitro* models to be developed in the context of skin pathology. In 1990, Krueger and Jorgensen developed a model composed of healthy or diseased dermal fibroblasts, and healthy keratinocytes separated by a porous membrane (Krueger & Jorgensen, 1990). However, this separation introduced a physical barrier that limited important interactions between the keratinocytes and fibroblasts.

A more advanced skin model was later developed by van den Bogaard *et al.* with the inclusion of immune cells (van den Bogaard *et al.*, 2012). The model was generated by pre-stimulated CD4⁺ cells from donor blood to facilitate Th1, Th2, and Th17 responses. These cells were then loaded on a membrane and covered with decellularized dermis. The authors demonstrated transdermal migration of the CD4⁺ cells towards the epidermis. The interaction between immune cells and keratinocytes in the epidermis increased the expression of biomarkers of inflammation (DEFB4, LCE3A and KRT16), as well the expression of pro-inflammatory cytokines (IL6, IL8, and IL23). However, the levels of pro-inflammatory cytokines were still 40 times lower than that of psoriatic skin lesions indicating a less-than-sufficient representation of disease-states, possibly due to the lack of the vascular compartment.

Capturing the ultrastructure and organization of the cutaneous microcirculation in both, normal physiology and disease-states, remains a challenge in the development of improved skin equivalents. The incorporation of microvasculature that can structurally, and functionally mimic *in vivo* responses may lead to better integration of engineered skin grafts with, and within, the host tissue as well as lead to the development of improved skin disease models.

I.4.2 *In Vitro* Skin Model of Melanoma

Cutaneous malignant melanomas are highly invasive and can easily metastasize to distant sites in the body. In the last decade, researchers have been trying to create appropriate *in vitro* models that can mimic human melanoma progression to address questions about the molecular mechanisms of melanoma invasion (please see review by Beaumont, Mohana-Kumaran, and Haass 2013 for further details). Melanoma progression is characterized by three phases: radial growth phase (RGP), vertical growth phase (VGP) and metastatic melanoma (Miller & Mihm, 2006). During RGP, melanoma cells grow as individual cells or small clusters along the basement membrane whereas VGP melanoma cells are more aggressive as they gain the ability to invade the dermis by breaking through the basement membrane. Metastatic melanoma cells can invade both epidermis and dermis, reach vascular or lymphatic vessels, and subsequently spread to distant sites. Current models of melanoma attempt to recapitulate this multiphasic nature of melanoma progression through the integration of RGP, VGP and metastatic melanoma cells in skin constructs.

Meier *et al.* have successfully demonstrated that *in vitro* response of these cells in a 3D skin model accurately reflects the responses observed *in vivo*: RGP melanoma cells grew but could not penetrate the basement membrane of the epidermis; VGP melanoma cells invaded into the dermis; and metastatic melanoma cells rapidly proliferated in the dermis (Meier et al., 2000).

In an attempt to create a more complex and relevant model of metastatic melanoma progression, Gibot *et al.* incorporated a microvasculature network within a reconstructed skin substitute to study the mechanisms of tumor angiogenesis (Gibot, Galbraith, Huot, & Auger, 2013). The presence of microvasculature within this model allowed the authors to demonstrate a correlation between high VEGF production by melanoma metastatic cells and migration of endothelial cells towards these cells. Moreover, the authors state "... the need to incorporate other structures such as lymphatic networks in melanoma models, since metastasis to the regional lymph nodes is one of the most important indicators of tumor aggressiveness, especially in melanomas" (Gibot et al., 2013).

As more becomes known about skin function, it also becomes clear that current skin models comprising of fibroblasts and keratinocytes alone lack the complexity of native human skin. Capturing the dynamic cross-talk between multiple cell types and structures in skin models is crucial and necessary to recapitulate the physiology of healthy and disease-states.

I.5 Efficacy Models for Drug and Formulation Screening

Many *in vitro* skin substitutes such as EpiSkin™, skinEthic™, Epiderm™ and GraftSkin™ have received regulatory approvals in Europe and United States for testing skin corrosion, acute skin irritation, and phototoxicity (Botham, Earl, Fentem, Roguet, & Van De Sandt, 1998; Netzlaff, Lehr, Wertz, & Schaefer, 2005). However, since these models lack rete ridges, vasculature, and other appendages such as hair follicles, they are limited in the detection of adverse drug reactions and prediction of percutaneous absorption across native human skin. Moreover, because these substitutes do not fully recapitulate the normal barrier function of human skin, none of them is currently approved for testing skin absorption. Skin equivalents have been shown to exhibit 10-to-30 times higher permeability of topical agents across the *stratum corneum* when compared to native skin (Perkins, Osborne, Rana, Ghassemi, & Robinson, 1999). This can result in an over-estimation of systemic exposure to irritants due to their higher penetration rates. Due to these limitations of the current models, many percutaneous permeation studies still rely on the use of human cadaveric skin and animal skin obtained from pigs, mice, and rabbits. These models have been extensively used to investigate the molecular mechanism responsible for the development of skin diseases and in the discovery of new drug candidates (Jung & Maibach, 2015). However, with increasing awareness for animal protection and regulation of the use of animals for the testing of cosmetics, companies are now increasing their efforts in developing *in vitro* skin models with better barrier function.

I.6 3D Bioprinting

I.6.1 3D Bioprinting Modalities

The complexity of skin microvasculature and other three-dimensional structures that are present in human skin are difficult to replicate *in vitro* through simple manual fabrication methods. 3D bioprinting is a flexible tool that allows precise deposition and patterning of different cell populations and biomaterials to create accurate geometries in three dimensions that mimic anatomical and biological structures such as tissues and organs (Knowlton, Yenilmez, & Tasoglu, 2016; Munoz-Abraham et al., 2016; Murphy & Atala, 2014).

The most commonly used bioprinting approaches to generate living tissues are inkjet, microextrusion and laser assisted technology (Figure I.6.1).

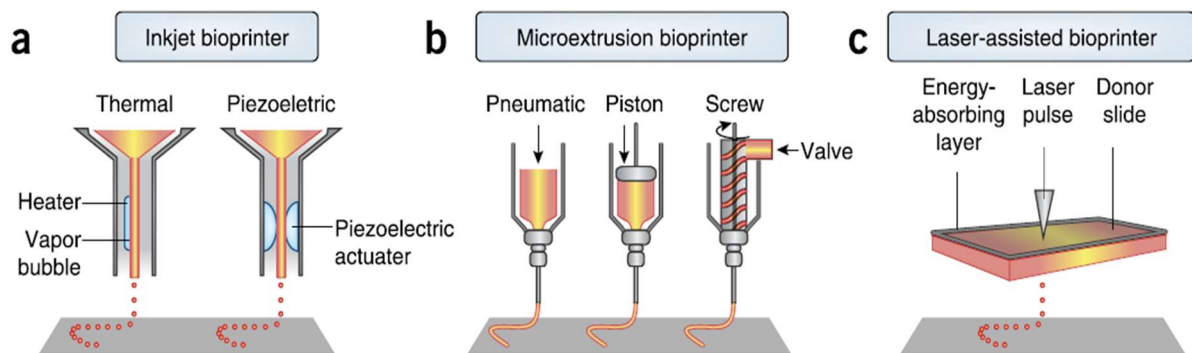


Figure 1.6.1 - Components of inkjet, microextrusion and laser-assisted bioprinting. **(a)** Thermal inkjet printers produce air-pressure pulses to produce droplets, whereas acoustic printers use pulses formed by piezoelectric or ultrasound pressure. **(b)** Microextrusion printers use pneumatic or mechanical systems to extrude continuous droplets of material. **(c)** Laser-assisted printers use lasers focused on an absorbing substrate to generate pressures that propel materials onto a collector material. Reprinted by permission from Springer Nature Publishers: Nature Biotechnology (Murphy & Atala, 2014), copyright 2014.

1.6.1.1 Inkjet Bioprinting

Inkjet printers are the most common of the 3 types of printers and have been used in broad range of application such as regeneration of functional skin and cartilage (Gao, Hubbell, Schilling, Dai, & Cui, 2017). These printers can use thermal or acoustic forces to eject droplets of material onto a substrate. In thermal inkjet printers, localized heating of the print head produces pulses of pressure that force droplets to be ejected from the nozzle (Cui, Boland, D’Lima, & Lotz, 2012). Although high printing speeds can be achieved with this technology, the risk of exposing cells and materials to thermal stress and the frequent clogging of the nozzle are considerable disadvantages for the use of these type of printers. Many inkjet printers rely on a piezoelectric crystal to create an acoustic wave to create droplets inside the print head at regular intervals. Due to the range of frequencies used to create the acoustic waves, these bioprinters have the potential to induce cell lysis (Chameettachal & Pati, 2018). Moreover, inkjet bioprinters are limited to relatively low viscosity materials due to the force required to eject droplets of solutions at higher viscosities (Murphy & Atala, 2014).

1.6.1.2 Microextrusion Bioprinting

Microextrusion bioprinting has been used to generate a broad range of tissues from aortic valves to tumor models (Ozbolat & Hospodiuk, 2016). This type of printer can extrude

materials into a substrate by a robotically-controlled mechanism. Rather than dispensing individual droplets of material, microextrusion printing produces a continuous array of droplets. Biomaterials and live cells can be extruded through *pneumatic* or *mechanical* forces generated at the printing head. While pneumatic dispensing systems require compressed air to push the biomaterial through the nozzle, mechanical-based bioprinting requires more complex components such as a piston or a screw to generate the forces to dispense the materials (Murphy & Atala, 2014). Although high viscosity materials can be easily dispensed with this type of printer, increasing the printing resolution and speed is still a challenge. Additional improvements in nozzle, syringe and motor control units may significantly reduce the printing times (Ozbolat & Yu, 2013).

1.6.1.3 Laser-assisted Bioprinting

Laser-assisted bioprinting is less common than inkjet or microextrusion bioprinting but has been successfully used to fabricate medical devices such as acellular tracheal splint implanted in a patient with tracheobronchomalacia (Morrison et al., 2015). A typical laser-assisted bioprinter consists of a pulsed laser beam, a focusing system, an optically transparent quartz disk (ribbon), and a layer of biomaterial (Schiele et al., 2010). Focused laser pulses on the ribbon surface generate a small bubble that ejects part of the coating material containing cells towards the collector surface. Since this technology is nozzle-free, the clogging of the nozzle is not a concern during printing. In addition, laser-assisted printing is compatible with high viscosity materials and has negligible effect on cell viability. However, as the preparation of a new ribbon is required for each printed cell and material type, laser-assisted bioprinting can be time consuming when multiple cell-types and materials are co-deposited (Guillemot, Souquet, Catros, & Guillotin, 2010).

1.6.2 3D Bioprinting of Human Skin

3D bioprinting of a human skin construct was first reported in the journal *Tissue Engineering. Part C* by Lee *et al.* in 2014 (Lee et al., 2014). The group of researchers demonstrated for the first time the potential of using 3D bioprinting to generate a human skin construct comprised of human foreskin fibroblasts and HaCaT cells, an immortalized cell line of human keratinocytes. In this study, a 3D solid freeform fabrication technology was used to precisely place cells and extracellular matrix. The liquid materials were dispensed by pneumatic pressure and the volume of dispensed droplets was manipulated by controlling valve opening time and air pressure. In the printing scheme, the printed skin structure contained eight

collagen layers. These include six collagen layers alternating with three layers of fibroblasts layers and two collagen layers separating the fibroblasts layers from keratinocytes (Figure I.6.2e). Two keratinocytes layers were printed on top of the dermal compartment to generate the epidermis. Although histological analysis demonstrated that the 3D printed construct was made of 2 distinct layers, an epidermal and a dermal compartment, the authors did not show the expression of any skin differentiation markers. In addition, the skin tissue did not show proper stratification and formation of a *stratum corneum* layer as observed in human skin. The authors hypothesize this was likely due to the use of HaCaT cells, an immortalized keratinocyte cell line, which is unable to form a *stratum corneum* layer.

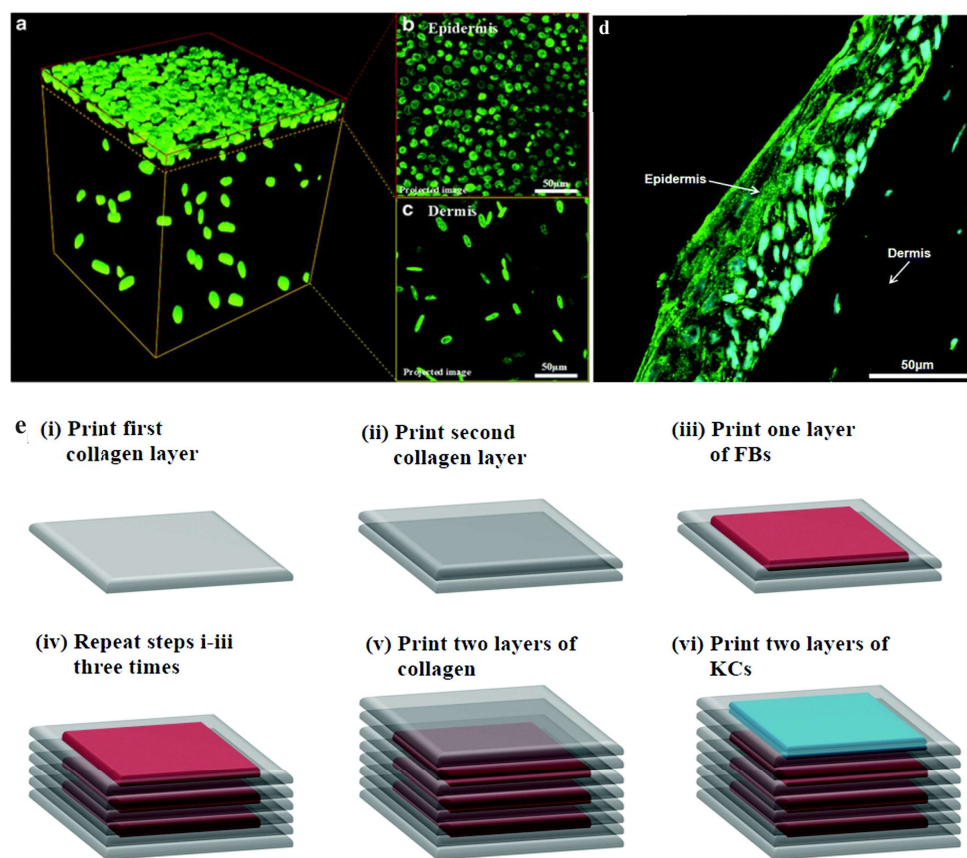


Figure I.6.2 – 3D bioprinting of human skin with HaCaT cells. **(a)** 3D reconstruction of confocal microscopy images of printed skin after 7 days in submerged culture conditions. Live cell nuclei are stained green and present compact and rounded (KC) or large and elongated (FB) morphologies. **(b, c)** Compressed z-projections of the epidermis and dermis showing KCs and FBs. **(d)** Printed skin structures were stained for N-cadherin tight junctions at day 14 of ALI culture. N-cadherin (green) was observed bordering adjacent epidermal cells, but it was not detected in the dermal compartment. **(e)** Construction of three-dimensional (3D) skin tissue. Collagen matrix, KCs, and FBs were printed in a layer-by-layer fashion to construct the dermal and epidermal compartments in a single structure.

More recently, Cubo *et al.* described the generation of a 3D bioprinted skin construct using primary human cells in a fibrin-based dermal matrix. The authors developed an extrusion bioprinting method with four separated dispensers (Figure I.6.3E). Each syringe driving screw had its own angular speed, which were calculated to obtain a constant mixture of three components (fibroblasts, plasma and CaCl₂) at the nozzle. Human keratinocytes were inserted in the fourth syringe which was controlled independently by a second step motor. The printed human skin was allowed to mature *in vitro* and engrafted onto an immunodeficient athymic nude mice. Eight weeks post-engraftment, the printed model presented characteristics of the skin from the donor's skin (Figure I.6.3B). Moreover, the authors reported the presence of small blood vessels beneath the epidermis of the bioprinted graft through positive staining of α -smooth muscle actin (Figure I.6.3D). However, printed fibroblasts that do not associate with endothelial cells can also stain positively for α -SMA, which makes it unclear that the structures observed in the dermis are vessels.

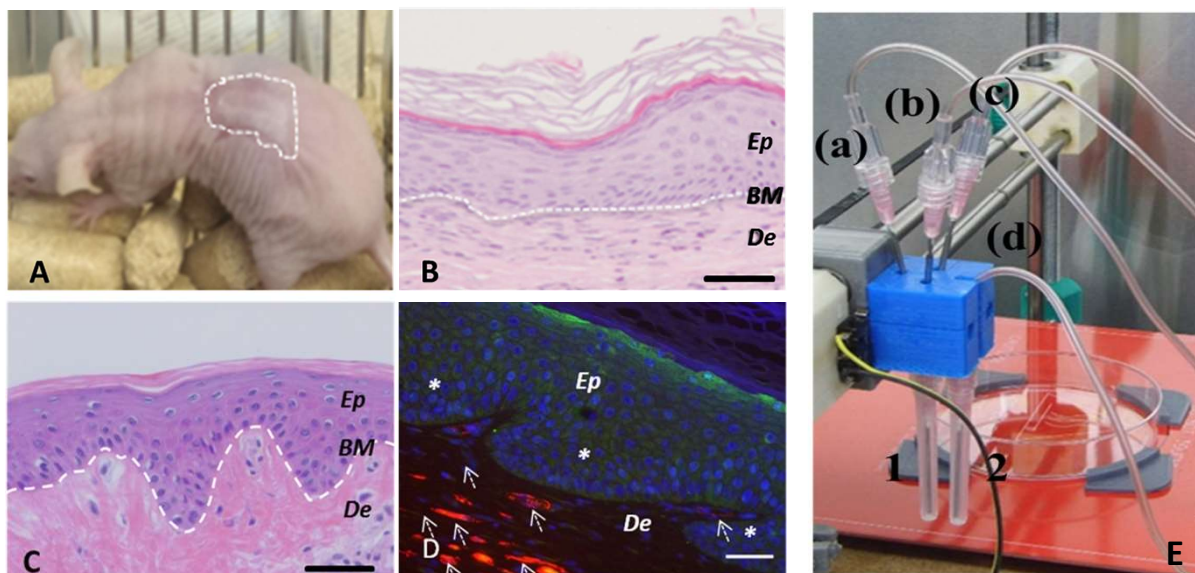


Figure I.6.3 – 3D bioprinting human skin. **(A)** Grafted human skin onto a immunodeficient mice. The dotted line marks the boundary between human and mouse skin. **(B)** Histological analysis 8 weeks post-grafting of bioprinted human skin. **(C)** H&E staining of normal human skin. The white dotted line in **(B)** and **(C)** indicates the dermo-epidermal junction (basal membrane, BM). Ep and De denote the epidermal and the dermal compartments, respectively. Scale bar: 100 μ m. **(E)** Picture of the printing head showing the three tubes **(a)–(c)** carrying the components of the dermal compartment (FBs, human plasma and CaCl₂), converging to the trifurcated connector connected to needle 1 and the fourth tube **(d)**, carrying the KCs, connected to needle 2. Reprinted by permission from IOP Publishers: Biofabrication (Cubo *et al.*, 2016), copyright 2016.

I.6.3 Incorporating 3D bioprinted vasculature in human skin equivalents

Although multiple approaches using 3D bioprinting technology have shown to successfully generate perfusable capillary-like structures *in vitro* (please see reviews by Hoch, Tovar, and Borchers 2014 and Frueh et al. 2016 for further details), these studies have not yet shown integration of the vascularized constructs in the skin context. A few research groups have recently demonstrated the combination of both tissue components into a single vascularized skin model (Abaci et al., 2016; Bibb, Nottrodt, & Gillner, 2016). Abaci *et al.* have successfully generated an *in vitro* skin model embedded with a 3D bioprinted and perfusable vascular network using both primary and induced pluripotent stem cell (iPSC)-derived endothelial cells (Abaci et al., 2016). The authors demonstrated in mice that blood flow was restored to the vascularized skin constructs 14 days after grafting through ingrowth of the host vessels that perfectly aligned with the patterns of the graft vessels (Figure I.6.4). After gel contraction, the final size of the printed vessels ranged from 100–250 μm . Although the authors reported the generation of smaller channels with their platform, the lowest diameter achieved was of 80 μm . This size is significantly larger than the capillaries found in the skin microvasculature: < 26 μm at the superficial horizontal plexus and < 50 μm at the dermal-subcutaneous plexus. In addition, a fully printed vascularized skin construct has yet to be realized.

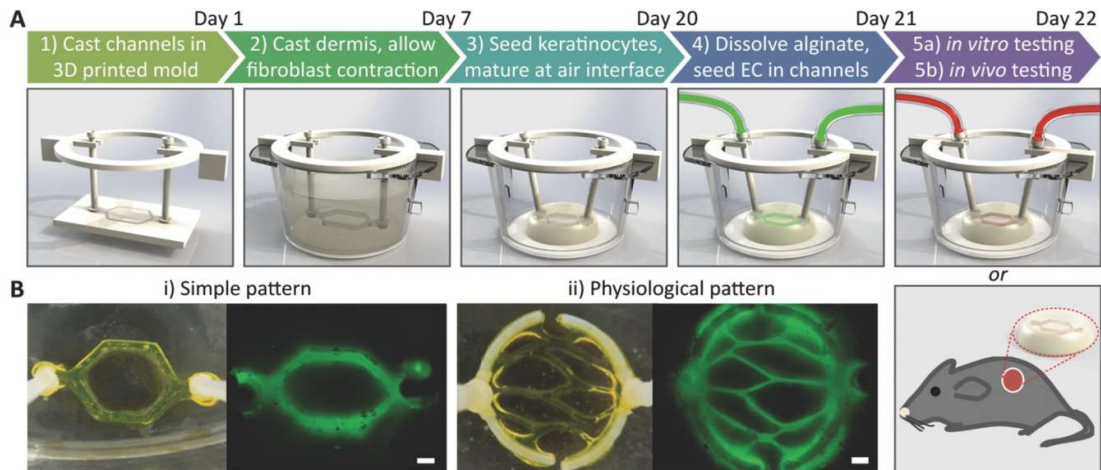


Figure I.6.4 - Development of vascularized human skin equivalents. **A)** A sacrificial layer of alginate microchannels was created in 3D-printed molds with the desired vasculature pattern. Then the dermal compartment that consisted of dermal fibroblasts and collagen gel was formed around the sacrificial layer, which was suspended in the transwell inserts using a ring-shaped holder. The sacrificial layer was dissolved by sodium citrate treatment through the inlet/outlet ports followed by EC seeding through the same ports. **B)** Two different vasculature patterns were used using fluorescently tagged alginate. Scale bar: 600 μm . Reprinted by permission from John Wiley and Sons: Advanced Healthcare Materials, (Abaci et al., 2016). copyright 2016.

The development of a full-thickness vascularized 3D printed skin model is not only important for the success of permanent engraftment but also for disease modeling of inflammatory conditions in systems such as organ-on-a-chip as it provides a platform for physiological integration with other organ systems.

I.6.4 Incorporating adnexal structures in human skin equivalents

The first attempt to include sweat glands in a human reconstructed skin model was made in 2010 by Huang *et al.* (Huang, Xu, Wu, Sha, & Fu, 2010). When gelatin microspheres containing sweat gland cells and epidermal growth factor were injected in a full thickness skin model, structures similar to sweat glands were generated (Huang et al., 2010). Furthermore, these constructs, when grafted on a wound in mice, improved tissue integration compared to control condition, demonstrating the importance of this skin appendage for tissue regeneration. Recently, the same group employed a 3D bioprinting platform as a tool to promote differentiation and regeneration of sweat gland cells (Huang, Yao, Xie, & Fu, 2016; Liu et al., 2016). The authors showed that the gelatin and alginate-based scaffold created an environment capable of inducing differentiation of epidermal progenitor cells into sweat gland cells (Huang et al., 2016). Additionally, the matrix induced sweat gland regeneration when it was directly printed on burn wounds in mice. Further experiments demonstrated the effect of the pore sizes and controlled growth factor release from the 3D-ECM, both guided by printing parameters, in the differentiation and self-organization of sweat gland cells (Liu et al., 2016). With this work, the group has demonstrated the advantages of using 3D bioprinting for precisely controlling scaffold structure aiming at the improvement in differentiation of sweat gland cells *in vitro*. The 3D bioprinting technology allows not only the creation of a scaffold with precise and a reproducible architecture, but also the simultaneous incorporation of multiple cells, with high cell viability, and matrix molecules during the fabrication of biological structures (Huang et al., 2016; Liu et al., 2016).

I.7 References

- Abaci, H. E., Guo, Z., Coffman, A., Gillette, B., Lee, W., Sia, S. K., & Christiano, A. M. (2016). Human Skin Constructs with Spatially Controlled Vasculature Using Primary and iPSC-Derived Endothelial Cells. *Advanced Healthcare Materials*, 5(14), 1800–1807. <https://doi.org/10.1002/adhm.201500936>
- Atkin, L. (2014). Understanding methods of wound debridement. *British Journal of Nursing*, 23(sup12), S10–S15. <https://doi.org/10.12968/bjon.2014.23.sup12.S10>
- BaoLin, G., & Ma, P. X. (2014). Synthetic biodegradable functional polymers for tissue engineering: a brief review. *Science China. Chemistry*, 57(4), 490–500. Retrieved from <https://www.ncbi.nlm.nih.gov/pubmed/25729390>
- Beaumont, K. a, Mohana-Kumaran, N., & Haass, N. K. (2013). Modeling melanoma in vitro and in vivo. *Healthcare*, 2(1), 27–46. <https://doi.org/10.3390/healthcare2010027>
- Bell, E., Ehrlich, H. P., Buttle, D. J., & Nakatsuji, T. (1981). Living tissue formed in vitro and accepted as skin-equivalent tissue of full thickness. *Science*, 211(4486), 1052 LP-1054. <https://doi.org/10.1126/science.7008197>
- Benichou, G., Yamada, Y., Yun, S.-H., Lin, C., Fray, M., & Tocco, G. (2011). Immune recognition and rejection of allogeneic skin grafts. *Immunotherapy*, 3(6), 757–770. <https://doi.org/10.2217/imt.11.2>
- Bernard, B. A. (2017). The Hair Follicle Enigma. *Experimental Dermatology*, 0, 1–6. <https://doi.org/10.1111/exd.13337>
- Bert, P. (1865). Notes sur un cas de greffe animale. *Comptes Rendus de La Societe de Biologie*, 61, 587.
- Bibb, R., Nottrodt, N., & Gillner, A. (2016). Artificial vascularized scaffolds for 3D-tissue regeneration — a report of the ArtiVasc 3D Project. *International Journal of Bioprinting*, 2(1), 93–102. <https://doi.org/10.18063/IJB.2016.01.004>
- Boehnke, K., Mirancea, N., Pavesio, A., Fusenig, N. E., Boukamp, P., & Stark, H.-J. J. J. (2007). Effects of fibroblasts and microenvironment on epidermal regeneration and tissue function in long-term skin equivalents. *European Journal of Cell Biology*, 86(11–12), 731–746. <https://doi.org/http://doi.org/10.1016/j.ejcb.2006.12.005>
- Botham, P. A., Earl, L. K., Fentem, J. H., Roguet, R., & Van De Sandt, J. J. M. (1998). Alternative Methods for Skin Irritation Testing: The Current Status. ECVAM Skin Irritation Task Force Report 1. *ATLA Alternatives to Laboratory Animals*, 26(2), 195–211.
- Bradshaw, C. E. (2011). An in vitro comparison of the antimicrobial activity of honey, iodine and silver wound dressings. *Bioscience Horizons: The International Journal of Student Research*, 4(1), 61–70. <https://doi.org/10.1093/biohorizons/hzr008>
- Braverman, I. M. (1989). Ultrastructure and Organization of the Cutaneous Microvasculature in Normal and Pathologic States. *Journal of Investigative Dermatology*, 93(s2), 2S–9S. <https://doi.org/10.1111/1523-1747.ep12580893>
- Braverman, I. M., & Sibley, J. (1982). Role of the microcirculation in the treatment and pathogenesis of psoriasis. *The Journal of Investigative Dermatology*, 78(1), 12–17. <https://doi.org/10.1111/1523-1747.ep12497850>
- Braverman, I. M., & Yen, A. (1977). Ultrastructure of the Human Dermal Microcirculation. *Journal of Investigative Dermatology*, 68(1), 44–52. <https://doi.org/10.1111/1523-1747.ep12485165>
- Brohem, C. A., da Silva Cardeal, L. B., Tiago, M., Soengas, M. S. M. S., de Moraes Barros, S. B., & Maria-Engler, S. S. (2011). Artificial skin in perspective: concepts and applications. *Pigment Cell*

- {&} *Melanoma Research*, 24(1), 35–50. <https://doi.org/10.1111/j.1755-148X.2010.00786.x>
- Cai, Y., Fleming, C., & Yan, J. (2012). New insights of T cells in the pathogenesis of psoriasis. *Cellular and Molecular Immunology*, 9(4), 302–309. <https://doi.org/10.1038/cmi.2012.15>
- Capla, J. M., Ceradini, D. J., Tepper, O. M., Callaghan, M. J., Bhatt, K. a, Galiano, R. D., Levine, J. P., & Gurtner, G. C. (2006). Skin graft vascularization involves precisely regulated regression and replacement of endothelial cells through both angiogenesis and vasculogenesis. *Plastic and Reconstructive Surgery*, 117(3), 836–844. <https://doi.org/10.1097/01.prs.0000201459.91559.7f>
- Chakrabarti, S., Bhattacharya, R., & Deb, K. (2016). Cell-based Wound Healing: Mechanisms and Treatments. *British Journal of Medicine and Medical Research*, 11(4), 1–17. <https://doi.org/10.9734/BJMMR/2016/21382>
- Chameettachal, S., & Pati, F. (2018). Inkjet-based 3D bioprinting. *3D Bioprinting in Regenerative Engineering:: Principles and Applications*.
- Chen, G., Gulbranson, D. R., Hou, Z., Bolin, J. M., Ruotti, V., Probasco, M. D., Smuga-Otto, K., Howden, S. E., Diol, N. R., Propson, N. E., Wagner, R., Lee, G. O., Antosiewicz-Bourget, J., ... Thomson, J. a. (2011). Chemically defined conditions for human iPSC derivation and culture. *Nature Methods*, 8(5), 424–429. <https://doi.org/10.1038/nmeth.1593>
- Converse, J. M., Smahel, J., Ballantyne, D. L. ., & Harper, A. D. (1975). Inosculation of vessels of skin graft and host bed: a fortuitous encounter. *British Journal of Plastic Surgery*, 28(1955), 274–282.
- Crompton, M. J., Dexter, T. M., Wright, N. A., & Watt, F. M. (1998). Epidermal stem cells: markers, patterning and the control of stem cell fate. *Philosophical Transactions of the Royal Society of London. Series B: Biological Sciences*, 353(1370), 831–837. <https://doi.org/10.1098/rstb.1998.0247>
- Cubo, N., Garcia, M., Del Canizo, J. F., Velasco, D., Jorcano, J. L., Cañizo, J. F., Velasco, D., Jorcano, J. L., del Cañizo, J. F., Velasco, D., & Jorcano, J. L. (2016). 3D bioprinting of functional human skin: production and in vivo analysis. *Biofabrication*, 9(1), 15006. <https://doi.org/10.1088/1758-5090/9/1/015006>
- Cui, X., Boland, T., D’Lima, D. D., & Lotz, M. K. (2012). Thermal inkjet printing in tissue engineering and regenerative medicine. *Recent Patents on Drug Delivery & Formulation*, 6(2), 149–155. Retrieved from <https://www.ncbi.nlm.nih.gov/pubmed/22436025>
- Driskell, R. R., Lichtenberger, B. M., Hoste, E., Kretzschmar, K., Simons, B. D., Charalambous, M., Ferron, S. R., Herault, Y., Pavlovic, G., Ferguson-Smith, A. C., & Watt, F. M. (2013). Distinct fibroblast lineages determine dermal architecture in skin development and repair. *Nature*, 504(7479), 277–281. <https://doi.org/10.1038/nature12783>
- Eckert, R. L. (1989). Structure, function, and differentiation of the keratinocyte. *Physiological Reviews*, 69(4), 1316–1346.
- Eming, S. A., Krieg, T., & Davidson, J. M. (2007). Inflammation in wound repair: molecular and cellular mechanisms. *The Journal of Investigative Dermatology*, 127(3), 514–525. <https://doi.org/10.1038/sj.jid.5700701>
- Frueh, F. S., Menger, M. D., Lindenblatt, N., Giovanoli, P., & Laschke, M. W. (2016). Current and emerging vascularization strategies in skin tissue engineering. *Critical Reviews in Biotechnology*, 8551(July), 1–13. <https://doi.org/10.1080/07388551.2016.1209157>
- Gao, G., Hubbell, K., Schilling, A. F., Dai, G., & Cui, X. (2017). Bioprinting Cartilage Tissue from Mesenchymal Stem Cells and PEG Hydrogel. *Methods in Molecular Biology (Clifton, N.J.)*, 1612, 391–398. https://doi.org/10.1007/978-1-4939-7021-6_28
- Garrè, C. (1889). Ueber die histologischen Vorgänge bei der Anheilung der Thiersch’schen Transplantationen. *Brun’s Beitr Klin Chir*, 4, 625–652.

- Gibot, L., Galbraith, T., Huot, J., & Auger, F. A. (2010). A Preexisting Microvascular Network Benefits *In Vivo* Revascularization of a Microvascularized Tissue-Engineered Skin Substitute. *Tissue Engineering Part A*, 16(10), 3199–3206. <https://doi.org/10.1089/ten.tea.2010.0189>
- Gibot, L., Galbraith, T., Huot, J., & Auger, F. A. (2013). Development of a tridimensional microvascularized human skin substitute to study melanoma biology. *Clinical and Experimental Metastasis*, 30(1), 83–90. <https://doi.org/10.1007/s10585-012-9511-3>
- Gilchrest, B. A. (1983). In vitro assessment of keratinocyte aging. *Journal of Investigative Dermatology*, 81(1), S184–S189.
- Glowacki, J., & Mizuno, S. (2008). Collagen scaffolds for tissue engineering. *Biopolymers*, 89(5), 338–344. <https://doi.org/10.1002/bip.20871>
- Griffiths, M., Ojeh, N., Livingstone, R., Price, R., & Navsaria, H. (2004). Survival of Apligraf in acute human wounds. *Tissue Engineering*, 10(7), 1180–1195. <https://doi.org/10.1089/ten.2004.10.1180>
- Guillemot, F., Souquet, A., Catros, S., & Guillotin, B. (2010). Laser-assisted cell printing: Principle, physical parameters versus cell fate and perspectives in tissue engineering. *Nanomedicine*, 5(3), 507–515. <https://doi.org/10.2217/nnm.10.14>
- Halstead, F. D., Rauf, M., Bamford, A., Wearn, C. M., Bishop, J. R. B., Burt, R., Fraise, A. P., Moiem, N. S., Oppenheim, B. A., & Webber, M. A. (2015). Antimicrobial dressings: Comparison of the ability of a panel of dressings to prevent biofilm formation by key burn wound pathogens. *Burns*, 41(8), 1683–1694. <https://doi.org/https://doi.org/10.1016/j.burns.2015.06.005>
- Han, G., & Ceilley, R. (2017). Chronic Wound Healing: A Review of Current Management and Treatments. *Advances in Therapy*, 34(3), 599–610. <https://doi.org/10.1007/s12325-017-0478-y>
- Hoch, E., Tovar, G. E. M. G. E. M., & Borchers, K. (2014). Bioprinting of artificial blood vessels: Current approaches towards a demanding goal. *European Journal of Cardio-Thoracic Surgery*, 46(5), 767–778. <https://doi.org/10.1093/ejcts/ezu242>
- Huang, S., Xu, Y., Wu, C., Sha, D., & Fu, X. (2010). In vitro constitution and in vivo implantation of engineered skin constructs with sweat glands. *Biomaterials*, 31(21), 5520–5525. <https://doi.org/10.1016/j.biomaterials.2010.03.060>
- Huang, S., Yao, B., Xie, J., & Fu, X. (2016). 3D bioprinted extracellular matrix mimics facilitate directed differentiation of epithelial progenitors for sweat gland regeneration. *Acta Biomaterialia*, 32, 170–177. <https://doi.org/10.1016/j.actbio.2015.12.039>
- Itoh, M., Umegaki-Arao, N., Guo, Z., Liu, L., Higgins, C. A., & Christiano, A. M. (2013). Generation of 3D Skin Equivalents Fully Reconstituted from Human Induced Pluripotent Stem Cells (iPSCs). *PLoS ONE*, 8(10), 1–9. <https://doi.org/10.1371/journal.pone.0077673>
- Jung, E. C., & Maibach, H. I. (2015). Animal models for percutaneous absorption. *Journal of Applied Toxicology*, 35(1), 1–10. <https://doi.org/10.1002/jat.3004>
- Kamoun, E. A., Kenawy, E.-R. S., & Chen, X. (2017). A review on polymeric hydrogel membranes for wound dressing applications: PVA-based hydrogel dressings. *Journal of Advanced Research*, 8(3), 217–233. <https://doi.org/https://doi.org/10.1016/j.jare.2017.01.005>
- Kirsner, R. S. S., Falanga, V., Kerdel, F. A. a, Katz, M. H. H., & Eaglstein, W. H. H. (1996). Skin grafts as pharmacological agents: pre-wounding of the donor site. *The British Journal of Dermatology*, 135(2), 292–296. <https://doi.org/10.1111/j.1365-2133.1996.tb01164.x>
- Klemp, P. (1987). Cutaneous and subcutaneous blood flow measurements in psoriasis. *Danish Medical Bulletin*, 34(3), 147–159. Retrieved from https://inis.iaea.org/search/search.aspx?orig_q=RN:18076556
- Knowlton, S., Yenilmez, B., & Tasoglu, S. (2016). Towards Single-Step Biofabrication of Organs on a

- Chip via 3D Printing. *Trends in Biotechnology*, 34(9), 685–688. <https://doi.org/10.1016/j.tibtech.2016.06.005>
- Krueger, G. G., & Jorgensen, C. M. (1990). Experimental Models for Psoriasis. *Journal of Investigative Dermatology*, 95(5), S56–S58. <https://doi.org/10.1111/1523-1747.ep12505791>
- Landén, N. X., Li, D., & Ståhle, M. (2016). Transition from inflammation to proliferation: a critical step during wound healing. *Cellular and Molecular Life Sciences: CMLS*, 73(20), 3861–3885. <https://doi.org/10.1007/s00018-016-2268-0>
- Lazic, T., & Falanga, V. (2011). Bioengineered skin constructs and their use in wound healing. *Plastic and Reconstructive Surgery*, 127 Suppl, 75S–90S. <https://doi.org/10.1097/PRS.0b013e3182009d9f>
- Lee, V., Singh, G., Trasatti, J., Bjornsson, C., Xu, X., Tran, T., Yoo, S., Dai, G., & Karande, P. (2014). Design and Fabrication of Human Skin by Three-Dimensional Bioprinting. *Tissue Engineering Part C: Methods*, 20(6), 473–484. <https://doi.org/10.1089/ten.tec.2013.0335>
- Lee, To, T., Nicholson, E., & Schrieber, L. (1994). Endothelial cell adhesion molecules in psoriasis. *The Australasian Journal of Dermatology*, 35(2), 65–70.
- Lim, C. P., Phan, T. T., Lim, I. J., & Cao, X. (2009). Cytokine profiling and Stat3 phosphorylation in epithelial-mesenchymal interactions between keloid keratinocytes and fibroblasts. *The Journal of Investigative Dermatology*, 129(4), 851–861. <https://doi.org/10.1038/jid.2008.337>
- Liu, N., Huang, S., Yao, B., Xie, J., Wu, X., & Fu, X. (2016). 3D bioprinting matrices with controlled pore structure and release function guide in vitro self-organization of sweat gland. *Scientific Reports*, 6, 34410.
- Lu, C., & Fuchs, E. (2014). Sweat Gland Progenitors in Development, Homeostasis, and Wound Repair. *Cold Spring Harbor Perspectives in Medicine*, 4(2), a015222. <https://doi.org/10.1101/cshperspect.a015222>
- Maas-Szabowski, N., Stärker, A., & Fusenig, N. E. (2003). Epidermal tissue regeneration and stromal interaction in HaCaT cells is initiated by TGF- α . *Journal of Cell Science*, 116(Pt 14), 2937–2948. <https://doi.org/10.1242/jcs.00474>
- MacNeil, S. (2008). Biomaterials for tissue engineering of skin. *Materials Today*, 11(5), 26–35. [https://doi.org/10.1016/S1369-7021\(08\)70087-7](https://doi.org/10.1016/S1369-7021(08)70087-7)
- Martin, P. (1997). Wound healing--aiming for perfect skin regeneration. *Science (New York, N.Y.)*, 276(5309), 75–81.
- Martin, P., & Leibovich, S. J. (2005). Inflammatory cells during wound repair: the good, the bad and the ugly. *Trends in Cell Biology*, 15(11), 599–607. <https://doi.org/https://doi.org/10.1016/j.tcb.2005.09.002>
- Mathes, S. H., Ruffner, H., & Graf-Hausner, U. (2014). The use of skin models in drug development. *Advanced Drug Delivery Reviews*, 69–70, 81–102. <https://doi.org/10.1016/j.addr.2013.12.006>
- Matoltsy, A. G., & Matoltsy, M. N. (1970). The chemical nature of keratohyalin granules of the epidermis. *The Journal of Cell Biology*, 47(3), 593–603.
- McGrath, J. A., Eady, R. A. J., & Pope, F. M. (2004). Anatomy and organization of human skin. *Rook's Textbook of Dermatology*, 3, 1–15.
- Mecklenburg, L., Tobin, D. J., Muller-Rover, S., Handjiski, B., Wendt, G., Peters, E. M., Pohl, S., Moll, I., & Paus, R. (2000). Active hair growth (anagen) is associated with angiogenesis. *The Journal of Investigative Dermatology*, 114(5), 909–916. <https://doi.org/10.1046/j.1523-1747.2000.00954.x>
- Meier, F., Nesbit, M., Hsu, M.-Y. Y., Martin, B., Van Belle, P., Elder, D. E., Schaumburg-Lever, G., Garbe, C., Walz, T. M., Donatien, P., Crombleholme, T. M., & Herlyn, M. (2000). Human

- melanoma progression in skin reconstructs: biological significance of bFGF. *The American Journal of Pathology*, 156(1), 193–200. [https://doi.org/10.1016/S0002-9440\(10\)64719-0](https://doi.org/10.1016/S0002-9440(10)64719-0)
- Meigel, W. N., Gay, S., & Weber, L. (1977). Dermal architecture and collagen type distribution. *Archives of Dermatological Research*, 259(1), 1–10.
- Miller, A. J., & Mihm, M. C. J. (2006). Melanoma. *The New England Journal of Medicine*, 355(1), 51–65. <https://doi.org/10.1056/NEJMra052166>
- Morrison, R. J., Hollister, S. J., Niedner, M. F., Mahani, M. G., Park, A. H., Mehta, D. K., Ohye, R. G., & Green, G. E. (2015). Mitigation of tracheobronchomalacia with 3D-printed personalized medical devices in pediatric patients. *Science Translational Medicine*, 7(285), 285ra64 LP-285ra64. <https://doi.org/10.1126/scitranslmed.3010825>
- Moulin, V. J., Mayrand, D., Laforce-Lavoie, A., Larochelle, S., & Genest, H. (2011). In Vitro Culture Methods of Skin Cells for Optimal Skin Reconstruction by Tissue Engineering. In D. Eberli (Ed.), *Regenerative Medicine and Tissue Engineering - Cells and Biomaterials*. InTech. <https://doi.org/10.5772/20341>
- Munoz-Abraham, A. S., Rodriguez-Davalos, M. I., Bertacco, A., Wengerter, B., Geibel, J. P., & Mulligan, D. C. (2016). 3D Printing of Organs for Transplantation: Where Are We and Where Are We Heading? *Current Transplantation Reports*, 3(1), 93–99. <https://doi.org/10.1007/s40472-016-0089-6>
- Murphy, S. V., & Atala, A. (2014). 3D bioprinting of tissues and organs. *Nature Biotechnology*, 32(8), 773–785. <https://doi.org/10.1038/nbt.2958>
- Mustoe, T. A., O'Shaughnessy, K., & Kloeters, O. (2006). Chronic wound pathogenesis and current treatment strategies: A unifying hypothesis. *Plastic and Reconstructive Surgery*. <https://doi.org/10.1097/01.prs.0000225431.63010.1b>
- Netzlaff, F., Lehr, C.-M., Wertz, P. W., & Schaefer, U. F. (2005). The human epidermis models EpiSkin®, SkinEthic® and EpiDerm®: An evaluation of morphology and their suitability for testing phototoxicity, irritancy, corrosivity, and substance transport. *European Journal of Pharmaceutics and Biopharmaceutics*, 60(2), 167–178. <https://doi.org/http://doi.org/10.1016/j.ejpb.2005.03.004>
- Niemann, C., & Horsley, V. (2012). Development and homeostasis of the sebaceous gland. *Seminars in Cell & Developmental Biology*, 23(8), 928–936. <https://doi.org/http://dx.doi.org/10.1016/j.semcdb.2012.08.010>
- Ozbolat, I. T., & Hospodiuk, M. (2016). Current advances and future perspectives in extrusion-based bioprinting. *Biomaterials*, 76, 321–343. <https://doi.org/https://doi.org/10.1016/j.biomaterials.2015.10.076>
- Ozbolat, I. T., & Yu, Y. (2013). Bioprinting toward organ fabrication: Challenges and future trends. *IEEE Transactions on Biomedical Engineering*, 60(3), 691–699. <https://doi.org/10.1109/TBME.2013.2243912>
- Panteleyev, A. A., Jahoda, C. A., & Christiano, A. M. (2001). Hair follicle predetermination. *Journal of Cell Science*, 114(Pt 19), 3419–3431.
- Pasparakis, M., Haase, I., & Nestle, F. O. (2014). Mechanisms regulating skin immunity and inflammation. *Nature Reviews. Immunology*, 14(5), 289–301. <https://doi.org/10.1038/nri3646>
- Perkins, M. A., Osborne, R., Rana, F. R., Ghassemi, A., & Robinson, M. K. (1999). Comparison of in vitro and in vivo human skin responses to consumer products and ingredients with a range of irritancy potential. *Toxicological Sciences*, 48(2), 218–229. Retrieved from <http://dx.doi.org/10.1093/toxsci/48.2.218>
- Phillips, T. J., Manzoor, J., Rojas, A., Isaacs, C., Carson, P., Sabolinski, M., Young, J., & Falanga, V. (2002). The longevity of a bilayered skin substitute after application to venous ulcers. *Archives of*

Dermatology, 138(8), 1079–1081. <https://doi.org/10.1001/archderm.138.8.1079>

- Rheinwald, J. G., & Green, H. (1977). Epidermal growth factor and the multiplication of cultured human epidermal keratinocytes. *Nature*, 265(5593), 421–424.
- Robson, M. C., Steed, D. L., & Franz, M. G. (2001). Wound healing: biologic features and approaches to maximize healing trajectories. *Current Problems in Surgery*, 38(2), 72–140. <https://doi.org/10.1067/msg.2001.111167>
- Salmon, J. K., Armstrong, C. A., & Ansel, J. C. (1994). The skin as an immune organ. *The Western Journal of Medicine*, 160(2), 146–152. Retrieved from <https://www.ncbi.nlm.nih.gov/pubmed/8160465>
- Schiele, N. R., Corr, D. T., Huang, Y., Raof, N. A., Xie, Y., & Chrisey, D. B. (2010). Laser-based direct-write techniques for cell printing. *Biofabrication*, 2(3), 32001. <https://doi.org/10.1088/1758-5082/2/3/032001>
- Schmidt-Ullrich, R., & Paus, R. (2005). Molecular principles of hair follicle induction and morphogenesis. *BioEssays*, 27(3), 247–261. <https://doi.org/10.1002/bies.20184>
- Sebastiano, V., Zhen, H. H., Derafshi, B. H., Bashkirova, E., Melo, S. P., Wang, P., Leung, T. L., Siprashvili, Z., Tichy, A., Li, J., Ameen, M., Hawkins, J., Lee, S., ... Oro, A. E. (2014). Human COL7A1-corrected induced pluripotent stem cells for the treatment of recessive dystrophic epidermolysis bullosa. *Science Translational Medicine*, 6(264), 264ra163 LP-264ra163. <https://doi.org/10.1126/scitranslmed.3009540>
- Sheu, H.-M., Chao, S.-C., Wong, T.-W., Lee, Y.-Y., & Tsai, J.-C. (1999). Human skin surface lipid film: an ultrastructural study and interaction with corneocytes and intercellular lipid lamellae of the stratum corneum. *British Journal of Dermatology*, 140(3), 385–391. <https://doi.org/10.1046/j.1365-2133.1999.02697.x>
- Singer, A. J., & Clark, R. A. F. (1999). Cutaneous Wound Healing. *New England Journal of Medicine*, 341(10), 738–746. <https://doi.org/10.1056/NEJM199909023411006>
- Sorrell, J. M., & Caplan, A. I. (2004). Fibroblast heterogeneity: more than skin deep. *Journal of Cell Science*, 117(Pt 5), 667–675. <https://doi.org/10.1242/jcs.01005>
- Sun, B. K., Siprashvili, Z., & Khavari, P. A. (2014). Advances in skin grafting and treatment of cutaneous wounds. *Science*, 346(6212), 941–945. <https://doi.org/10.1126/science.1253836>
- Swartz, M. A., & Lund, A. W. (2012). Lymphatic and interstitial flow in the tumour microenvironment: linking mechanobiology with immunity. *Nature Reviews Cancer*, 12(3), 210.
- Thiersch, C. (1869). Ueber die Entstehungsweise und operative Behandlung der Epispadie. *Arch Heilkunde*, 10, 20.
- Tremblay, P. L., Hudon, V., Berthod, F., Germain, L., & Auger, F. A. (2005). Inosculation of tissue-engineered capillaries with the host's vasculature in a reconstructed skin transplanted on mice. *American Journal of Transplantation*, 5(5), 1002–1010. <https://doi.org/10.1111/j.1600-6143.2005.00790.x>
- Tsur, H., Daniller, A., & Strauch, B. (1980). Neovascularization of Skin Flaps: Route and Timing. *Plastic and Reconstructive Surgery*, 66(1), 85–90.
- Uchi, H., Terao, H., Koga, T., & Furue, M. (2000). Cytokines and chemokines in the epidermis. *Journal of Dermatological Science*, 24(SUPPL. 1), 29–38. [https://doi.org/10.1016/S0923-1811\(00\)00138-9](https://doi.org/10.1016/S0923-1811(00)00138-9)
- van den Bogaard, E. H., Rodijk-Olthuis, D., Jansen, P. A. M., van Vlijmen-Willems, I. M. J. J., van Erp, P. E., Joosten, I., Zeeuwen, P. L. J. M., & Schalkwijk, J. (2012). Rho Kinase Inhibitor Y-27632 Prolongs the Life Span of Adult Human Keratinocytes, Enhances Skin Equivalent Development,

- and Facilitates Lentiviral Transduction. *Tissue Engineering. Part A*, 18(17–18), 1827–1836. <https://doi.org/10.1089/ten.tea.2011.0616>
- Velasquillo, C., Galue, E. A., Rodriguez, L., Ibarra, C., & Ibarra-Ibarra, L. G. (2013). Skin 3D Bioprinting. Applications in Cosmetology. *Journal of Cosmetics, Dermatological Sciences and Applications*, 3(1A), 85–89. <https://doi.org/10.4236/jcdsa.2013.31A012>
- Vijayavenkataraman, S., Lu, W. F., & Fuh, J. Y. H. (2016). 3D bioprinting of skin: a state-of-the-art review on modelling, materials, and processes. *Biofabrication*, 8(3), 32001. <https://doi.org/10.1088/1758-5090/8/3/032001>
- Wong, R., Geyer, S., Weninger, W., Guimberteau, J.-C., & Wong, J. K. (2016). The dynamic anatomy and patterning of skin. *Experimental Dermatology*, 25(2), 92–98. <https://doi.org/doi:10.1111/exd.12832>
- Yannas, I. V, & Burke, J. F. (1980). Design of an artificial skin. I. Basic design principles. *Journal of Biomedical Materials Research*, 14(1), 65–81. <https://doi.org/10.1002/jbm.820140108>
- Yano, K., Brown, L. F., & Detmar, M. (2001). Control of hair growth and follicle size by VEGF-mediated angiogenesis. *Journal of Clinical Investigation*, 107(4), 409–417.

CHAPTER II: 3D bioprinting of non-vascularized human skin

II.1 Introduction

Skin is one of the most investigated tissues for *in vitro* reconstruction, possibly, due to the relatively simple, hierarchical and layer-by-layer structure formed by the dermal compartment (papillary and reticular dermis) and the multiple epidermal layers (*stratum basale*, *spinosum*, *granulosum* and *stratum corneum*) that can be reproduced *in vitro* with relative ease (Eckert & Rorke, 1989; Harper & Grove, 1979; Moulin, Mayrand, Laforce-Lavoie, Larochelle, & Genest, 2011; Reijnders et al., 2015; Zhang & Michniak-Kohn, 2012). The reconstructed skin models typically contain fibroblasts embedded in a collagenous matrix to simulate the dermis and augmented with a layer of keratinocytes atop the dermis to simulate the epidermis. When exposed to optimal and biologically-/physiologically-relevant conditions, this assembly can differentiate and mature to form a stratified multi-layered structure that resembles human skin. Nonetheless, this uniform and quite predictable structure recreated *in vitro* does not recapitulate the complexity of the skin. *In vivo*, skin presents a diverse population of cells, and a complex and heterogenous distribution of proteins and growth factors that cannot be adequately represented in the simplified models fabricated in the laboratory (Panteleyev, Jahoda, & Christiano, 2001). Furthermore, many of these cells are organized and compartmentalized in distinct structures within the skin, such as vasculature, and adnexal structures (for e.g., hair follicles, sweat glands, and sebaceous glands), which confers an even higher level of complexity to this organ.

In the last four decades, a variety of acellular and cellular matrices have been developed to promote skin wound healing, such as Alloderm™, Biobrane™, Dermagraft™ and Apligraf™ (please see reviews by Lazic and Falanga 2011 and Brohem et al. 2011 for further details). However, these do not integrate with the host skin. Instead, these artificial grafts act as pharmacological agents that stimulate wound healing by inducing re-epithelization from the wound edges, a process known as the edge effect (Kirsner, Falanga, Kerdel, Katz, & Eaglstein, 1996). Moreover, cultured allografts work to provide immediate wound coverage from injuries and infections; release of healing growth factors (for e.g., TGF- α and β , GM-CSF, β FGF, PDGF, TNF- α) and cytokines (for e.g., IL-1, 3, 6, and 8) (Lim, Phan, Lim, & Cao, 2009; Maas-Szabowski, Stärker, & Fusenig, 2003; Uchi, Terao, Koga, & Furue, 2000); and biosynthesis of new matrix components (Boehnke et al., 2007). Phillips *et al.* have shown that allogeneic cells were rarely detected in patients with venous ulcers treated with Apligraf™ at 2 months after grafting (Phillips et al., 2002). In agreement with this observation, Griffiths *et al.* demonstrated that Apligraf™ does not persist beyond 4 weeks in the host skin (Griffiths, Ojeh, Livingstone, Price, & Navsaria, 2004). The relatively short clinical persistence of Apligraf™ and other cultured allografts can be a disadvantage, particularly in the treatment of

chronic wounds which require more than 4 weeks to heal. Since these grafts do not integrate with the host skin and are only temporary, patients often need multiple rounds of treatment until re-epithelization is achieved. This makes the use of cultured allografts expensive, burdensome, time-consuming, and with sub-optimal clinical outcomes.

The complexity of skin three-dimensional structures that are present in human skin are difficult to replicate *in vitro* through simple manual fabrication methods. 3D bioprinting is a flexible tool that allows precise deposition and patterning of different cell populations and biomaterials to create accurate geometries in three dimensions that mimic anatomical and biological structures such as tissues and organs (Knowlton, Yenilmez, & Tasoglu, 2016; Munoz-Abraham et al., 2016; Murphy & Atala, 2014).

The main aim of this chapter is to establish a 3D printing protocol for robust, consistent and scalable production of skin grafts composed entirely of human primary cells. Different printing parameters and culture conditions will be tested to generate a 3D bioprinted graft morphologically and functionally similar to native skin. The successful generation of a non-vascularized skin graft will serve as the first step for further optimization studies such as the inclusion of endothelial cells to produce a 3D printed full-thickness vascularized human skin graft, reported in more detail in chapter IV.

II.2 Materials and Methods

II.2.1. 3D bioprinter

The overall schematic of the printing platform is shown in Figure II.2.1. The printer consists of an array of eight microvalves as dispensers, a three-axis robotic stage and an optional temperature control unit. The microvalve dispensers, each with a pneumatically driven control mechanism, were mounted to the horizontal (x–y) robotic stage (Newmark Systems). The target substrate was mounted to another robotic stage that moved along the z-axis. To maintain sterility, the printer was placed in a laminar flow hood and syringes were replaced in each printing experiment.

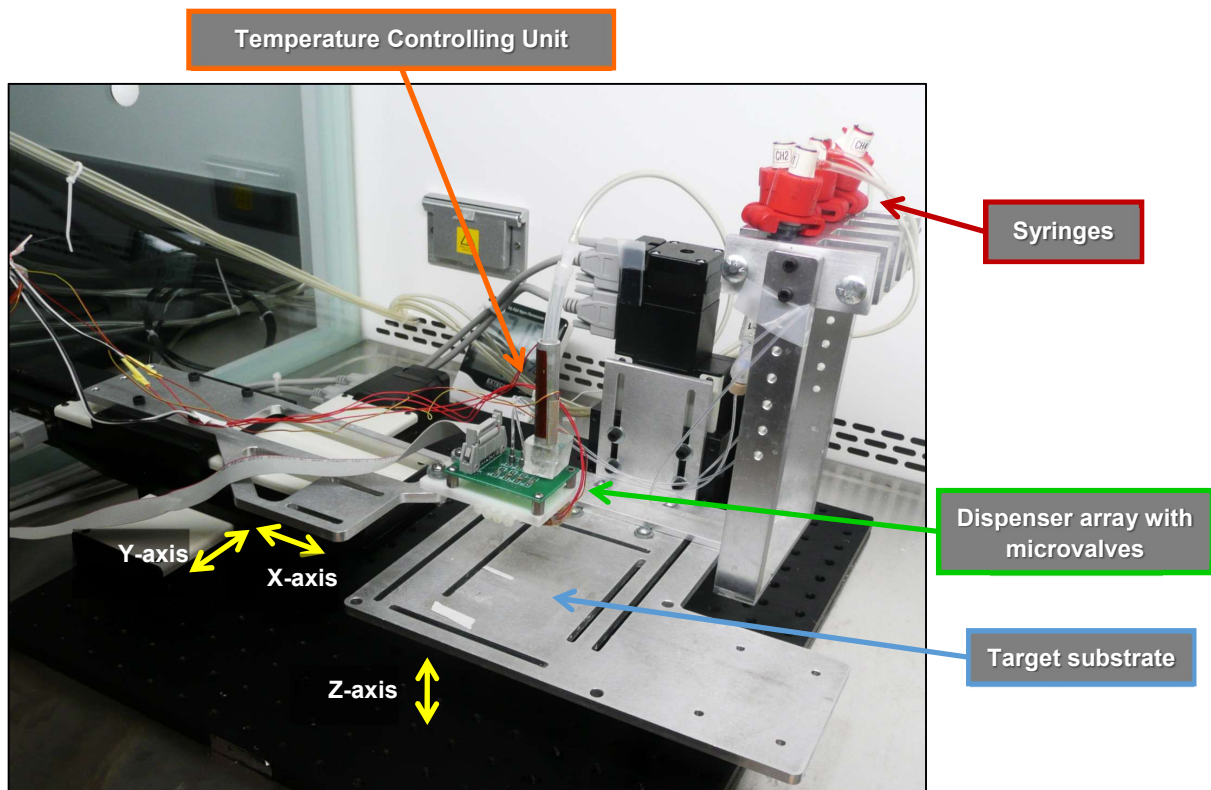


Figure II.2.1 - Modular tissue printing platform. The photograph shows 4 syringes as ‘cartridges’ to load cell suspensions and bioinks; horizontal stage with an array of 8-channel dispensers; vertical stage/target substrate and an optional heating unit.

The general operating principle of the dispensing mechanism is as follows. Cell suspensions in culture media or dermal and epidermal bioinks were placed in 10 mL disposable syringes. Each syringe was pressurized using an air tank and independently controlled by a digital pressure regulator (DPGA-05; Dwyer, USA). The formation of droplets, under pneumatic

pressure, was gated by a set of electromagnetic microvalves (SMLD; Fritz Gyger AG, 150 μm nozzle diameters). When there is no current, the valve ball in the microvalve blocks the exit of fluids through the nozzle. When there is a current feed through the valve coil, the mobile anchor attached to the valve ball is pulled by the magnetic field of the stationary anchor ball, opening the microvalve nozzle, allowing for a droplet to form (Figure II.2.2).

A user-friendly MATLAB computing interface (Mathworks) was used to generate the printing pattern and dispensing spatial coordinates. The 3D pattern was generated by combining 2D slice profiles, in which each slice was defined by its resolution (the distance between each dispensing points), size, pattern, coordinates and dispensing microvalve channel. The generated control codes were sequentially executed by scripts generated by Active-X Toolkit (Galil Motion Control, Inc.) programmed in Visual Basic (Microsoft).

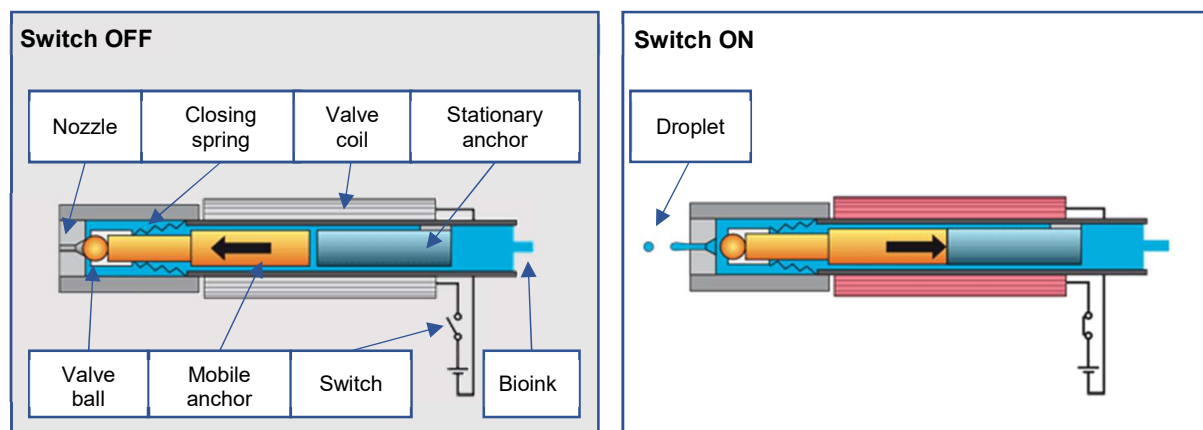


Figure II.2.2 - Microvalve components and operating modes. Adapted from www.fgyger.ch

II.2.2. Cell isolation

Human dermal fibroblasts and keratinocytes were obtained from donated foreskin samples from the University of Pennsylvania (UPenn). Foreskin samples were received in saline solution and washed with phosphate buffered saline (PBS) containing antibiotics (Pen/Strep - Gibco). Samples were cleaned and fragmented prior to digestion with 4 mg/mL dispase II (Roche) overnight at 4°C. The epidermis was carefully peeled off from the dermis using precision stainless steel tweezers (Cole-Parmer). The dermis was subsequently incubated with 1 mg/mL Collagenase (Gibco) for 6 hours at room temperature to induce detachment of the fibroblasts from the collagen matrix. The epidermis was incubated with 0.05% trypsin for 15 minutes at 37°C to promote cell dissociation. Fibroblasts obtained from dermis, and keratinocytes obtained from epidermis were centrifuged at 1500 g for 3 minutes and plated with specific culture media as described below.

II.2.3. Cell culture

Keratinocytes were cultured in KGM Gold medium (Lonza), fibroblasts were cultured in Dulbecco's Modified Eagle Medium (DMEM; Gibco) supplemented with 10% fetal bovine serum (Atlanta Biologics) and 1% Pen/Strep (Gibco), and human umbilical vein endothelial cells (HUVEC) were cultured in EGM2 medium (Lonza). Fibroblasts, keratinocytes and endothelial cells were maintained in a humidified incubator at 37°C containing 5% CO₂. At approximately 80% confluency, cells were routinely passaged by treatment with 0.1% trypsin-EDTA.

II.2.4. Dermal and epidermal bioinks

Nebulization method. The composition of the dermal and epidermal bioinks were based on a protocol previously described by Lee *et al.* (Lee et al., 2014). Briefly, to print the dermal compartment two inks were prepared: (1) collagen type I precursor (Rat tail, type I; BD Biosciences) at 3mg/mL and (2) human dermal fibroblasts resuspended in DMEM supplemented with 10% Fetal Bovine Serum and 1% Penicillin/Streptomycin. To prepare the epidermal bioink, human keratinocytes were resuspended in KGM Gold medium.

Pre-mixing method. The composition of the dermal and epidermal bioinks were based on a protocol previously described by Brohem *et al.* (Brohem et al., 2011). The dermal bioink was generated by resuspension of human dermal fibroblasts in a collagen mixture consisting of 750 µL/mL of 2.5 mg/mL of type I collagen (Corning), 50 µL/mL of FBS (Atlanta Biologics), 100 µL/mL of Reconstitution Buffer 10X (0.05 M NaOH, 2.2% NaHCO₃, and 200 mM HEPES), and 100 µL/mL of HAM-F12 medium 10X(Gibco). To avoid gelation before printing, the dermal bioink was kept on ice. The epidermal bioink was generated by resuspension of human keratinocytes in a 1:1 ratio culture medium composed of KGM medium and ***skin differentiation medium***: DMEM/HAM's F-12 (3:1) supplemented with 10% FBS, 0.1 nM cholera toxin (Sigma), 5 µg/ml insulin (Sigma), 5 µg/ml apo-transferrin (Sigma), 0.4 µg/ml hydrocortisone-21 (Sigma) and 0.5 ng/ml epidermal growth factor (Peprotech).

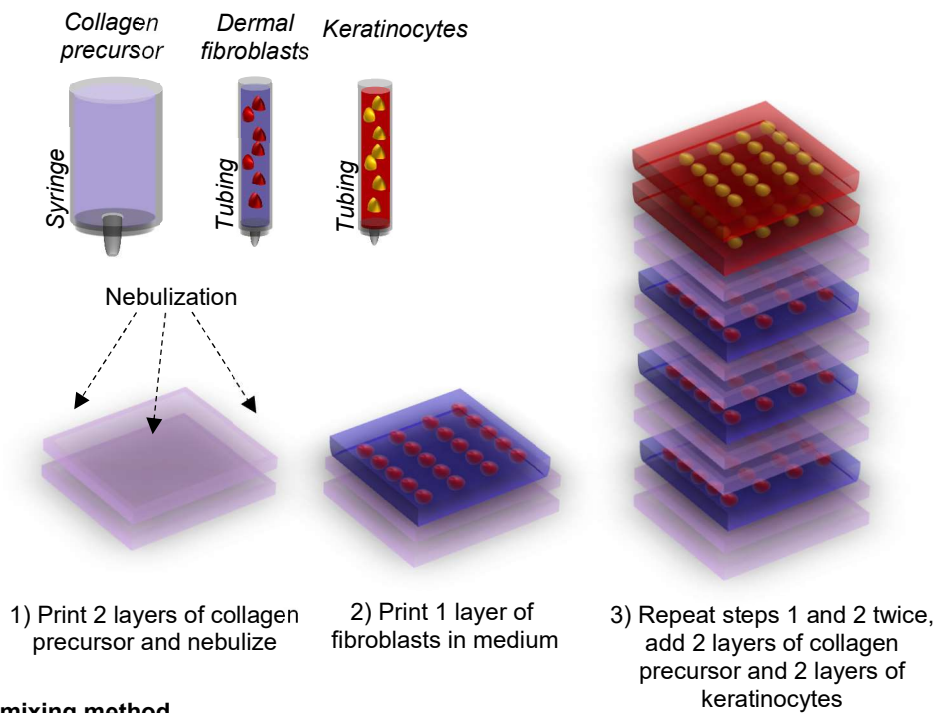
II.2.5. 3D bioprinting of dermal and epidermal compartments

Nebulization method. The printed skin construct was generated by printing six collagen layers (300 µm, 2.5 psi) alternating with three layers of fibroblasts (300 µm, 2.5 psi) and two collagen layers separating the stacked dermal layers from keratinocytes as shown in Figure II.2.3A. Two layers of keratinocytes (300 µm, 2.5 psi) were printed to achieve the desired cell density

within the epidermis. Upon completion of the printing steps, the composite structure was placed in an incubator for 1 hour to complete gelation of collagen. The whole tissue structure was then submerged in culture media. To avoid cell settling and aggregation in the printer's syringe and tubing during the printing process, volumes of 100 μ L of resuspended fibroblasts and keratinocytes, in the respective media, were repeatedly pipetted directly into the tubing connecting the microvalve dispenser to the syringe.

Pre-mixing method. The printed skin construct was generated by printing 17 layers (300 μ m, 2.5 psi) of cold dermal bioink on top of a Transwell insert PET membrane (Figure II.2.3B). Upon complete gelation of dermal layers at 37°C, 2, 3 or 5 layers of epidermal bioink (300 μ m, 2.5 psi) were printed on top of the 3D construct.

A. Nebulization method



B. Pre-mixing method

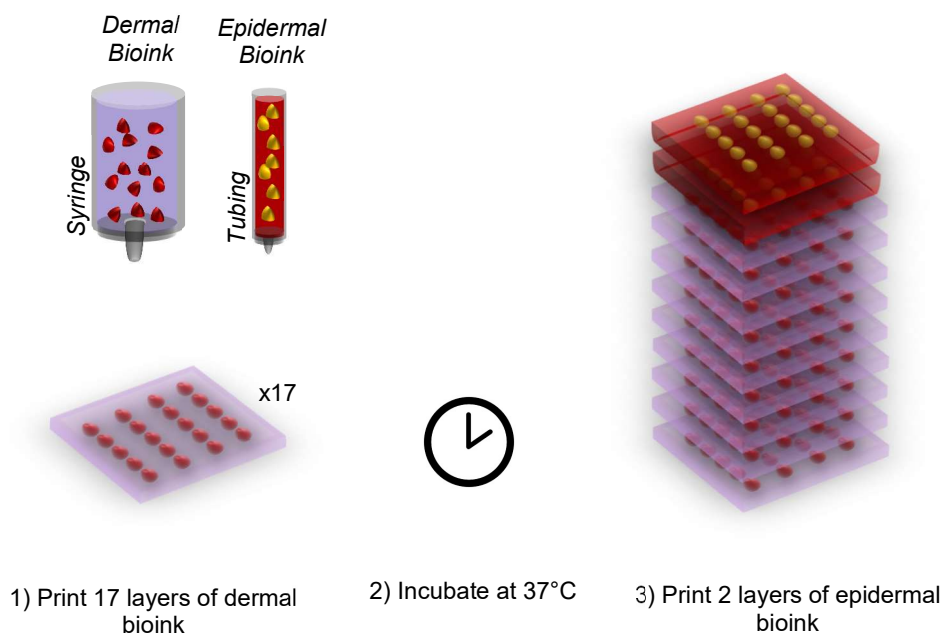


Figure II.2.3 – Layer-by-layer printing of human skin equivalents. Two modes of dermal compartment printing were tested based on two methods for collagen crosslinking: (A) **nebulization** of printed collagen precursor layers or (B) **pre-mixing** of collagen precursor with dermal fibroblasts, reconstitution buffer 10x and HAM-F12 medium before printing.

II.2.6. Bioprinted skin maturation

After printing, 1 mL of epidermal bioink without keratinocytes was added to the bottom compartment of the 12-well Transwell insert. Twenty-four hours after incubation at 37°C, the medium on top and bottom of the Transwell insert was removed and changed to 100% skin differentiation medium. After 4 days under medium submersion, the Transwell insert containing the skin equivalent was carefully transferred to air-liquid interface on top of a 100 µm pore cell strainer placed in a Falcon® 6-well Deep Well Plate (Corning). The medium on top of the skin construct was removed and 9 mL of skin differentiation medium were slowly added to the bottom of the cell strainer, making sure that no bubbles were trapped under the Transwell insert. The medium below the cell strainer was replaced every 3 days for two weeks.

II.2.7. Viability analysis

Before cell printing or manual deposition was initiated, a 10 x 10 mm collagen layer was printed on a 35 mm culture dish and subsequently nebulized with sodium bicarbonate (NaHCO₃) vapor. Cell suspensions of 3x10⁶ cells/mL in medium were inserted in the printer syringe or manually pipetted on top of the collagen layer. Cell viability was measured 4 hours, 1, 3 and 5 days after deposition using a Live/Dead assay kit (ThermoFisher Scientific), according to the manufacturer's instructions. Briefly, a solution of 10 mL of DPBS containing 5µL of calcein AM and 2 µL of propidium iodide was prepared and added directly to the cells. The culture dishes were incubated for 30 minutes at room temperature. Each sample was imaged at 4 different fields of view under an inverted fluorescence microscope and the images were loaded into Fiji (ImageJ) software for automatic cell counting. Green and red fluorescent images, representing live and dead cells, respectively, were extracted from the original image and processed separately with "*find maxima*" algorithm. The "*find maxima*" detection algorithm detects the local maximum intensity values in each image outputting the number of single points per maximum, and thus, the total number of cells per field of view (Figure II.2.4). The percentage of live cells was determined by calculating the ratio of calcein-positive cells to the total number of cells (the sum of calcein-positive live cells and propidium iodide-positive dead cells).

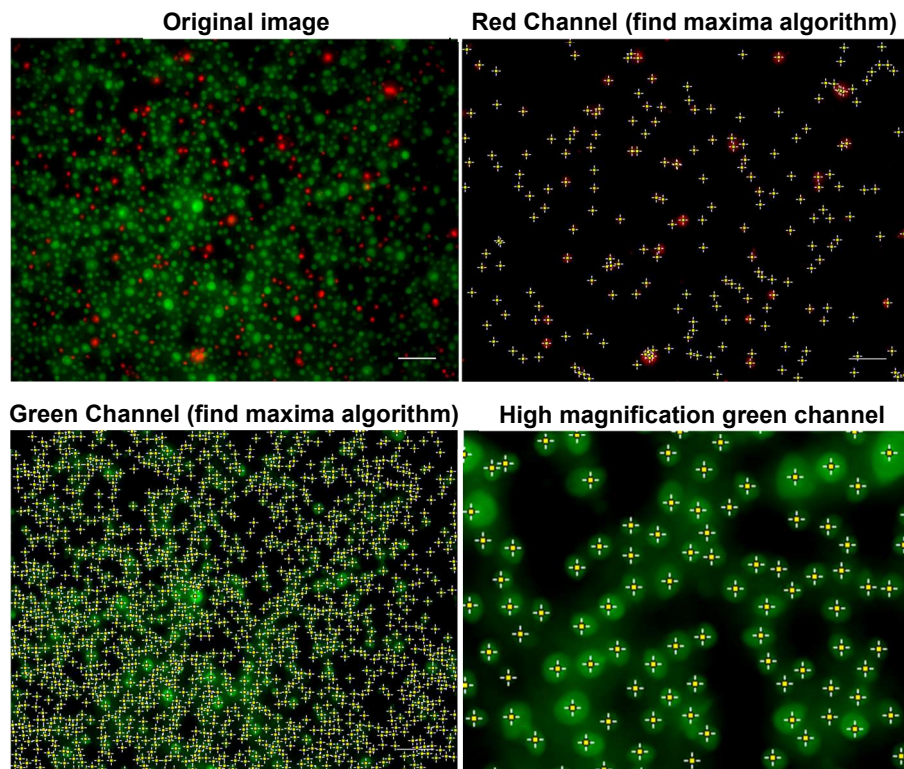


Figure II.2.4 - Representative images of LIVE/Dead staining of printed human keratinocytes at day 1. Green and red channel images were processed with “find maxima algorithm” in Fiji software. Measured maximum intensity points in the field of view are represented in yellow. Scale bar: 100 μm .

II.2.8. 3D projection of skin constructs

Twenty-four hours before printing, at ~70% confluency, human dermal fibroblasts and keratinocytes were fluorescently labeled with CellTracker™ Red CMPTX and CellTracker™ Green CMFDA dyes (ThermoFisher Scientific), respectively, according to the manufacturer’s instructions. Three days after printing, the constructs were imaged on Nikon Eclipse Ti-E inverted fluorescence microscope (Nikon Instruments, USA) with a motorized stage and multiple Z-stack images were taken to evaluate fibroblasts and keratinocyte spatial distribution in the 3D printed constructs. The Z-stack images were processed in NIS-Elements software (Nikon Instruments) to generate 3D projections of each sample.

II.2.9. Histological and immunofluorescence analysis of skin constructs

Skin samples were placed in an aluminum foil mold (10mm x 20mm x 15mm) containing Optimum Cutting Temperature compound (O.C.T., Tissue-Tek®). The molds were placed on a bath of dry-ice and 100% ethanol until snap-frozen and kept at -80°C until sectioning. O.C.T. blocks were cut into 10 µm sections in a cryostat chamber set to -25°C, collected in Superfrost Plus charges slides and stored at -20°C until use.

Epidermal differentiation was evaluated with Hematoxylin & Eosin staining. Hematoxylin dye (Millipore®) was added for 7 min followed by rinsing with running tap water for 1 min. Then eosin dye (Millipore®) was added for 2 min followed by washing with water and dehydration through ethanol graded series. The slides were then immersed in xylene (Sigma) for 10 minutes and mounted with Distyrene Plasticizer Xylene (DPX; Sigma) mounting medium. All histological images were captured on Olympus IX-71 microscope with a couple-charge device (CCD) camera (Olympus, USA).

For immunofluorescence analysis, tissue sections were immersed in cold acetone for 10 minutes and blocked for 1 hour with 10% Normal Goat Serum in PBS. Slides were then incubated overnight at 4°C, in humid chamber, with primary monoclonal antibodies anti-cytokeratin 10 (rabbit, 1:200, clone EP1607IHCY; Abcam), anti-cytokeratin 14 (mouse, 1:200, clone LL002; Abcam), anti-filaggrin (mouse, 1:200, clone FLG/1561, Abcam) and anti-collagen IV (mouse; 1:200, clone COL-94; Abcam). Next day, the slides were washed three times with PBS and incubated for 1 hour at room temperature with anti-mouse or anti-rabbit IgG H&L secondary antibodies Alexa Fluor™ 488 or Alexa Fluor™ 568 (goat, 1:500; Abcam). Slides were mounted with VECTASHIELD antifade mounting medium containing DAPI (Vector Labs) for nuclear staining and imaged on Nikon Eclipse Ti-E inverted fluorescence microscope (Nikon Instruments, USA).

All images were analyzed by Fiji (ImageJ) software. Measurements of suprabasal and basal layers thickness were carried out using 10 images from each experimental condition and, for each image, 5 thickness measurements were performed. The mean values obtained for each of the 10 images were used to perform statistical analysis in Prism 7 software (GraphPad, USA).

II.2.10. Barrier Function

To evaluate and compare the barrier function of our 3D printed skin model to human skin, other mammalian skin models and *in vitro* skin equivalents reported in the literature, we used two fluorescein-dextran molecules of different molecular weight sizes, 10 kDa (FD-10) and 20 kDa (FD-20). To measure barrier function we used a simple assay that measures permeability in a Transwell insert (Hsu et al., 2018). Since maturation of the 3D printed skin equivalent occurs at air-liquid interface in a Transwell insert, this assay does not require transfer of 3D bioprinted skin samples to a measuring apparatus. This offers the advantage of avoiding any possible damage to the sample during the transferring procedure. The penetrants, FD-10 and FD-20 were applied directly to the top of the skin and 10 μ L samples were collected from the bottom compartment of the Transwell insert at different time points. The fluorescence signal intensity was measured with a Synergy HT plate-reader (Ex: 485/20 nm, Em: 528/20 nm; BioTek, USA) and converted to mass of permeated drug ($y=352.6x+158$, $r^2=0.99$). The area of the 3D printed skin sample was 1cm² and the initial concentration of the penetrants was 1mg/mL in 1X Phosphate-Buffered Saline.

II.2.11. Determination of steady state flux and permeability coefficient

The passive diffusion of a drug through skin can be described by Fick's first law. It describes the time course of the transfer of a penetrant between two compartments and is given by the following equation:

$$J = -D \frac{dc}{dx}$$

Equation II.2.1- Fick's first law

where, J is the flux, D the diffusion coefficient of the penetrant and dc/dc is the concentration gradient. The flux of a drug can be approximated as the slope of the linear part in the plot of the cumulative amount permeated per area as a function of time. The lag-time, which is the time from when the penetrant is applied to the skin surface until it can be detected on the other side of the skin, is the time intercept of the linear portion of the graph. The apparent permeability coefficient (K_p) can be calculated as the ratio of the flux and the initial concentration of the drug. This parameter is particularly important when comparing different drugs if different initial concentrations are used between studies. The correct estimation of these parameters assumes that: (i) the full thickness of the stratum corneum contributes to

the diffusion barrier; (ii) no active transport occurs; (iii) the stratum corneum is a homogeneous medium; (iv) there is no carrier effect of the vehicle molecules; (v) there are no size-limiting pores in the system; (vi) the stratum corneum is not changed overtime by the penetrant or vehicle properties; and (vii) penetrant concentration changes do not alter the stratum corneum. Moreover, accurate estimation of flux and permeability coefficient requires a duration equal to at least three lag times to achieve a linear concentration gradient and a uniform steady state flux across the skin (Shah, 1993).

In order to calculate the flux of FD-10 in the bioprinted constructs, we have considered the period between 0.15 and 2.0 h as the linear range of the permeation profile ($r^2=0.97$). For FD-20 flux estimation, we have considered the period between 1.25 and 3.25 hours as the linear range ($r^2=0.99$). Notice that estimation of J and K_p of FD-20 may be in error since three lag times (3.75 hours) is smaller than the linear range period (2 hours).

II.2.12. Statistical analysis

Statistical analyses were performed using Prism 7 software (GraphPad, USA). Data are expressed as mean standard deviation. When the means of 2 variables of more than 2 groups were compared, a two-way ANOVA analysis was performed. Results were considered significant when the P-value (P) < 0.05: * = $P < 0.05$, ** = $P < 0.01$, *** = $P < 0.001$, **** = $P < 0.0001$, ns = non-significant.

II.3 Results

II.3.1. Resolution and Pressure

Before 3D multi-layered printing, the dispensing pressure and droplet size were optimized in order to achieve homogeneous cell distribution within each printed layer. Since fast gelation of small droplets can promote cell encapsulation and clustering, we aimed at finding printing conditions to dispense a continuous stream of droplets without significantly affecting cell spatial resolution. Droplets of collagen type I at a concentration of 3 mg/mL were printed at 2.5, 5.5 and 7 psi, and spacing of 800 and 300 μm between droplets (Figure II.3.1). An opening valve time of 750 μs was kept constant between conditions. Low printing resolution (800 μm) failed to produce a continuous stream of droplets, producing gaps between droplets. With decreasing pressure values, smaller droplets volumes were dispensed, causing collagen gelation and evaporation of each droplet to happen within seconds. On the contrary, higher printing resolutions (300 μm) generated a continuous stream of droplets, while increasing pressures generated bigger droplets and wider streams. In addition, the rate of collagen gelation was visibly decreased above 2.5 psi, causing the array of deposited droplets to quickly flatten on the printing surface. As slow gelation rates can promote gravity-settling of printed cells inside each droplet, the loss of three-dimensional resolution was a concern. In order to preserve homogenous 3D cell distribution within each printed layer, we chose 2.5 psi and 300 μm spacing between droplets as good printing parameters to generate a 3D multi-layered human skin construct.

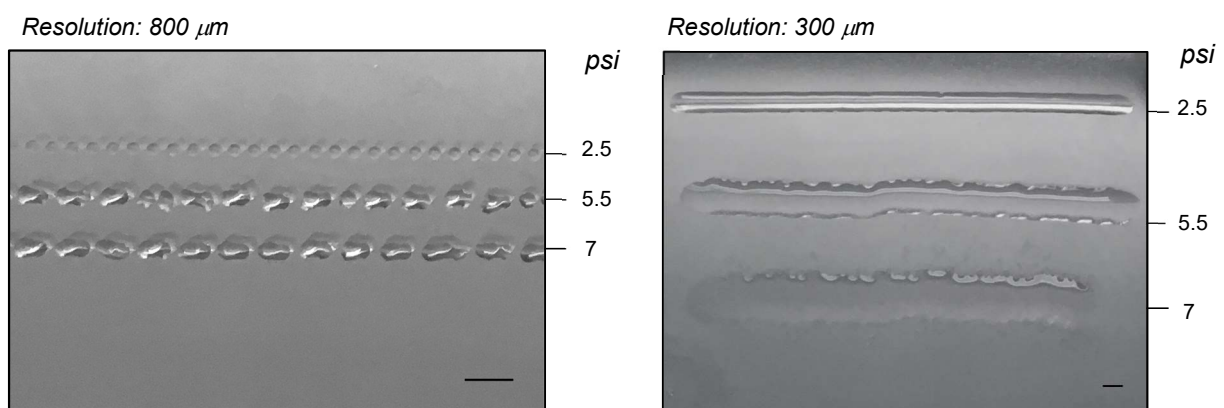
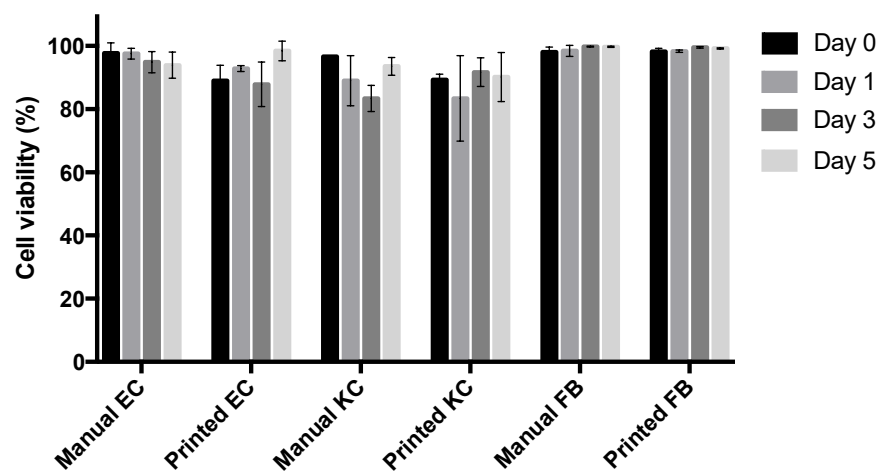


Figure II.3.1 - Droplet-based bioprinting. Bright field images of collagen type I droplets printed at 2.5, 5.5 and 7 psi at resolution of 800 and 300 μm . Scale bar: 1 mm.

II.3.2. Cell viability

To assess the effect of the above printing parameters on primary cells, the viability of printed human keratinocytes, umbilical vein endothelial cells and dermal fibroblasts were compared to the viability of manually deposited cells (Figure II.3.2). Four hours after manual deposition, the cell viability of human keratinocytes, endothelial cells and fibroblasts was $96.7 \pm 0.2\%$, $97.8 \pm 3.2\%$, $98.1 \pm 1.5\%$, respectively. A reduction, but weakly significant, in cell viability was observed on printed human keratinocytes ($89.3 \pm 1.7\%$, $p=0.13$) and printed endothelial cells ($88.9 \pm 4.9\%$, $p=0.11$). At day 1, the viability of manually deposited and printed human

A



B

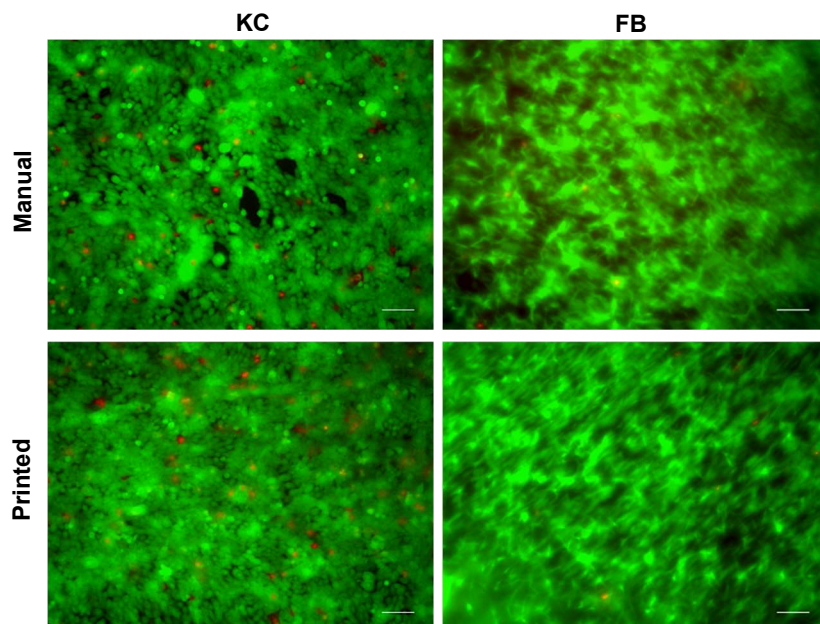


Figure II.3.2 - Cell viability of manually deposited and printed cells. **(A)** Cell viability was analyzed by LIVE/DEAD staining assay up to 5 days. Live and dead cell counts were determined in 4 randomly chosen fields of view. **(B)** Representative images of LIVE/DEAD (green/ red) staining of manually deposited and printed keratinocytes and fibroblasts at day 5. Scale bar: 100 μm .

keratinocytes decreased to $89.0 \pm 7.9\%$ ($p=0.058$) and $83.4 \pm 13.5\%$ ($p=0.0002$), respectively. After 5 days in culture, all manually deposited and printed cell types retained $>90\%$ viability.

II.3.3. 3D Bioprinting of the Dermal Compartment

Lee *et al.* have reported the generation of the first 3D bioprinted human skin equivalent composed of human fibroblasts and HaCaT cells in a collagen type I gel (Lee et al., 2014). In their model, 8 layers of collagen precursor were sequentially deposited. Between each layer of collagen and fibroblasts, nebulized NaHCO_3 was applied as a crosslinking agent. We tested this collagen gelation method and varied the nebulization time from 5 to 10 seconds. Visualization of the 3D data showed that when collagen layers were nebulized for 5 seconds, dermal fibroblasts deposited at the bottom of the Transwell insert, while nebulization for 10 seconds produced a striated pattern with visible separation between the layers of fibroblasts (Figure II.3.3A).

In agreement with these observations, histological analysis of the printed constructs at day 20 showed aggregation of dermal fibroblasts near the Transwell insert membrane when collagen layers were nebulized for 5 seconds, while nebulization for 10 seconds led to spatial separation of the collagen and fibroblasts layers. Interestingly, both conditions showed none or poor epidermal differentiation (Figure II.3.3B). Since our goal was to obtain homogeneous distribution of fibroblasts within the dermis by 3D printing, we tested a second method for collagen cross-linking by mixing dermal fibroblasts with a pH reconstitution buffer before printing, with subsequent incubation at 37°C . This gelation method not only showed significant improvement on the distribution of fibroblasts within the dermis, but also revealed the presence of an epidermal compartment by H&E staining.

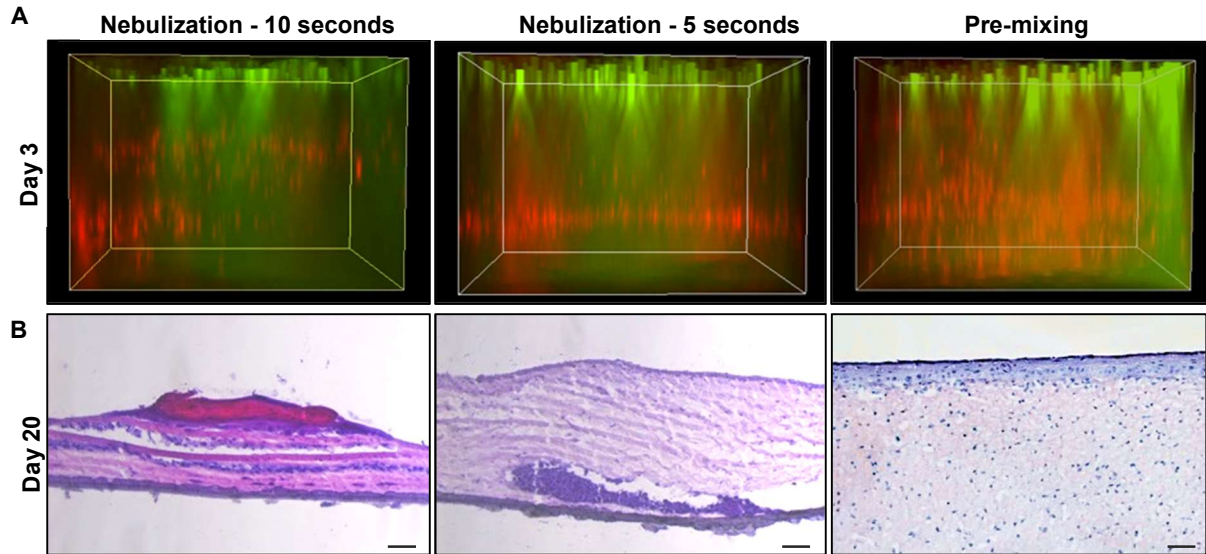


Figure II.3.3 – Evaluation of collagen cross-linking method on dermal fibroblasts distribution and epidermal differentiation in 3D printed constructs. **(A)** Images are shown as maximum projections of z-stacks epifluorescence images of printed constructs at day 3. Fibroblasts and keratinocytes were fluorescently labeled with CellTracker™ Red CMPTX and CellTracker™ Green CMFDA dyes, respectively. **(B)** H&E staining of printed constructs 20 days after printing showing heterogeneous distribution of fibroblasts when the collagen layers were nebulized. Scale bar: 100 μ m.

II.3.4. 3D Bioprinting of the Epidermal Compartment

Another important challenge in the printing protocol is the incubation time required to allow for complete gelation of the dermis compartment before printing the layers of keratinocytes. This step is particularly important to avoid mixture of fibroblasts and keratinocytes and to allow for proper development of the epidermal layers. In order to evaluate the incubation time required between printing of dermal and epidermal compartments, two layers of dermal bioink were printed and incubated at 37°C for 15, 30 and 40 minutes with subsequent printing of 1 layer of epidermal bioink. Twenty-four hours later, bright-field images were taken with the printed layer of keratinocytes in-focus. Results showed that when fibroblasts layers were incubated for shorter periods of time, a larger area was out-of-focus in the field of view (Figure II.3.4A, B). Approximately $61.7 \pm 6.7\%$, $35.0 \pm 5.2\%$ and $11.7 \pm 4.1\%$ of the printed keratinocyte layer was out-of-focus when incubated for 15, 30 and 40 minutes, respectively. This result suggests that printed keratinocytes tend to penetrate and become embedded in the dermal layers depending on the degree of collagen cross-linkage.

To confirm this hypothesis, we performed histological analysis of skin constructs incubated for 15 or 40 minutes at 37°C prior to printing of the epidermal compartment. Incubation for 15 minutes gave rise to structures of entrapped differentiated keratinocytes within the dermis (Figure II.3.4C). On the contrary, incubation of the printed dermal compartments for 40 minutes showed polarization of columnar keratinocytes in the basal layer, formation of a distinct dermal-epidermal junction and absence of keratinocytes within the dermis.

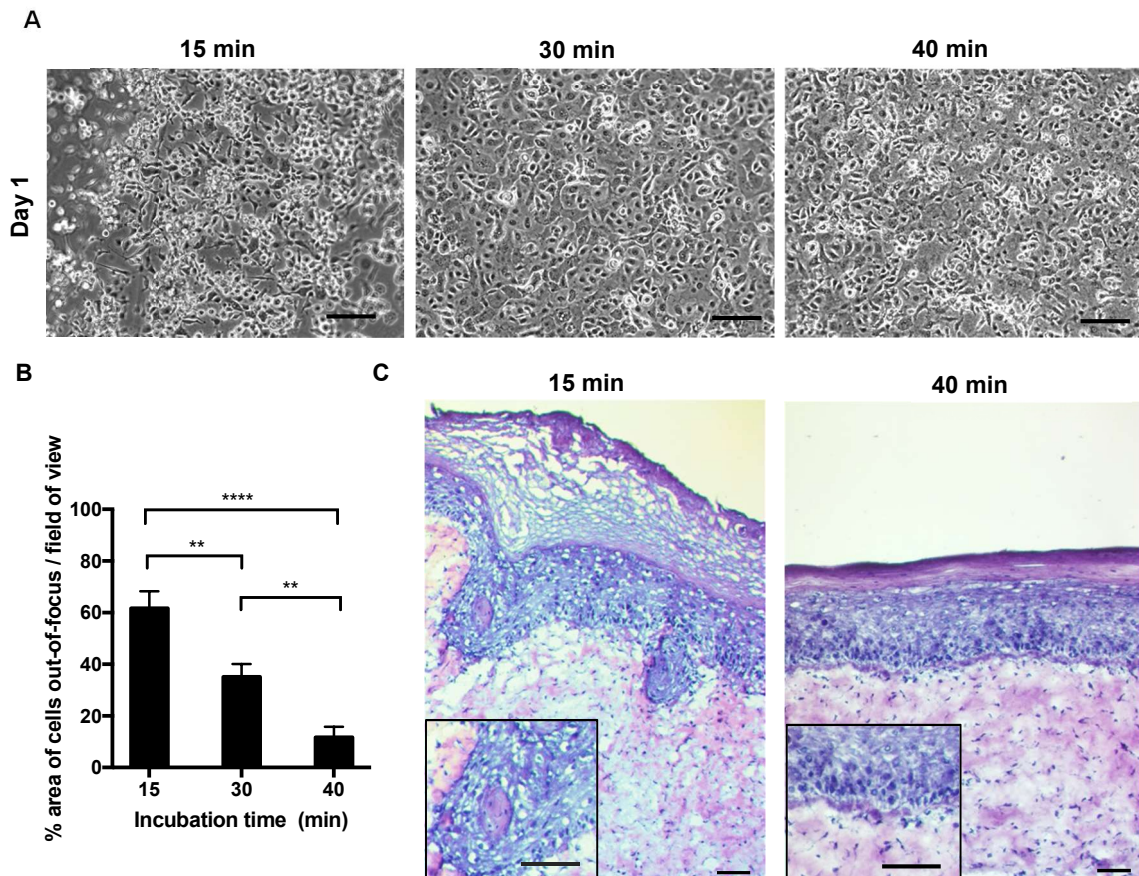


Figure II.3.4- Evaluation of dermal compartment incubation time on the spatial distribution of printed keratinocytes and its effects on epidermal differentiation. **(A)** Representative bright-field images of in-focus keratinocyte layer after 15, 30 and 40 minutes incubation of dermal layers at 37°C. **(B)** The percentage of out-of-focus area was measured in 4 fields of view in Fiji software and is presented as mean \pm SEM, ** p-value \leq 0.01, **** p-value \leq 0.0001. **(C)** H&E staining of 3D printed constructs incubated for 15 and 40 minutes at 37°C prior to printing of epidermal layers, 2 weeks after printing.

Scale bar: 100 μ m.

II.3.5. Epidermal and Dermal Bioink Optimization

Depending on the donor and region, keratin thickness of skin grafts can vary significantly (Robertson & Rees, 2010). The generation of a skin equivalent morphologically similar to the recipient's human skin requires optimization of the number of printed fibroblasts and keratinocytes in the dermal and epidermal bioink. For the purpose of this study, we chose human foreskin as the putative recipient's region. In order to assess the optimal number of dermal fibroblasts and keratinocytes in each bioink, we varied the number of printed fibroblasts and keratinocytes from 1.5 to 3.5×10^5 (Table II.3.1) and compared the thickness of the suprabasal and basal layers of the 3D printed construct to *in vivo* human foreskin.

Table II.3.1 - Summary of printing parameters used to generate bioprinted skin constructs.

Dermal Bioink				
Fibroblast density in bioink	Estimated number of fibroblasts per droplet (~52nL)	Total volume dispensed per layer (μL)	Number of printed layers	Number of fibroblasts in printed dermis
$1.87 \times 10^5/\text{mL}$	8	47	17	1.5×10^5
$3.13 \times 10^5/\text{mL}$	13	47	17	2.5×10^5
$4.4 \times 10^5/\text{mL}$	18	47	17	3.5×10^5
Epidermal Bioink				
Keratinocyte density in bioink	Estimated number of keratinocytes per droplet (~52nL)	Total volume dispensed per layer (μL)	Number of printed layers	Number of keratinocytes in printed epidermis
$1.6 \times 10^6/\text{mL}$	83	47	2	1.5×10^5
$1.6 \times 10^6/\text{mL}$	83	47	3	2.2×10^5
$1.6 \times 10^6/\text{mL}$	83	47	5	3.7×10^5

Results are summarized in Table II.3.2 and Figure II.3.5. The data shows that the number of printed keratinocytes and fibroblasts had significant effect on the thickness of both suprabasal (cytokeratin 10 positive) and basal (cytokeratin 14 positive) layers. At the highest number of printed fibroblasts (3.5×10^5) and keratinocytes (3.7×10^5), the basal and suprabasal layers were about 2- and 3-fold thicker in the printed constructs than in human foreskin, respectively.

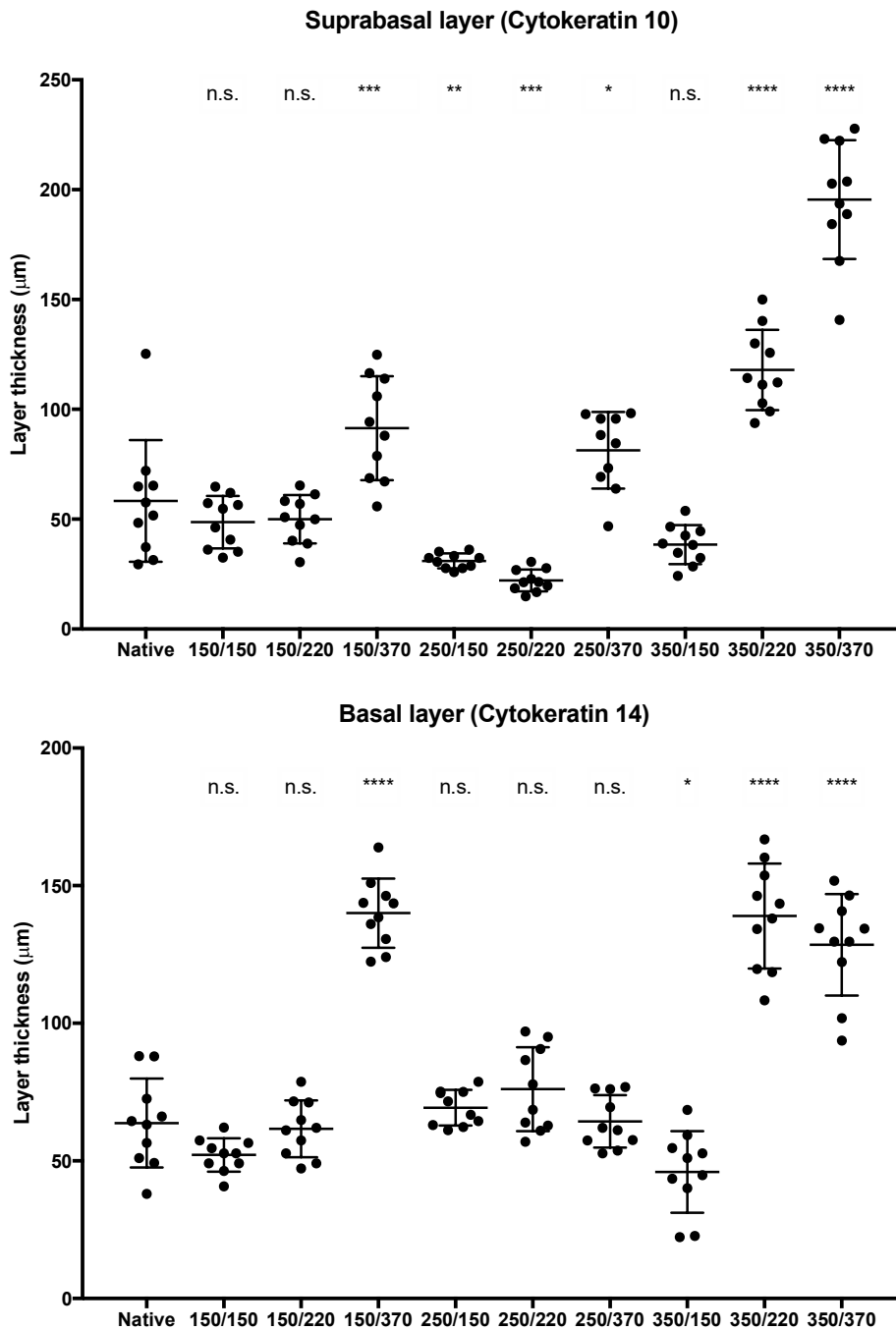


Figure II.3.5 – Thickness of suprabasal (CK10+) and basal (CK14+) layers of 3D bioprinted constructs and native human foreskin. The number of printed fibroblasts (FB) and keratinocytes (KC) per skin constructs was varied from 150×10^3 , 250×10^3 and 350×10^3 and 150×10^3 , 220×10^3 and $370 \times 10^3 \times 10^3$, respectively. Measurements of suprabasal and basal layers thickness were carried out using 10 images from each experimental condition and, for each image, 5 thickness measurements were performed. The mean values \pm SEM are represented. N.s - non-significant, * - p-value ≤ 0.1 , ** - p-value ≤ 0.01 , *** - p-value ≤ 0.001 , **** - p-value ≤ 0.0001 .

Table II.3.2 - Summary of the thickness mean and SEM values of suprabasal (CK10+) and basal (CK14+) layers of 3D bioprinted constructs and native foreskin.

	Layer thickness (μm)									
	Native Foreskin	Fibroblasts/Keratinocytes ($\times 10^3$ cells)								
		150/1 50	150/2 20	150/3 70	250/1 50	250/2 20	250/3 70	350/1 50	350/2 20	350/3 70
Suprabasal (CK10)	58.35 \pm 27.7	48.66 \pm 11.93 <i>n.s.</i>	50.02 \pm 10.99 <i>n.s.</i>	91.44 \pm 23.62 ***	31.05 \pm 3.41 **	22.12 \pm 5.0 ***	81.38 \pm 17.42 *	38.47 \pm 8.87 <i>n.s.</i>	117.5 \pm 18.24 ****	195.5 \pm 27.06 ****
Basal (CK14)	63.74 \pm 16.2	52.1 \pm 6.1 <i>n.s.</i>	61.6 \pm 10.3 <i>n.s.</i>	140 \pm 12.59 ****	69.3 \pm 6.47 <i>n.s.</i>	76.1 \pm 15.3 <i>n.s.</i>	64.3 \pm 9.53 <i>n.s.</i>	45.97 \pm 14.8 *	138.9 \pm 19.04 ****	128.5 \pm 18.4 ****

Overall, the number of printed fibroblasts had no effect on the thickness of the basal layer, except at the highest concentration tested. When 5 layers of keratinocytes were printed, the thickness of the suprabasal and basal layers increased significantly, independently of the number of printed fibroblasts. However, this effect was augmented by 2-fold in the suprabasal layer at the highest concentration of printed fibroblasts. Based on these results, 3D constructs generated by printing of 1.5×10^5 fibroblasts and 2 or 3 layers of keratinocytes, were the only printing conditions that did not show statistically significant differences in the thickness of suprabasal and basal layers compared to human foreskin. Since printing of 3 layers of keratinocytes showed to be the condition morphologically closest to human foreskin by H&E analysis (Figure II.3.6), these printing parameters were used to generate a 3D construct comprised of FB, KC and EC, explored in more detail in chapter IV.

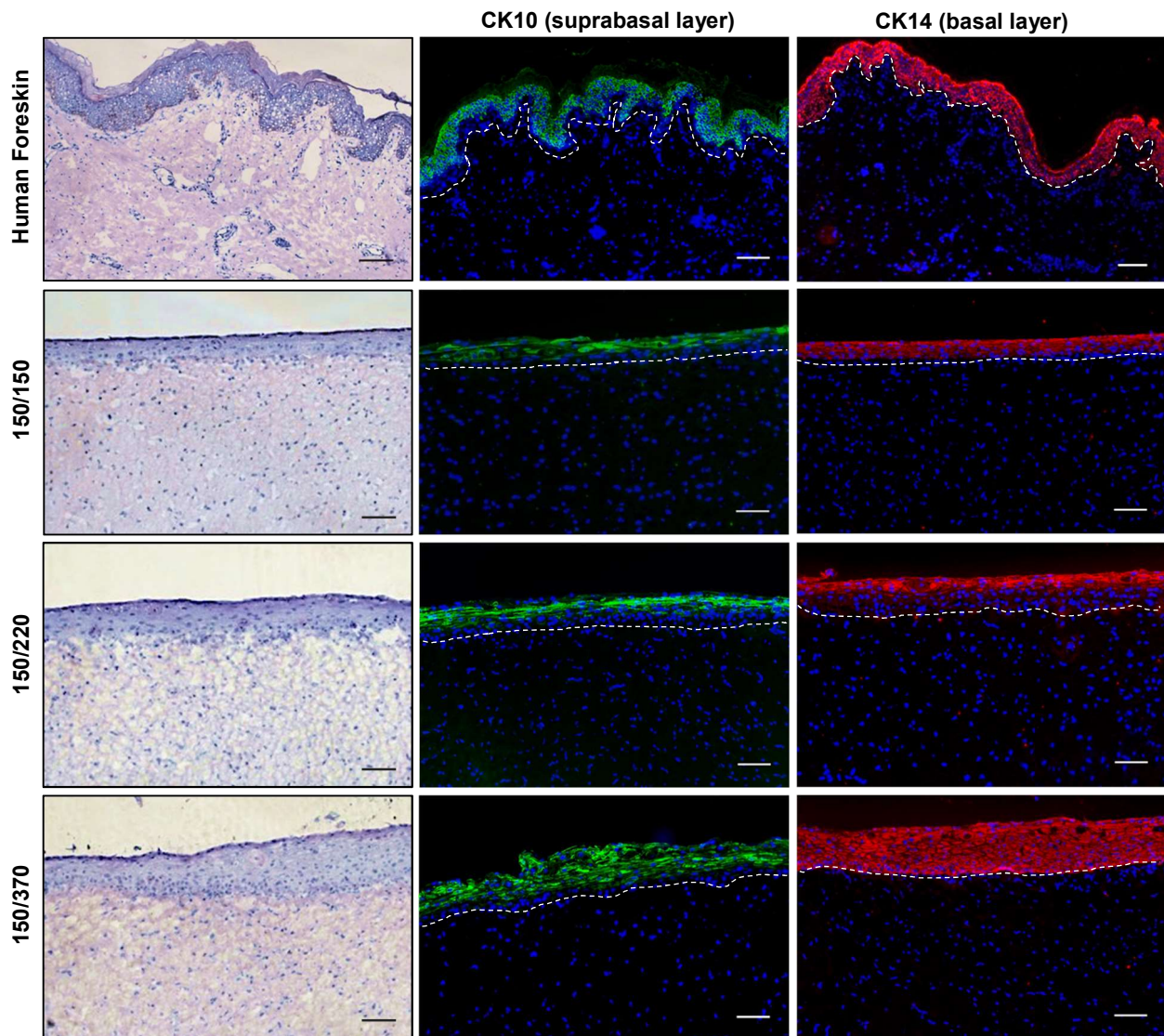
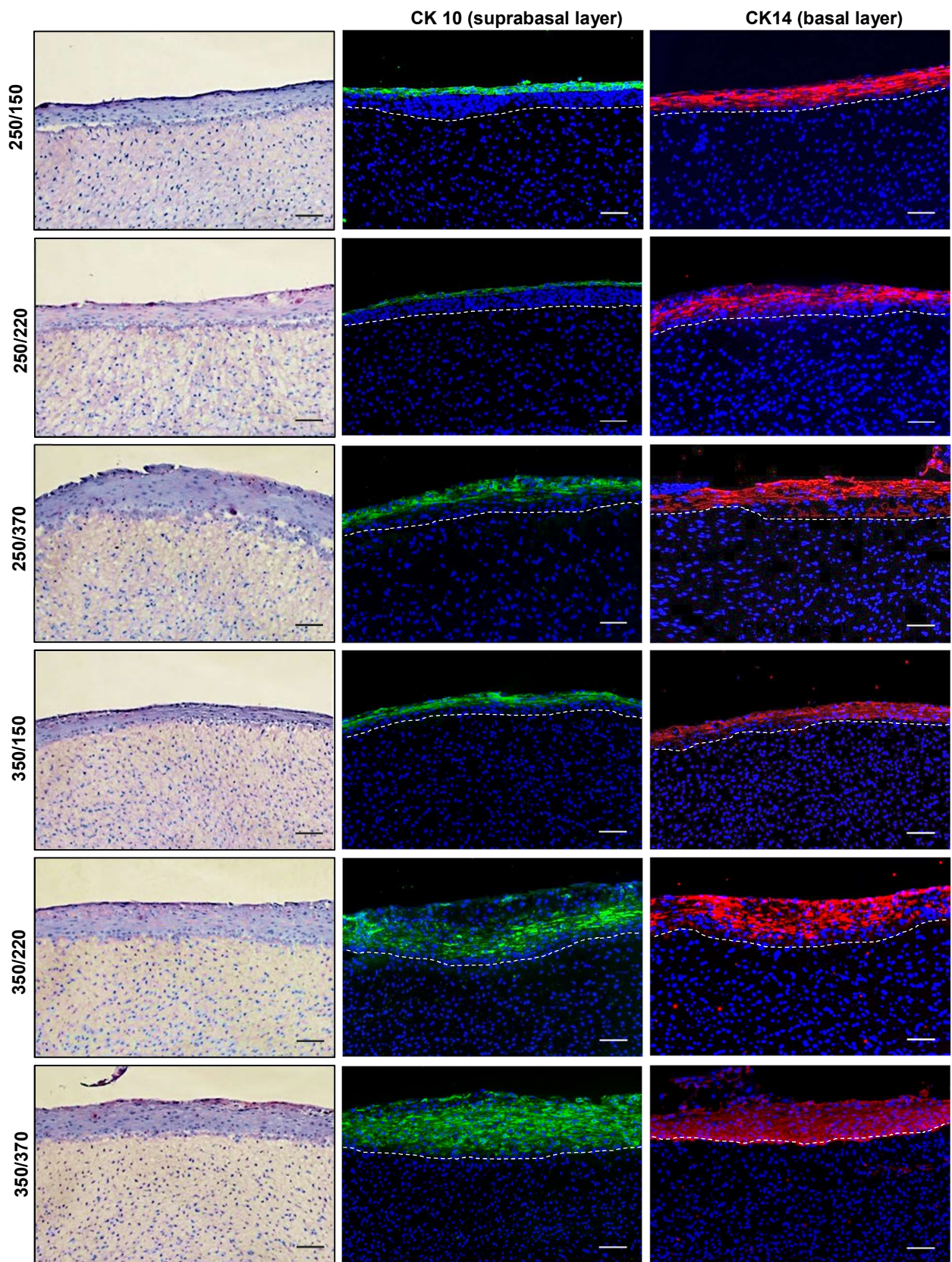


Figure II.3.6 – H&E and immunofluorescence staining of bioprinted constructs generated with varying numbers of dermal fibroblasts and keratinocytes. Representative images of H&E staining and immunofluorescence staining of cytokeratin 10 (green) and cytokeratin 14 (red). Cell nuclei was stained with DAPI (blue). Scale bar: 100 μ m. Figure continues in the next page.



II.3.6. Skin maturation/ ALI culture

Printed skin constructs were grown at air-liquid interface (ALI) from day 4 until day 30. During the 4 days of submerged culture, the thickness of the skin constructs was constant, approximately 8 mm thick. Twenty-four hours after ALI was initiated, the thickness of the printed constructs decreased significantly to 2.2 mm. During ALI culture, the thickness continued to decrease gradually to 450 μm by the end of 30 days (Figure II.3.7). H&E staining was performed to visualize the progression of the cultured constructed at different stages of maturation (Figure II.3.8). Bioprinted skin constructs cultured for 11 days under ALI, showed positive staining of filaggrin (*stratum corneum*), CK14 (*stratum basal*) and CK10 (suprabasal layers) but not collagen type IV (basement membrane). The lack of basement membrane at the dermal-epidermal junction suggests incomplete epidermal stratification and maturation of the printed constructs at this stage of differentiation. At day 26 of ALI, bioprinted constructs stained positively for the outer cornified layer, basal layer, suprabasal layers and basement membrane, indicative of the development of a more mature tissue. In addition, the epithelium showed a greater degree of tissue organization, demonstrated by the presence of well-organized cuboidal basal cells adherent to the basement membrane.

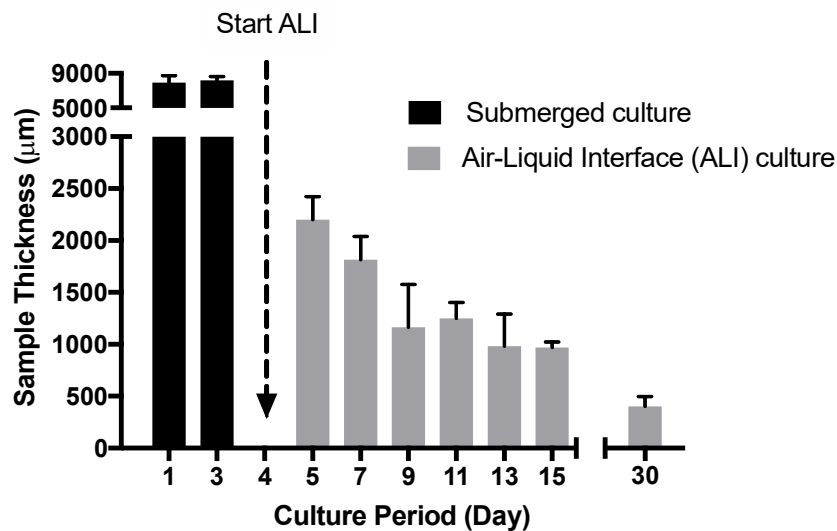


Figure II.3.7 – Thickness of printed skin tissues over the course of 4 weeks. Bioprinted constructs were cultured under submerged culture for 4 days and lifted to the air-liquid interface from day 4 until day 30 of *in vitro* maturation.

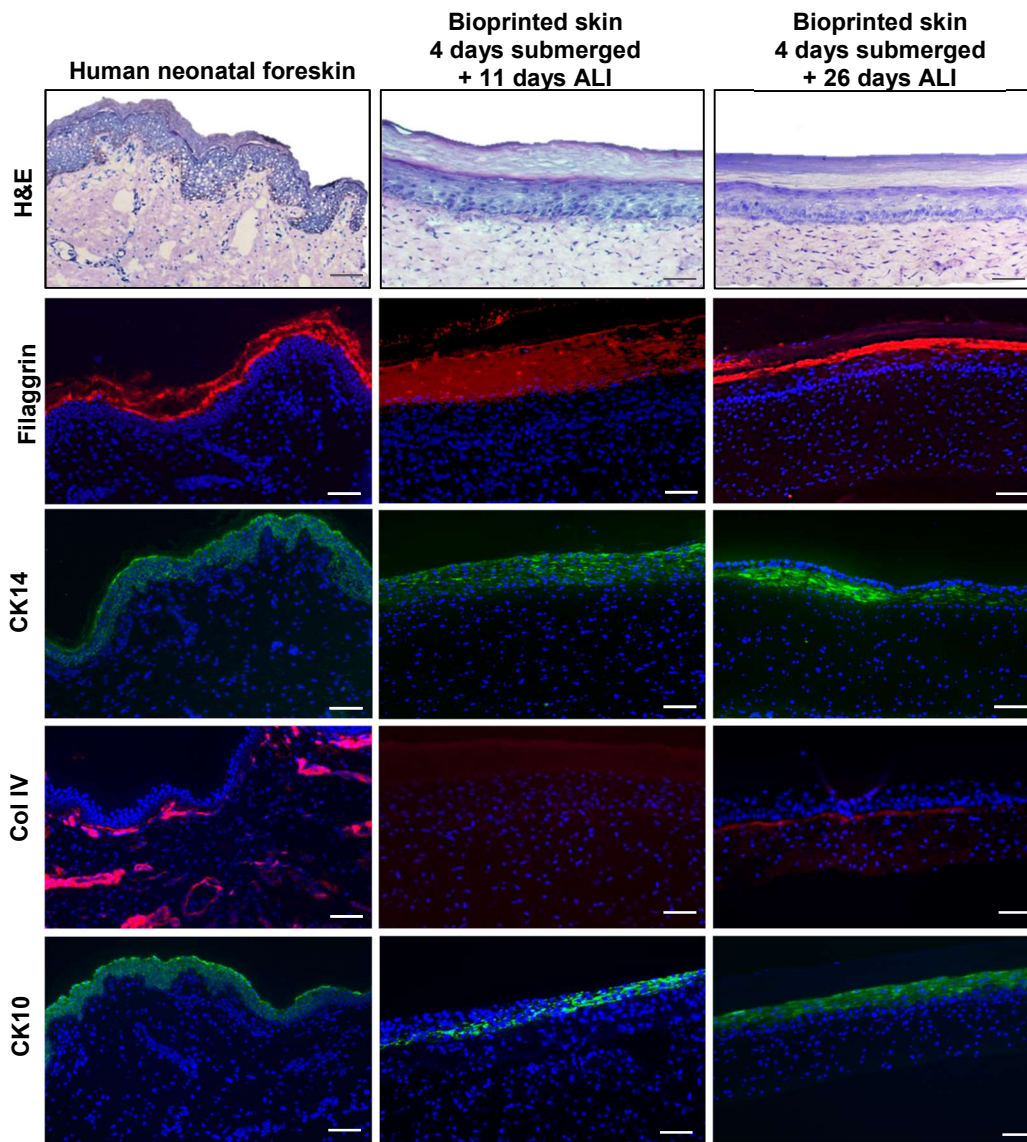


Figure II.3.8 - H&E and immunofluorescence staining of bioprinted constructs at different stages of *in vitro* maturation. Representative images of H&E staining and immunofluorescence staining of filaggrin (stratum corneum), cytokeratin 14 (suprabasal layer), collagen type IV (basement membrane) and cytokeratin 10 (basal layer). Cell nuclei was stained with DAPI (blue). Scale bar: 100 μ m.

II.3.7 Barrier Function

Based on the printing and culture parameters optimized in the previous sections, we generated a bioprinted skin construct and assessed barrier function after 26 days under ALI culture through periodic measurements of permeated fluorescein labeled dextran molecules of different molecular weights: 10 and 20 kDa. The flux of fluorescein dextran-20kDa, was found to be approximately two-fold lower than FD-10, revealing a direct correlation between higher molecular weight and slower permeation rate of the penetrant through the bioprinted skin (Figure II.3.9, Table II.3.3). In addition, FD-10 showed a lag-time inferior to the first sample measurement (15 minutes), while FD-20 was detected in the acceptor's compartment after 1.25 hours. In comparison to previously reported permeability coefficients values for the penetrant FD-10, the 3D printed skin construct showed 19-times higher permeability than intact human breast skin and 7-times less permeability than rat skin stripped of stratum corneum. Moreover, Hsu *et al.* have generated a skin equivalent composed of primary fibroblasts and HaCaT cells in a collagen gel (Hsu et al., 2018), and found that the permeability coefficient of FD-10 was $594 \pm 18 \times 10^{-5} \text{cm/h}$, about 230-times higher compared to human breast skin and 12-times higher than our 3D printed model (Table II.3.4).

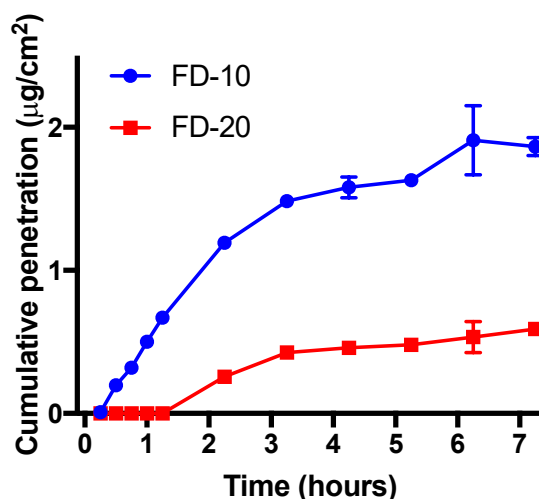


Figure II.3.9 - Cumulative permeation profile of fluorescein dextran-10 kDa (FD-10) and fluorescein dextran-20 kDa (FD-20) molecules in 3D bioprinted constructs cultured *in vitro* for 30 days. The steady state flux rate of each penetrant was calculated from the linear portion of the graph. (Mean \pm SD, n = 3).

Table II.3.3 – Summary of calculated steady state flux, lag-time and permeability coefficients of FD-10 and FD-20 molecules in bioprinted constructs cultured *in vitro* for 30 days.

Penetrant	Flux ($\mu\text{g}/\text{cm}^2/\text{h}$)	Lag-time (h)	Permeability coefficient ($\times 10^{-5}\text{cm}/\text{h}$)
Fluorescein dextran -10 kDa	0.501	0	50.1
Fluorescein dextran -20 kDa	0.213	1.25	21.3

Table II.3.4 – Summary of reported permeability coefficient values for FD-10 and FD-20 molecules in different skin models. ND - not detectable.

MW (kDa)	Permeability coefficient ($\times 10^{-5}\text{cm}/\text{h}$)			
	Intact rat skin (Ogiso, Paku, Iwaki, & Tanino, 1994)	Tape-stripped rat skin (Ogiso et al., 1994)	Intact human breast tissue (Dave, Alsharif, & Perumal, 2016)	Skin equivalent (Hsu et al., 2018)
FD-10	1.22 ± 0.25	373.7 ± 0.52	2.6 ± 0.7	594 ± 18
FD-70	0.45 ± 0.16	35.57 ± 8.16	ND	-

II.4 Discussion

In this chapter, we describe the development, optimization and characterization of a layer-by-layer construct comprised of human primary cells using a pneumatically driven printing system. The advantage of such system is that various types of liquid materials with viscosities up to 200 Pa s can be dispensed by adjusting the pressure and microvalve gating time (Lee et al., 2014). Our studies indicate that printing of dermal fibroblasts, keratinocytes and endothelial cells had no significant effect on cell viability. Unlike the potential pressure-related cell damage which can occur in inkjet or piezoelectric element-driven dispensing systems (Derakhshanfar et al., 2018), high cell viability was observed in this study due to low operational pneumatic pressure, which was in the order of 2.5 psi. However, an interesting negative trend in cell viability was observed on both manually deposited and printed keratinocytes at day 1 and 3. We hypothesize that this effect on human keratinocytes might be associated with poor cell-to-substrate interaction. Murray *et al.* and Terranova *et al.* have reported a direct correlation of growth rate, adhesion and cell morphology depending on the substrate protein used for human keratinocyte culture (Murray, Stingl, Kleinman, Martin, & Katz, 1979; Terranova, Rohrbach, & Martin, 1980). Particularly, preferential attachment and growth of keratinocytes to collagen type IV was shown, a major constituent of skin basement membrane, compared to other types of collagen. Furthermore, it has been found that human foreskin keratinocytes cultured on collagen type I gels, but not in non-fibrous collagen, undergo apoptosis soon after seeding due to the lack of laminin deposition on the collagen gels (Fujisaki & Hattori, 2002). Successful deposition of laminins produced by keratinocytes on collagen type I is linked to increasing levels of Phosphoinositide 3-kinase (PI3K) and Serine-Threonine kinase (Akt) activity, which is essential for avoidance of apoptosis (Franke, Kaplan, & Cantley, 1997; Madrid et al., 2000). Particularly, the amount of Akt expressed by human foreskin keratinocytes cultured on collagen I gels was found to be almost absent within 1 day of culture, but slowly increased overtime, which seems to agree with our findings. We hypothesize that the inclusion of a thin layer of collagen type IV between the dermal and epidermal compartments might significantly improve keratinocyte proliferation and epidermal maturation. This hypothesis was not tested in this model and will require future validation.

Moreover, we were able to effectively improve the distribution of dermal fibroblasts in the dermis by mixing a pH reconstitution buffer prior to printing rather than using nebulized NaHCO₃ as a collagen cross-linking agent as previously described by Lee *et al.* (Lee et al., 2014). When collagen layers were nebulized for 10 seconds, complete collagen crosslinking was achieved resulting in high gel stiffness. When fibroblasts were subsequently printed, these adhered to the stiff collagen surface and grew as monolayers, producing a striated

dermis pattern. On the contrary, nebulization for 5 seconds led to incomplete gelation of the collagen layers, resulting in quick fibroblast settling by gravity on the Transwell insert membrane. In addition, nebulization was found to be highly variable and dependent on the ambient conditions at the time of printing, such as humidity and temperature. These factors, which vary significantly depending on the time of the year, can impact the aerosol droplet size distribution and, consequently, the rate by which the printed collagen layers transition to a higher pH (Haddrell et al., 2014; Phipps & Gonda, 1990). Overall, the pre-mixing gelation method showed to be the preferable method to achieve homogeneous distribution of dermal fibroblasts within the 3D printed dermal compartment. However, under these printing conditions several important factors have to be kept in mind. For example, the mixture of collagen precursor with a pH reconstitution buffer quickly initiates a crosslinking reaction, leading to increasing viscosity and gelation of the bioink, which can cause clogging of bioink in the printer's tubing and dispensing microvalves. To slow down collagen crosslinking during bioprinting, the components of the dermal bioink were individually refrigerated at 4°C and the bioink mixture was repeatedly loaded in small volumes (100 µL) into the printer's syringe just before printing. The low temperature of the dermal bioink at the time of printing significantly decreased the collagen gelation rate, which was then completed when the entire printed dermal compartment was incubated at 37°C. Since this method requires frequent user's attention to repeatedly mix and load the dermal bioink in the printer's syringe, further upgrades to the printing platform will be required to completely automate the printing protocol. First, integration of a cooling module in the printer's syringes to hold large volumes of the individual components of the dermal bioink; second, integration of in-line static mixer that converges the components of the dermal bioink into a single tubing connected to a dispensing microvalve; third, integration of a precision flow rate control device to mix the components of the dermal bioink consistently and in the right proportions over the course of printing. Successful implementation of these upgrades to the current printing platform will be crucial for robust, consistent and high-throughput fabrication of bioprinted skin grafts.

Other key parameter in the printing protocol is the incubation time required to achieve complete gelation of the printed dermal layers prior to keratinocyte printing. H&E staining of printed constructs showed that incubation of the dermal compartment for 30 minutes or less at 37°C led to penetration and encapsulation of keratinocytes in the dermis. Incubation for at least 40 minutes at 37°C was sufficient to avoid penetration of keratinocytes in the dermal layers and to enable normal epidermal stratification *in vitro*. Although we aimed at finding conditions to avoid keratinocyte penetration in the dermis in this particular study, further optimization of dermal compartment gelation and keratinocyte bioprinting may provide a way to effectively mimic *in vivo* skin rete ridges, which skin equivalents still fail to reproduce. Rete

ridges are particularly important as they form invaginations at the dermal-epidermal junction that serve to increase the contact area between the two layers, thus strengthening their adhesion and scattering the external forces to which they are exposed (Xiong, Wu, & He, 2013). In addition, encapsulation of dermal papilla cells (DPs) in the dermis may be of potential interest to generate more complex skin models, since DPs play an important role in the development and growth of hair follicles (Driskell, Clavel, Rendl, & Watt, 2011). As hair follicles develop as downgrowth's of the epidermis into the dermis, successful encapsulation and differentiation of DP cells using 3D printing technology may potentially be used as a tool to effectively induce hair follicle formation.

For skin grafting applications, depending on the host wound bed and region, 3D printed skin grafts will require optimization of cell suspension density and the number of printed layers to reproduce the thickness and cellular distribution observed in the recipient's skin. In this chapter, we analyzed the thickness of basal and suprabasal layers in bioprinted skin constructs by varying the number of printed fibroblasts and keratinocytes and compared it to neonatal human foreskin. The data showed that the number of printed keratinocytes and fibroblasts had significant effect on the thickness of both suprabasal (cytokeratin 10 positive) and basal (cytokeratin 14 positive) layers. The dynamic cross-talk between fibroblasts and keratinocytes in *in vitro* co-cultures has been studied by several investigators (Boehnke et al., 2007; Kunz-Schughart et al., 2006; Sorrell & Caplan, 2004). Particularly, it has been shown that the proliferation of keratinocytes that were in contact with fibroblasts in the early stage of the co-culture was significantly enhanced compared to cultures containing only keratinocytes (Wang, Wang, Farhangfar, Zimmer, & Zhang, 2012). In addition, the data showed that up-regulation of heparin-binding EGF-like growth factor (HB-EGF) by IL-1 α and TGF β 1 appears to be the major driving force behind the effects of co-cultured fibroblasts on the proliferation and migration of keratinocytes.

The ultimate goal of skin equivalent development is to generate a construct with the same barrier properties found in native human skin. Exposure to air-liquid interface along with maturation culture conditions are used to induce epidermal differentiation of skin equivalents overtime (Frankart et al., 2012; Pruniéras, Régnier, & Woodley, 1983). We have shown by histological characterization of bioprinted constructs at different times of maturation that after 11 days of ALI culture, markers of epidermal stratification (CK14, CK10 and filaggrin) were present but the basement membrane along the dermal-epidermal junction was absent, indicative of immature skin development. At day 26 of ALI, bioprinted constructs stained positively for the outer cornified layer, basal layer, suprabasal layers and basement membrane. In addition, the epithelium showed a greater degree of tissue organization, demonstrated by the presence of well-organized cuboidal basal cells adherent to the

basement membrane by H&E staining. The skin basement membrane is known to be the foundation of epidermal integrity as it is indispensable for normal skin functions, including acting as a permeability barrier, forming an adhesive interface between dermis and epidermis, and controlling cellular organization and differentiation (Breitkreutz, Koxholt, Thiemann, & Nischt, 2013; Jayadev & Sherwood, 2017; Yurchenco & Schittny, 1990). Depletion or functional deficiencies of the basement membrane caused by mutations in genes encoding components of the basement membrane are often associated with inherited skin disorders such as epidermolysis bullosa (EB), characterized by skin fragility (Bruckner-Tuderman & Has, 2014). A potential solution for the treatment of EB is the fabrication of skin equivalents comprised of autologous skin cells from EB patients with the corrected gene (Gache et al., 2004; Woodley et al., 2003).

The molecular weight of a drug can significantly influence its penetration through skin. Larger drugs will take longer to permeate, while smaller drugs will quickly penetrate the skin barrier (Cevc, 1997; Karande, Jain, & Mitragotri, 2004). To evaluate barrier function of 3D bioprinted skin constructs, we measured the steady state flux and permeability coefficient of two fluorescein dextran molecules of different size: 10 and 20 kDa. As predicted, the penetrant with lowest molecular weight, FD-10, permeated rapidly, whereas the flux of FD-20 was slow, suggesting size-dependent penetration through the bioprinted skin. In addition, the lag time increased with increasing molecular size of the penetrant. In comparison to reported values in the literature for fluorescein dextran-10kDa, the 3D printed skin construct showed 19-fold more permeability than human skin. This result was expected since permeability in skin models is known to be less developed and thus, more permeable to molecules than human skin (Welss, Basketter, & Schröder, 2004). However, Hsu *et al.* have measured the permeability of FD-10 in a skin equivalent composed of primary fibroblasts and HaCaT in a collagen gel and was found to be about 230-times more permeable than in intact human skin and about 12-fold higher than our 3D printed model (Hsu et al., 2018). This significant difference in barrier permeability observed between the 2 skin equivalents might be explained in part by the source of keratinocytes. Boelsma *et al.*, have reported that HaCaT cells fail to produce free fatty acids and present very low content and incomplete profile of ceramides, leading to impaired capacity to synthesize lipids that are necessary for a proper barrier formation (Boelsma, Verhoeven, & Ponc, 1999). Although we have shown significant improvement of barrier function by bioprinting a skin equivalent composed of human primary cells, further improvements are still required to completely replace the use of cadaver human skin or other skin models, such as rat, pig and rabbit in transdermal delivery studies. Barrier function of skin equivalents may be improved with longer *in vitro* maturation culture and with further optimization of the *in vitro* culture conditions, such as medium composition, to promote comparable keratinocyte

differentiation and skin maturation to *in vivo* skin. Furthermore, current skin equivalents lack appendages, such as hair follicles and sweat glands, which might significantly affect overall skin homeostasis and, consequently, barrier function. 3D bioprinting technology can be used to generate such complex structures as it offers the unique advantage of accurate 3D placement of cells and biomaterials at various length scales.

II.5 Conclusions

The present chapter explores the development of a 3D printing protocol for robust, consistent and scalable production of skin grafts composed entirely of human primary cells. First, it described the optimization of several printing and culture parameters; then, it described the morphological and functional characterization of the bioprinted skin construct.

Results have shown that printing of dermal fibroblasts, keratinocytes and endothelial cells at 300um printing resolution and 2.5 psi had no significant effect on cell viability. In addition, we were able to effectively improve the distribution of dermal fibroblasts in the dermis by mixing a pH reconstitution buffer prior to printing. This step in the protocol will likely require future upgrades to the current printing platform to achieve complete automation in the generation of bioprinted skin constructs. Bioprinting of the epidermal compartment was found to require an incubation of the dermal compartment for at least 40 minutes at 37°C.

Moreover, the 3D printed skin constructs seem to achieve comparable maturation to human skin after 26 days in ALI, as seen by the presence of basement membrane. At this stage of maturation, the printed construct showed to be more permeable than human skin to fluorescein dextran-10 kDa, but less permeable than a skin equivalent composed of HaCaT cells. Although we have shown significant improvement of barrier function by bioprinting a skin equivalent composed of human primary cells, further improvements are still required.

Together, these results demonstrate the successful generation of a non-vascularized skin graft which will serve as the first optimization step for further optimization of the printed skin constructs, such as the inclusion of microvascular network, to produce a 3D printed full-thickness vascularized human skin graft, reported in more detail in chapter III.

II.6 References

- Boehnke, K., Mirancea, N., Pavesio, A., Fusenig, N. E., Boukamp, P., & Stark, H.-J. J. J. (2007). Effects of fibroblasts and microenvironment on epidermal regeneration and tissue function in long-term skin equivalents. *European Journal of Cell Biology*, 86(11–12), 731–746. <https://doi.org/http://doi.org/10.1016/j.ejcb.2006.12.005>
- Boelsma, E., Verhoeven, M. C. H., & Ponc, M. (1999). Reconstruction of a Human Skin Equivalent Using a Spontaneously Transformed Keratinocyte Cell Line (HaCaT). *Journal of Investigative Dermatology*, 112(4), 489–498. <https://doi.org/https://doi.org/10.1046/j.1523-1747.1999.00545.x>
- Breitkreutz, D., Koxholt, I., Thiemann, K., & Nischt, R. (2013). Skin basement membrane: the foundation of epidermal integrity--BM functions and diverse roles of bridging molecules nidogen and perlecan. *BioMed Research International*, 2013, 179784. <https://doi.org/10.1155/2013/179784>
- Brohem, C. A., da Silva Cardeal, L. B., Tiago, M., Soengas, M. S. M. S., de Moraes Barros, S. B., & Maria-Engler, S. S. (2011). Artificial skin in perspective: concepts and applications. *Pigment Cell & Melanoma Research*, 24(1), 35–50. <https://doi.org/10.1111/j.1755-148X.2010.00786.x>
- Bruckner-Tuderman, L., & Has, C. (2014). Disorders of the cutaneous basement membrane zone--the paradigm of epidermolysis bullosa. *Matrix Biology: Journal of the International Society for Matrix Biology*, 33, 29–34. <https://doi.org/10.1016/j.matbio.2013.07.007>
- Cevc, G. (1997). Drug delivery across the skin. *Expert Opinion on Investigational Drugs*, 6(12), 1887–1937. <https://doi.org/10.1517/13543784.6.12.1887>
- Dave, K., Alsharif, F. M., & Perumal, O. (2016). Transpapillary (Nipple) Delivery of Macromolecules to the Breast: Proof of Concept Study. *Molecular Pharmaceutics*, 13(11), 3842–3851. <https://doi.org/10.1021/acs.molpharmaceut.6b00634>
- Derakhshanfar, S., Mbeleck, R., Xu, K., Zhang, X., Zhong, W., & Xing, M. (2018). 3D bioprinting for biomedical devices and tissue engineering: A review of recent trends and advances. *Bioactive Materials*, 3(2), 144–156. <https://doi.org/https://doi.org/10.1016/j.bioactmat.2017.11.008>
- Driskell, R. R., Clavel, C., Rendl, M., & Watt, F. M. (2011). Hair follicle dermal papilla cells at a glance. *Journal of Cell Science*, 124(Pt 8), 1179–1182. <https://doi.org/10.1242/jcs.082446>
- Eckert, R. L., & Rorke, E. A. (1989, March). Molecular biology of keratinocyte differentiation. *Environmental Health Perspectives*.
- Frankart, A., Malaise, J., De Vuyst, E., Minner, F., de Rouvroit, C. L., & Poumay, Y. (2012). Epidermal morphogenesis during progressive in vitro 3D reconstruction at the air-liquid interface. *Experimental Dermatology*, 21(11), 871–875. <https://doi.org/10.1111/exd.12020>
- Franke, T. F., Kaplan, D. R., & Cantley, L. C. (1997). PI3K: Downstream AKTion Blocks Apoptosis. *Cell*, 88(4), 435–437. [https://doi.org/10.1016/S0092-8674\(00\)81883-8](https://doi.org/10.1016/S0092-8674(00)81883-8)

- Fujisaki, H., & Hattori, S. (2002). Keratinocyte apoptosis on type I collagen gel caused by lack of laminin 5/10/11 deposition and Akt signaling. *Experimental Cell Research*, *280*(2), 255–269.
- Gache, Y., Baldeschi, C., Del Rio, M., Gagnoux-Palacios, L., larcher, F., Lacour, J.-P., & Meneguzzi, G. (2004). Construction of Skin Equivalents for Gene Therapy of Recessive Dystrophic Epidermolysis Bullosa. *Human Gene Therapy*, *15*(10), 921–933. <https://doi.org/10.1089/hum.2004.15.921>
- Griffiths, M., Ojeh, N., Livingstone, R., Price, R., & Navsaria, H. (2004). Survival of Apligraf in acute human wounds. *Tissue Engineering*, *10*(7), 1180–1195. <https://doi.org/10.1089/ten.2004.10.1180>
- Haddrell, A. E., Davies, J. F., Miles, R. E. H., Reid, J. P., Dailey, L. A., & Murnane, D. (2014). Dynamics of aerosol size during inhalation: Hygroscopic growth of commercial nebulizer formulations. *International Journal of Pharmaceutics*, *463*(1), 50–61. <https://doi.org/https://doi.org/10.1016/j.ijpharm.2013.12.048>
- Harper, R. A., & Grove, G. (1979). Human skin fibroblasts derived from papillary and reticular dermis: differences in growth potential in vitro. *Science (New York, N.Y.)*, *204*(4392), 526–527.
- Hsu, H.-H., Kracht, J.-K., Harder, L. E., Rudnik, K., Lindner, G., Schimek, K., Marx, U., & Pörtner, R. (2018). A Method for Determination and Simulation of Permeability and Diffusion in a 3D Tissue Model in a Membrane Insert System for Multi-well Plates. *Journal of Visualized Experiments : JoVE*, (132), 56412. <https://doi.org/10.3791/56412>
- Jayadev, R., & Sherwood, D. R. (2017). Basement membranes. *Current Biology : CB*, *27*(6), R207–R211. <https://doi.org/10.1016/j.cub.2017.02.006>
- Karande, P., Jain, A., & Mitragotri, S. (2004). Discovery of transdermal penetration enhancers by high-throughput screening. *Nature Biotechnology*, *22*, 192. Retrieved from <https://doi.org/10.1038/nbt928>
- Kirsner, R. S. S., Falanga, V., Kerdel, F. A. a, Katz, M. H. H., & Eaglstein, W. H. H. (1996). Skin grafts as pharmacological agents: pre-wounding of the donor site. *The British Journal of Dermatology*, *135*(2), 292–296. <https://doi.org/10.1111/j.1365-2133.1996.tb01164.x>
- Knowlton, S., Yenilmez, B., & Tasoglu, S. (2016). Towards Single-Step Biofabrication of Organs on a Chip via 3D Printing. *Trends in Biotechnology*, *34*(9), 685–688. <https://doi.org/10.1016/j.tibtech.2016.06.005>
- Kunz-Schughart, L. a, Schroeder, J. a, Wondrak, M., van Rey, F., Lehle, K., Hofstaedter, F., & Wheatley, D. N. (2006). Potential of fibroblasts to regulate the formation of three-dimensional vessel-like structures from endothelial cells in vitro. *American Journal of Physiology. Cell Physiology*, *290*(5), C1385-98. <https://doi.org/10.1152/ajpcell.00248.2005>
- Lazic, T., & Falanga, V. (2011). Bioengineered skin constructs and their use in wound healing. *Plastic and Reconstructive Surgery*, *127* Suppl, 75S–90S. <https://doi.org/10.1097/PRS.0b013e3182009d9f>

- Lee, V., Singh, G., Trasatti, J. P., Bjornsson, C., Xu, X. W., Tran, T. N., Yoo, S.-S. S., Dai, G. H., & Karande, P. (2014). Design and fabrication of human skin by three-dimensional bioprinting. *Tissue Engineering. Part C, Methods*, 20(6), 473–484. <https://doi.org/10.1089/ten.TEC.2013.0335>
- Lim, C. P., Phan, T. T., Lim, I. J., & Cao, X. (2009). Cytokine profiling and Stat3 phosphorylation in epithelial-mesenchymal interactions between keloid keratinocytes and fibroblasts. *The Journal of Investigative Dermatology*, 129(4), 851–861. <https://doi.org/10.1038/jid.2008.337>
- Maas-Szabowski, N., Stärker, A., & Fusenig, N. E. (2003). Epidermal tissue regeneration and stromal interaction in HaCaT cells is initiated by TGF- α . *Journal of Cell Science*, 116(Pt 14), 2937–2948. <https://doi.org/10.1242/jcs.00474>
- Madrid, L. V, Wang, C.-Y., Guttridge, D. C., Schottelius, A. J. G., Baldwin, A. S., & Mayo, M. W. (2000). Akt Suppresses Apoptosis by Stimulating the Transactivation Potential of the RelA/p65 Subunit of NF- κ B. *Molecular and Cellular Biology*, 20(5), 1626 LP-1638. Retrieved from <http://mcb.asm.org/content/20/5/1626.abstract>
- Moulin, V. J., Mayrand, D., Laforce-Lavoie, A., Larochelle, S., & Genest, H. (2011). In Vitro Culture Methods of Skin Cells for Optimal Skin Reconstruction by Tissue Engineering. In D. Eberli (Ed.), *Regenerative Medicine and Tissue Engineering - Cells and Biomaterials*. InTech. <https://doi.org/10.5772/20341>
- Munoz-Abraham, A. S., Rodriguez-Davalos, M. I., Bertacco, A., Wengerter, B., Geibel, J. P., & Mulligan, D. C. (2016). 3D Printing of Organs for Transplantation: Where Are We and Where Are We Heading? *Current Transplantation Reports*, 3(1), 93–99. <https://doi.org/10.1007/s40472-016-0089-6>
- Murphy, S. V., & Atala, A. (2014). 3D bioprinting of tissues and organs. *Nature Biotechnology*, 32(8), 773–785. <https://doi.org/10.1038/nbt.2958>
- Murray, J. C., Stingl, G., Kleinman, H. K., Martin, G. R., & Katz, S. I. (1979). Epidermal cells adhere preferentially to type IV (basement membrane) collagen. *The Journal of Cell Biology*, 80(1), 197–202.
- Ogiso, T., Paku, T., Iwaki, M., & Tanino, T. (1994). Mechanism of the enhancement effect of n-octyl-beta-D-thioglycoside on the transdermal penetration of fluorescein isothiocyanate-labeled dextrans and the molecular weight dependence of water-soluble penetrants through stripped skin. *Journal of Pharmaceutical Sciences*, 83(12), 1676–1681.
- Panteleyev, A. A., Jahoda, C. A., & Christiano, A. M. (2001). Hair follicle predetermination. *Journal of Cell Science*, 114(Pt 19), 3419–3431.
- Phillips, T. J., Manzoor, J., Rojas, A., Isaacs, C., Carson, P., Sabolinski, M., Young, J., & Falanga, V. (2002). The longevity of a bilayered skin substitute after application to venous ulcers. *Archives of Dermatology*, 138(8), 1079–1081. <https://doi.org/10.1001/archderm.138.8.1079>
- Phipps, P. R., & Gonda, I. (1990). Droplets produced by medical nebulizers. Some factors affecting

- their size and solute concentration. *Chest*, 97(6), 1327–1332.
- Pruniéras, M., Régnier, M., & Woodley, D. (1983). Methods for cultivation of keratinocytes with an air-liquid interface. *The Journal of Investigative Dermatology*. <https://doi.org/10.1111/1523-1747.ep12540324>
- Reijnders, C. M. A., van Lier, A., Roffel, S., Kramer, D., Scheper, R. J., & Gibbs, S. (2015). Development of a Full-Thickness Human Skin Equivalent In Vitro Model Derived from TERT-Immortalized Keratinocytes and Fibroblasts. *Tissue Engineering. Part A*, 21(17–18), 2448–2459. <https://doi.org/10.1089/ten.TEA.2015.0139>
- Robertson, K., & Rees, J. L. (2010). Variation in epidermal morphology in human skin at different body sites as measured by reflectance confocal microscopy. *Acta Dermato-Venereologica*, 90(4), 368–373. <https://doi.org/10.2340/00015555-0875>
- Shah, J. C. (1993). Analysis of permeation data: evaluation of the lag time method. *International Journal of Pharmaceutics*, 90(2), 161–169. [https://doi.org/https://doi.org/10.1016/0378-5173\(93\)90152-6](https://doi.org/https://doi.org/10.1016/0378-5173(93)90152-6)
- Sorrell, J. M., & Caplan, A. I. (2004). Fibroblast heterogeneity: more than skin deep. *Journal of Cell Science*, 117(Pt 5), 667–675. <https://doi.org/10.1242/jcs.01005>
- Terranova, V. P., Rohrbach, D. H., & Martin, G. R. (1980). Role of laminin in the attachment of PAM 212 (epithelial) cells to basement membrane collagen. *Cell*, 22(3), 719–726.
- Uchi, H., Terao, H., Koga, T., & Furue, M. (2000). Cytokines and chemokines in the epidermis. *Journal of Dermatological Science*, 24(SUPPL. 1), 29–38. [https://doi.org/10.1016/S0923-1811\(00\)00138-9](https://doi.org/10.1016/S0923-1811(00)00138-9)
- Wang, Z., Wang, Y., Farhangfar, F., Zimmer, M., & Zhang, Y. (2012). Enhanced keratinocyte proliferation and migration in co-culture with fibroblasts. *PloS One*, 7(7), e40951. <https://doi.org/10.1371/journal.pone.0040951>
- Welss, T., Basketter, D. A., & Schröder, K. R. (2004). In vitro skin irritation: Facts and future. State of the art review of mechanisms and models. *Toxicology in Vitro*, 18(3), 231–243. <https://doi.org/10.1016/j.tiv.2003.09.009>
- Woodley, D. T., Atha, T., Huang, Y., Chen, M., Krueger, G. G., Jorgensen, C. M., Fairley, J. A., Chan, L., & Keene, D. R. (2003). Normal and Gene-Corrected Dystrophic Epidermolysis Bullosa Fibroblasts Alone Can Produce Type VII Collagen at the Basement Membrane Zone. *Journal of Investigative Dermatology*, 121(5), 1021–1028. <https://doi.org/https://doi.org/10.1046/j.1523-1747.2003.12571.x>
- Xiong, X., Wu, T., & He, S. (2013). Physical forces make rete ridges in oral mucosa. *Medical Hypotheses*, 81(5), 883–886. <https://doi.org/10.1016/j.mehy.2013.07.005>
- Yurchenco, P. D., & Schittny, J. C. (1990). Molecular architecture of basement membranes. *FASEB Journal: Official Publication of the Federation of American Societies for Experimental Biology*, 4(6), 1577–1590.

Zhang, Z., & Michniak-Kohn, B. B. (2012). Tissue Engineered Human Skin Equivalents. *Pharmaceutics*, 4(1), 26–41. <https://doi.org/10.3390/pharmaceutics4010026>

CHAPTER III: Microvascular network development *in vitro*

III.1 Introduction

Successful transplantation of bioengineered tissues, such as skin, will require the development of strategies that can quickly restore oxygen and nutrients supply to the tissue to ensure its proper function and survival. This is particularly important in large grafts since diffusion is often limited to <1mm thick tissues and formation of new vessels by angiogenesis can take several days, often resulting in poor graft take (Mooney & Mikos, 1999). However, if graft and host vessels are present and in close proximity, anastomoses between graft and host vessels can occur rapidly and guarantee graft acceptance soon after transplantation (Converse, Smahel, Ballantyne, & Harper, 1975; Laschke & Menger, 2012). Thus, the generation of a pre-assembled microvascular network within the graft is one of the strategies that could support the rapid re-establishment of blood supply to the graft and significantly improve the outcome of transplantation.

In recent years, a number of approaches have been developed to generate capillary-like structures *in vitro*. Some of these efforts have attempted to identify agents that can stimulate angiogenesis (Matkar, Ariyagunaratnam, Leong-Poi, & Singh, 2017). Other studies have explored the role of matrix components and endothelial cell type in different systems (i.e., microfluidics, spheroid, monolayer). All of these approaches have their advantages and limitations, as discussed in several comprehensive reviews (Auger, Gibot, & Lacroix, 2013; E. Saik, K. McHale, & L. West, 2012; Lovett, Lee, Edwards, & Kaplan, 2009; Rouwkema & Khademhosseini, 2016; van Hinsbergh, Collen, & Koolwijk, 2001; Wong, Chan, Kamm, & Tien, 2012). Although there has been considerable progress in the generation of capillary-like structures *in vitro*, there is still a lack of understanding on the particular role of each component known to control angiogenesis and network morphology. Moreover, the heterogeneity between protocols, such as matrices scaffolds, cell sources, cell density and media composition used makes it difficult to interpret, compare and translate some of the findings to different culture systems, which often requires optimization and fine-tuning of culture conditions (Staton et al., 2004). Better understanding of these principles might offer a way to precisely control endothelial network formation and morphology *in vitro* and *in vivo*.

The main aim of this chapter is the optimization of culture conditions to successfully induce endothelial network formation in collagen type I gels, a step towards the generation of a vascularized full-thickness skin equivalent. In addition, we aimed at finding conditions that could significantly accelerate angiogenesis and reduce gel contraction. These factors are particularly important for successful engraftment of a functional vascularized skin equivalent that could rapidly anastomose with the host vasculature to restore blood perfusion to the graft.

III.2 Materials and methods

III.2.1. Cell culture

Human umbilical vein endothelial cells (HUVECs) and human dermal fibroblasts were cultured at 37°C in 5% CO₂ in EGM2 Endothelial Cell Growth Medium (Lonza). Culture media was changed every 2 days. Endothelial cells (ECs) and fibroblasts (FBs) were routinely passaged at ~80% confluency and were discarded at passage 8 and 12, respectively, before reaching senescence. For live visualization of endothelial cell sprouting and network formation, ECs were transfected at passage 2 with lentivirus overexpressing red fluorescent protein (RFP), kindly donated by Dr. Dai at Rensselaer Polytechnic Institute. Dermal fibroblasts were not labeled.

III.2.2. Preparation of telo- and atelo-collagen type I gels

Endothelial cells and dermal fibroblasts were harvested using 0.25% Trypsin–EDTA, and then combined in a single tube at the desired EC:FB ratio and cell density. Collagen hydrogel precursor (Rat tail, telo-collagen type I, Corning; or bovine hide, atelo-collagen type I, Advanced Biomatrix) was diluted to 2 or 3 mg/mL and kept on ice until use. The pellet of combined endothelial cells and dermal fibroblasts was resuspended in a collagen mixture consisting of 112.5 µL of collagen, 7.5 µL of fetal bovine serum (Atlanta Biologics), 15 µL of Reconstitution Buffer 10X (0.05 M NaOH, 2.2% NaHCO₃, and 200 mM HEPES), and 15 µL of HAM-F12 medium 10X (Gibco). The mixture was quickly deposited on a 12-well culture plate or 12-well Transwell-insert and allowed to crosslink at 37°C for 30 minutes. EGM2 medium was then added to the well and changed every day until the end of the experiment.

III.2.3. Analysis of RFP-expressing HUVEC area coverage

For each quantification, top-view images of the entire gel size were acquired on a Nikon Eclipse Ti-E inverted fluorescence microscope (Nikon Instruments, USA) by automatic stitching of multiple adjacent frames and then processed through Angiotool software (Zudaire, Gambardella, Kurcz, & Vermeren, 2011). Briefly, Angiotool identifies vessel profiles using a skeletonization approach (Figure III.2.1). Parameters measured by Angiotool include average and total vessel length, “branching index” (branch points/unit area of the explant), and percentage of total vessels. Segments inferior to 20 µm were considered to be single cells or background noise and were automatically removed from the analysis. Due to the 3-

dimensional distribution of endothelial networks in the collagen gels, only the percentage of total vessels was used as read-out to accurately compare different experimental conditions.

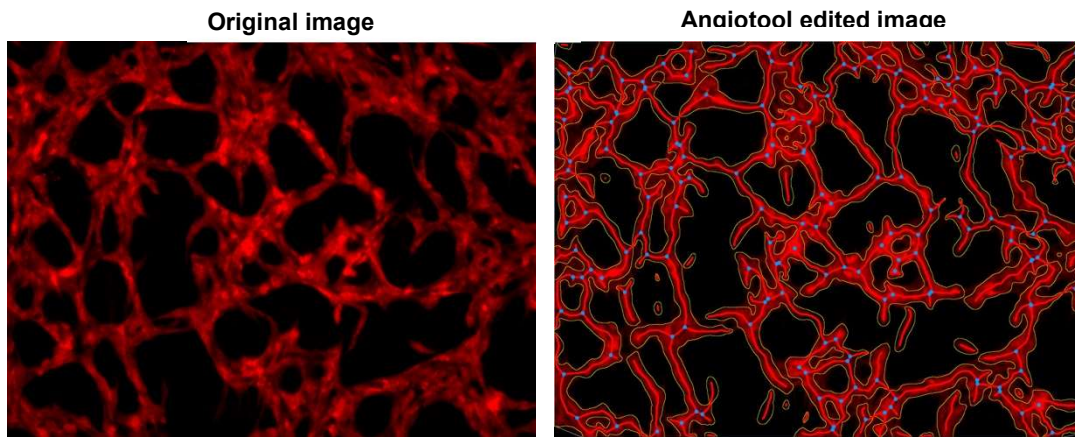


Figure III.2.1 – Representative image of endothelial cell networks in 3 mg/mL collagen type I gel at day 10 (left) and resulting image after analysis in Angiotool software (right). The vessels outlines are shown in yellow, the skeletons in red and the branching points in blue.

III.2.4. Confocal fluorescence and reflectance microscopy of collagen gels

For immunofluorescence analysis, collagen gels were fixed in 4% paraformaldehyde for 30 minutes and incubated overnight at 4°C with primary monoclonal antibodies anti-collagen IV (mouse; 1:200, clone COL-94; Abcam). The next day, the gels were washed three times with PBS and incubated for 1 hour at room temperature with anti-mouse IgG H&L secondary antibodies Alexa Fluor™ 568 (goat, 1:500; Abcam). To simultaneously visualize collagen fibers density and distribution in the collagen gels, confocal reflectance microscopy (CRM) was performed using a confocal microscope (Zeiss LSM 510 Meta) with a 60x 1.2 N.A. water immersion lens. The collagen gels were excited with 488 nm laser, and light between 485 nm and 495 nm was collected. Z-stack images were processed with Fiji (ImageJ) software. For 3-D reconstruction of vessel structures, Z-stack confocal images (1 μm between sections) were saved in the LSM format and processed using Imaris software (Bitplane, USA).

III.2.5. Statistical analysis

Statistical analyses were performed using Prism 7 software (GraphPad, USA). Data are expressed as mean standard deviation. When the means of 2 variables of more than 2 groups were compared, a two-way ANOVA analysis was performed. Results were considered significant when the P-value (P) < 0.05: * = P < 0.05, ** = P < 0.01, *** = P < 0.001, **** = P < 0.0001, ns = non-significant.

III.3 Results

III.3.1. The effect of collagen type I concentration in vessel formation and gel contraction *in vitro*

Extracellular matrix proteins, such as collagen type I, have unique mechanical properties that have been shown to significantly influence angiogenesis. The concentration of collagen precursor is a key determining factor of the mechanical structure and stiffness of collagen gels. We evaluated vessel density in collagen type I gels by varying the collagen precursor concentration and total density of seeded endothelial cells and dermal fibroblasts. Live cell imaging analysis at day 5 showed that the initial concentration of collagen had a significant effect on vascular network formation (Figure III.3.1 and Figure III.3.2). Particularly, RFP-

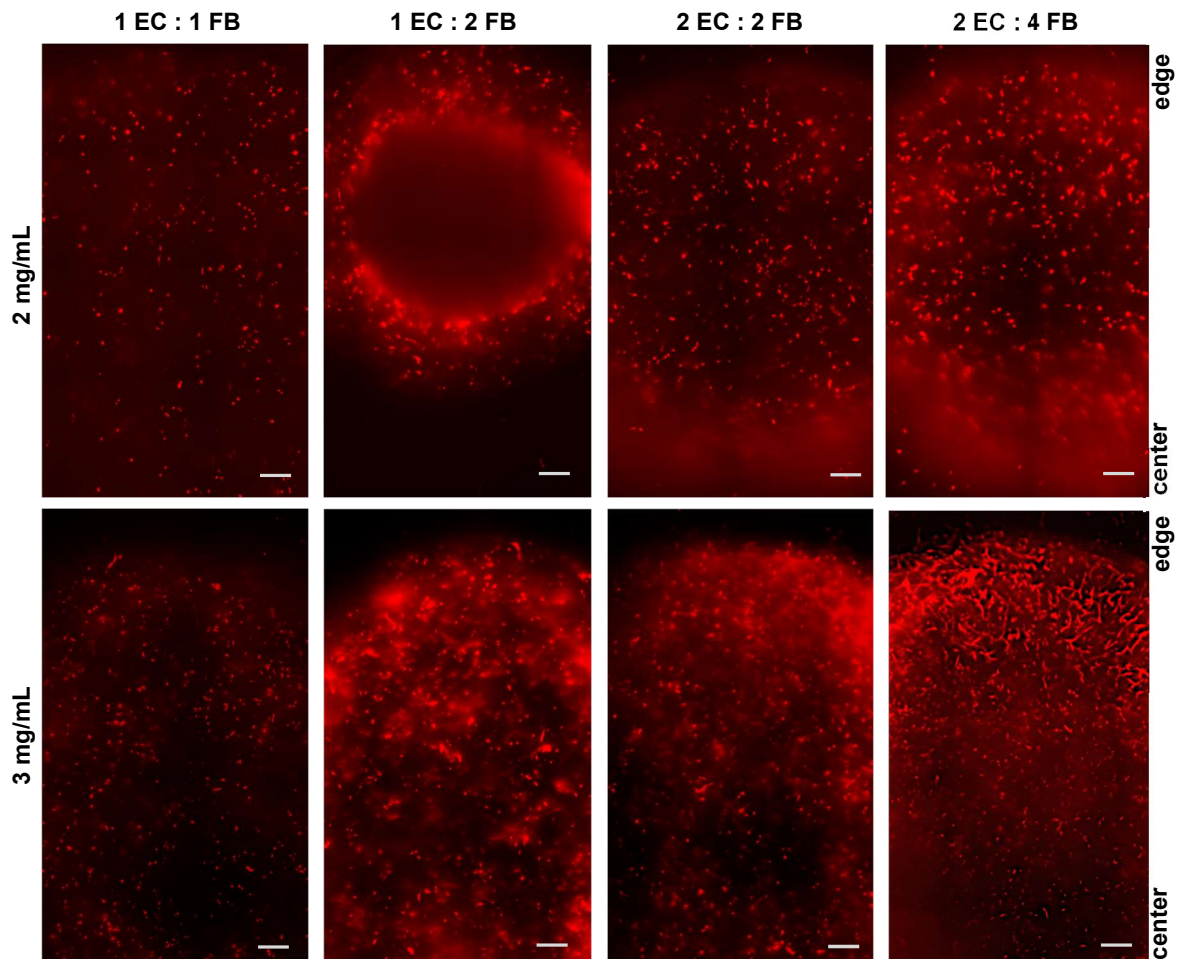


Figure III.3.1- Live epifluorescence imaging of 2 and 3 mg/mL collagen type I gels at day 5 with varying number of endothelial cells and fibroblasts ($\times 10^5$ cells). Representative images of center and edge regions of collagen gels containing RFP-expressing HUVEC and dermal fibroblasts. Scale bar: 100 μm .

expressing HUVEC in collagen gels at an initial concentration of 2 mg/mL showed significantly less RFP+ area coverage than in 3 mg/mL collagen gels, indicative of poor survival and diminished sprouting of endothelial cells. Moreover, vessel-like structures were found near the edge of 3 mg/mL gels at 2 EC: 4 FB ($\times 10^5$ cells). A decrease in the initial gel size was also observed at day 5 in both 2 and 3 mg/mL collagen gels, which was shown to be more pronounced in the 2 mg/mL collagen gels (Figure III.3.3).

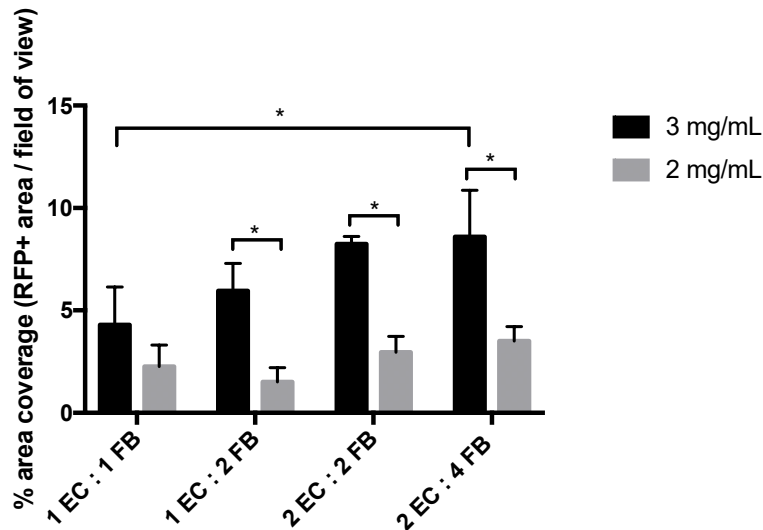


Figure III.3.2 – Area covered at day 5 by RFP-expressing HUVEC in 2 and 3 mg/mL collagen type I gels at varying number of endothelial cell and fibroblasts ($\times 10^5$ cells). Measurements were carried out using 3 images from each experimental condition. The mean values \pm SEM are represented. * - p-value \leq 0.1.

In an attempt to reduce contraction, collagen gels were deposited on top of a Transwell-insert membrane. We hypothesized that the Transwell-insert containing a porous PET membrane of 4 μ m in diameter could act as an anchor and counteract cell contractile forces. Results showed that gel contraction at day 5 was significantly reduced by approximately 96% when collagen gels were deposited on top of the Transwell porous membrane (Figure III.3.3). No significant differences in gel contraction were observed between gels with 2.0×10^5 or 4.0×10^5 fibroblasts.

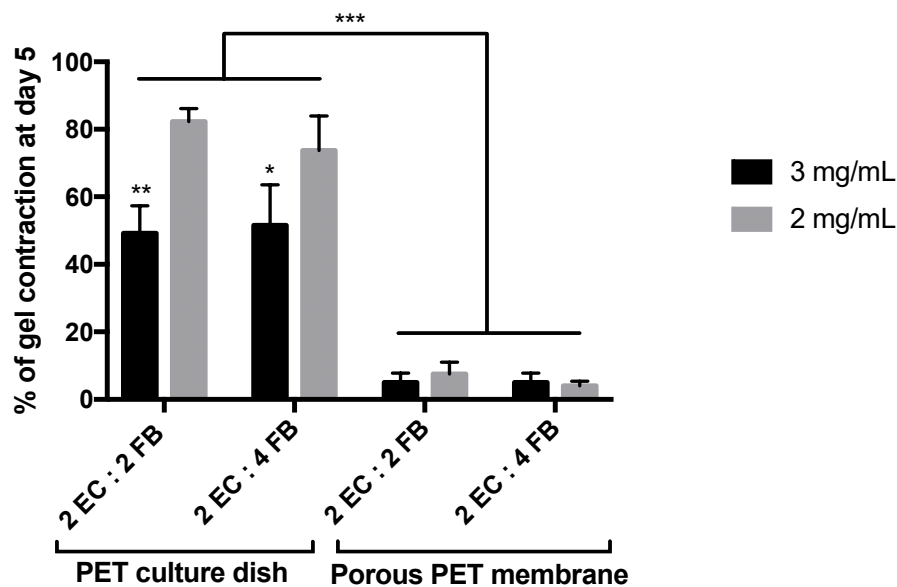


Figure III.3.3 - Percentage of gel contraction observed at day 5 at varying number of endothelial cells and fibroblasts ($\times 10^5$ cells). 2 and 3 mg/mL collagen gels were crosslinked directly on top of a PET culture dish surface or a Transwell-insert porous PET membrane. Measurements were carried out using 3 images from each experimental condition. The mean values \pm SEM are represented. * - p-value \leq 0.1, ** - p-value \leq 0.01, *** - p-value \leq 0.001.

III.3.2. The effect of collagen source and extraction method on vessel formation *in vitro*

Another important factor in endothelial network formation is the source and extraction method of fibrillar collagen used to form gels. Here, we co-cultured RFP-expressing HUVEC and dermal fibroblasts in telo-collagen type I solution extracted from rat tail tendon and atelo-collagen type I solution extracted from bovine hide. Live imaging analysis at day 15 showed decreased angiogenesis in bovine atelo-collagen type I gels (Figure III.3.4). More vessel-like structures were formed near the edges of the collagen gels when 2×10^5 fibroblasts were combined with 2×10^5 endothelial cells. In addition, no significant differences were observed in gel size overtime between atelo and telo-collagen type I gels except at the highest density of fibroblasts tested (Figure III.3.5). Bovine atelo-collagen gels at 2 EC : 2 FB ($\times 10^5$) ratio contracted 15% more than rat tail telo-collagen gels. In further optimization studies, rat tail collagen was chosen as the optimal biomaterial to generate vascularized gel constructs.

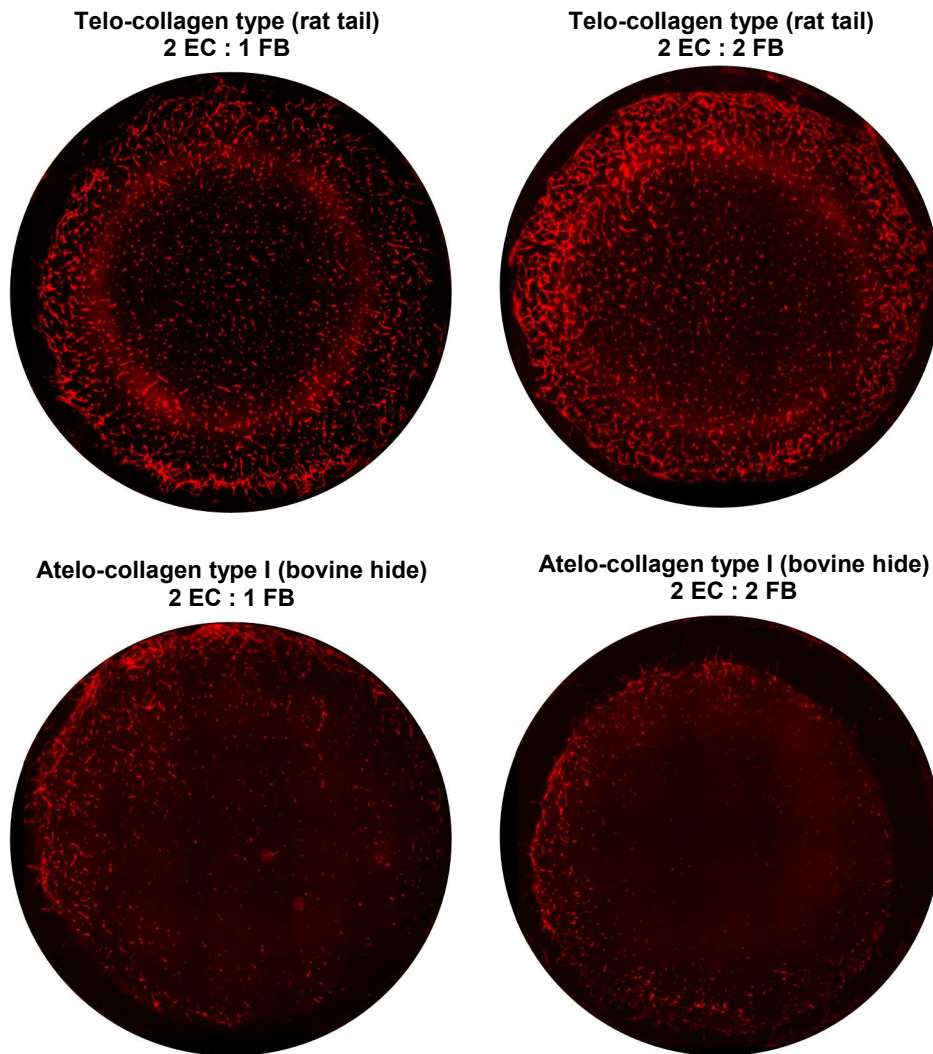


Figure III.3.4 - Live epifluorescence imaging of Telo and Atelo-collagen type I gels at day 5 with varying number of endothelial cells and fibroblasts ($\times 10^5$ cells). Representative top view images of whole collagen gels containing RFP-expressing HUVEC and dermal fibroblasts.

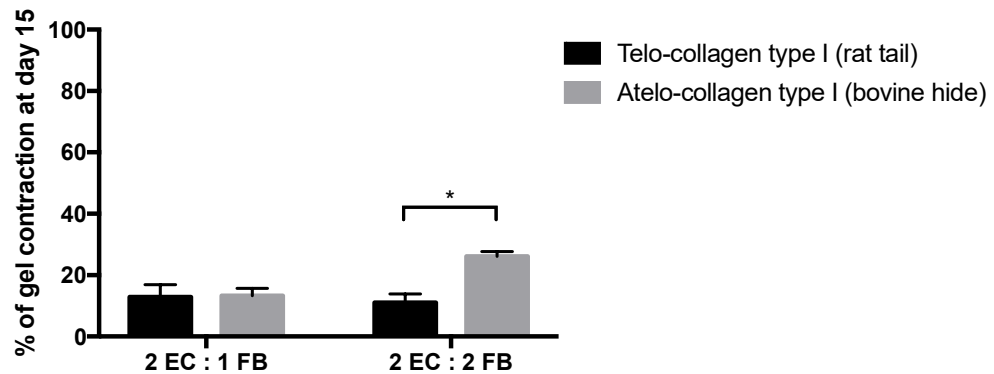


Figure III.3.5 - Percentage of gel contraction observed at day 15 at varying number of endothelial cells and fibroblasts ($\times 10^5$ cells). Telo- and Atelo-collagen type I gels were crosslinked directly on top of a Transwell-insert porous PET membrane. Measurements were carried out using 3 images from each experimental condition. The mean values \pm SEM are represented. * - p-value ≤ 0.1 .

III.3.3. The effect of endothelial cells to fibroblasts ratio and total cell number in endothelial network formation *in vitro*

As previously described, increasing number of endothelial cells and fibroblasts in 3 mg/mL collagen gels significantly improved angiogenesis *in vitro*. However, the percentage of area covered by RFP-expressing HUVEC was still low (~ 10 - 15% of the total gel area), and vessels only formed near the borders of the gel at the highest cell density tested. To induce homogeneous vessel formation in the entire gel structure, the number of encapsulated endothelial cells was increased from 3.0 to 5.0×10^5 and mixed with dermal fibroblasts at 1:1 and 1:2 ratios. Live imaging analysis of collagen gels at day 5 showed higher vessel density with increasing numbers of seeded endothelial cells and fibroblasts (Figure III.3.6). However, when more than 5.0×10^5 endothelial cells and fibroblasts were cultured, gels seeded on top of Transwell inserts contracted and detached from the porous Transwell membrane. In addition, with increasing cell densities more vascular structures were observed both in the center of the gels and at the edge of the gels (Figure III.3.7).

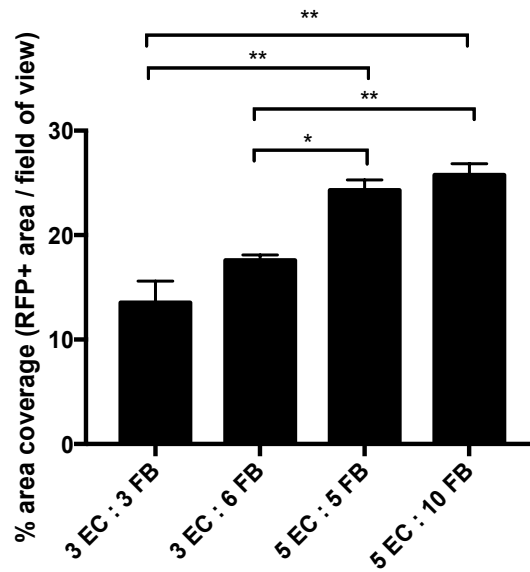


Figure III.3.6 - Area covered at day 5 by RFP-expressing HUVEC in 3 mg/mL collagen type I gels at varying number of endothelial cell and fibroblasts ($\times 10^5$ cells). Measurements were carried out using 3 images from each experimental condition. The mean values \pm SEM are represented. * - p-value \leq 0.1, ** - p-value \leq 0.01.

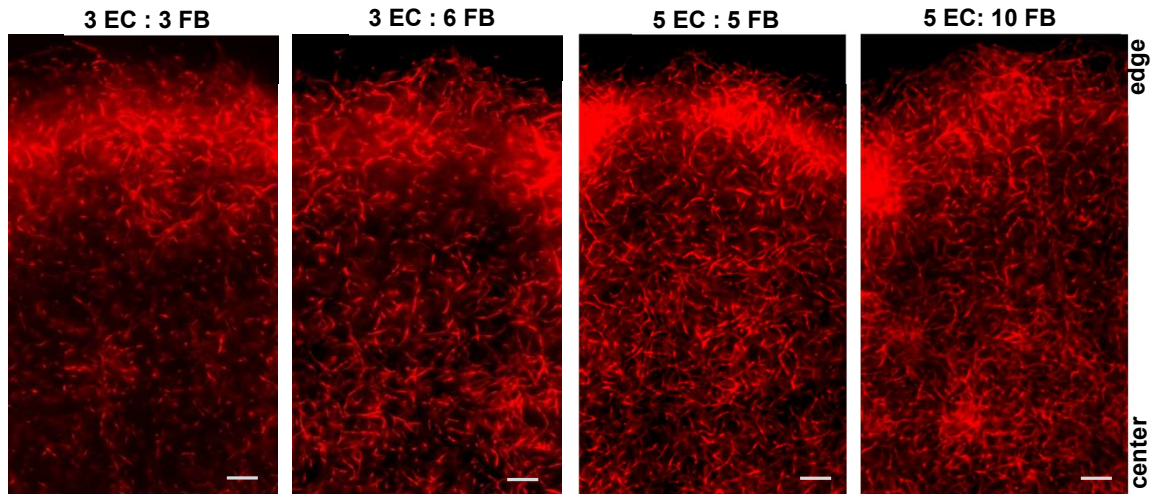


Figure III.3.7- Live epifluorescence imaging of 3 mg/mL collagen type I gels at day 5 with varying number of endothelial cells and fibroblasts ($\times 10^5$ cells) . Representative images of center and edge regions of collagen gels containing RFP-expressing HUVEC and dermal fibroblasts.

Scale bar: 100 μ m.

III.3.4. The effect of vascular endothelial growth factor media supplementation in the absence of dermal fibroblasts in endothelial network formation *in vitro*

We have shown that increasing numbers of endothelial cells and fibroblasts enhances endothelial network formation. However, 5×10^5 endothelial cells and 1×10^6 fibroblasts was the maximum number that could be incorporated in collagen gels to successfully induce endothelial network self-assembly without significant gel contraction in a Transwell-insert. We attempted to reduce the number of fibroblasts in the collagen gels by recapitulating the proangiogenic effects of fibroblasts through Vascular Endothelial Growth Factor (VEGF) supplementation to the culture medium. The concentration of VEGF in the EGM2 culture medium was increasing by 50-fold, at a final concentration of 25 ng/mL. Results showed that supplementation of 25 ng/mL VEGF alone to the EGM2 medium did not support endothelial network formation *in vitro* (Figure III.3.8). Co-culture of endothelial cells and fibroblasts in collagen gels successfully induced endothelial cell sprouting and network formation overtime, an indication that cell-to-cell interactions and/or secretion of other important proangiogenic factors besides VEGF by dermal fibroblasts is required to successfully induce angiogenesis *in vitro*.

III.3.5. The effect of fetal bovine serum in endothelial network formation *in vitro*

To further understand the impact of fetal bovine serum, a main component of EGM2 media, in angiogenesis, the content of FBS in EGM2 medium was increased by 10%. Live cell imaging analysis from day 1 until day 9 showed that supplementation of fetal bovine serum to EGM2 media significantly accelerated angiogenesis compared to the control condition (EGM2; 2% FBS) (Figure III.3.9).

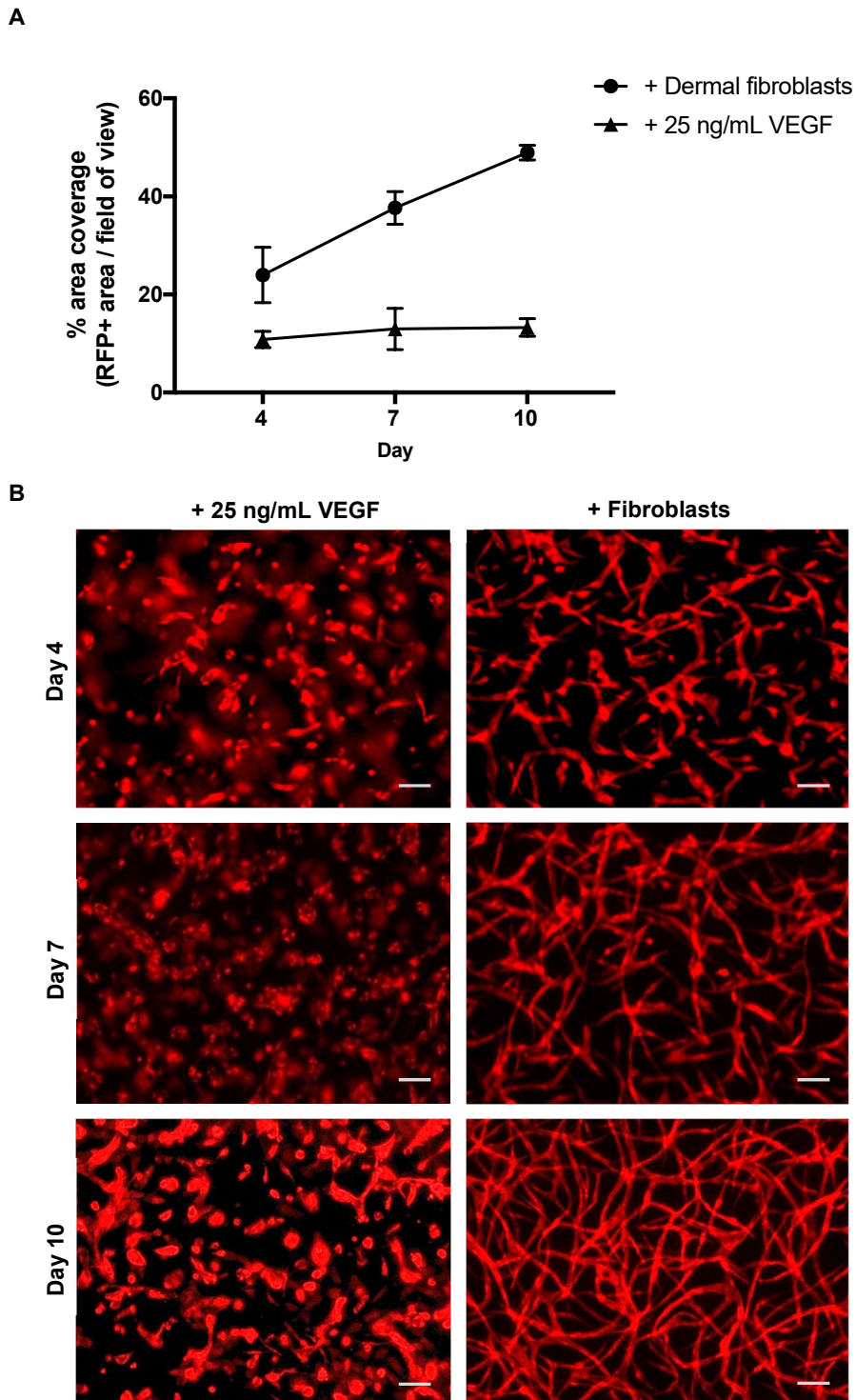


Figure III.3.8 – Collagen gels containing RFP-expressing HUVEC in the presence of dermal fibroblasts or with VEGF media supplementation in the absence of fibroblasts. **(A)** Area covered by RFP-expressing HUVEC in 3 mg/mL collagen type I gels at 5 EC : 10 FB ($\times 10^5$ cells) ratio. Measurements were carried out using 3 images from each experimental condition. The mean values \pm SEM are represented. **(B)** Live epifluorescence imaging of 3 mg/mL collagen type I gels, at day 4, 7 and 10; at 5 EC : 10 FB ($\times 10^5$ cells) ratio. Representative images of center region of collagen gels. Scale bar: 100 μ m.

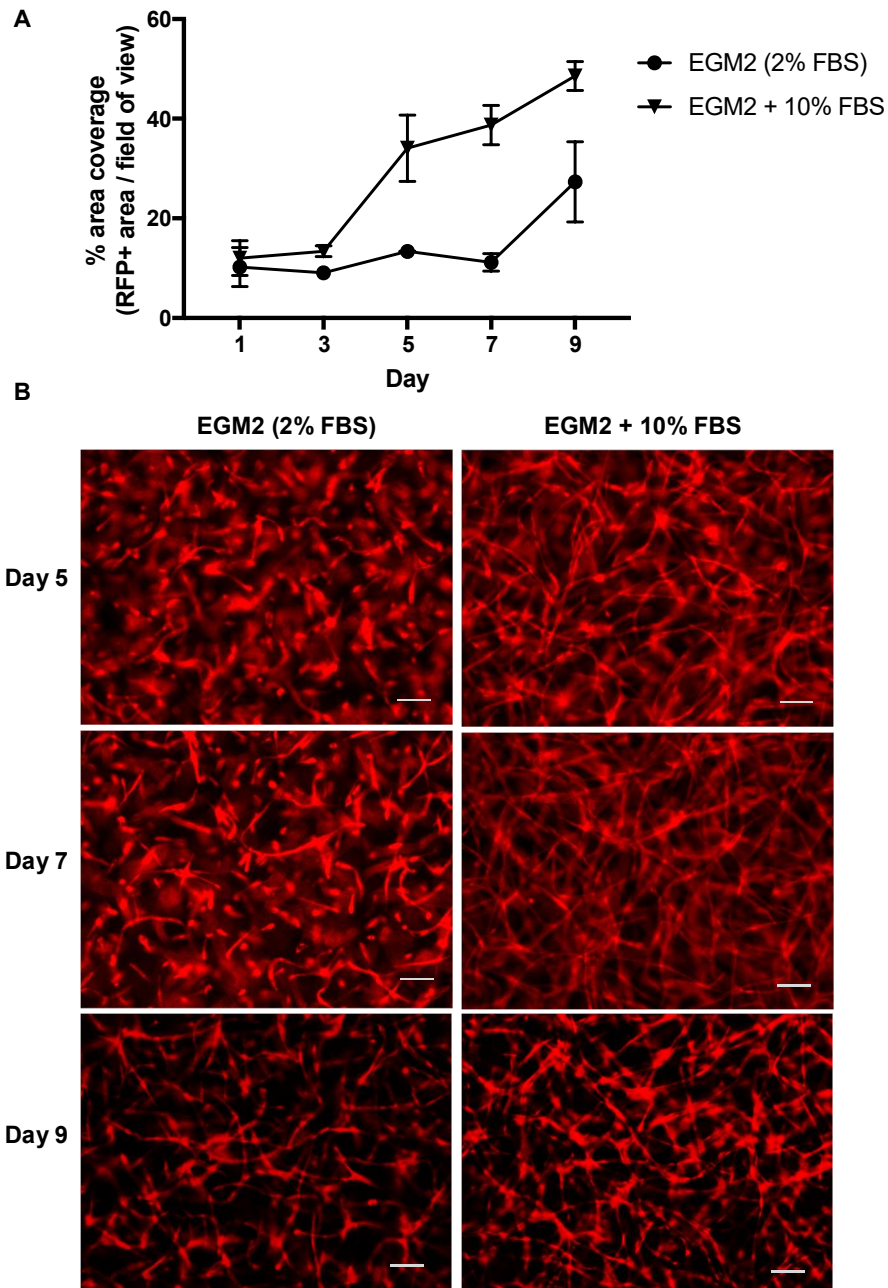


Figure III.3.9 - Collagen gels containing RFP-expressing HUVEC in the presence of 2% or 2 % supplemented with 10% Fetal Bovine Serum. **(A)** Area covered by RFP-expressing HUVEC in 3 mg/mL collagen type I gels at 5 EC : 10 FB ($\times 10^5$ cells) ratio. Measurements were carried out using 3 images from each experimental condition. The mean values \pm SEM are represented. **(B)** Live epifluorescence imaging of 3 mg/mL collagen type I gels, at day 5, 7 and 9; at 5 EC : 10 FB ($\times 10^5$ cells) ratio. Representative images of center region of collagen gels. Scale bar: 100 μ m.

III.3.6. 3D organization of endothelial cell networks *in vitro*

To assess the three-dimensional structure of the self-assembled endothelial cell networks within the collagen gels, z-stack confocal images were taken at day 10 and processed through Imaris software to generate 3-dimensional reconstructed images. Gels were approximately 50 μm thick and at least 2-3 layers of endothelial networks were found to be interconnected along the z-axis (Figure III.3.10). Moreover, endothelial networks generated open lumens and secreted collagen type IV, a main component of the basement membrane of the capillary endothelium. Highly packed collagen fibers were also found surrounding the vessel structures and were particularly denser in vicinity of endothelial cells (Figure III.3.11).

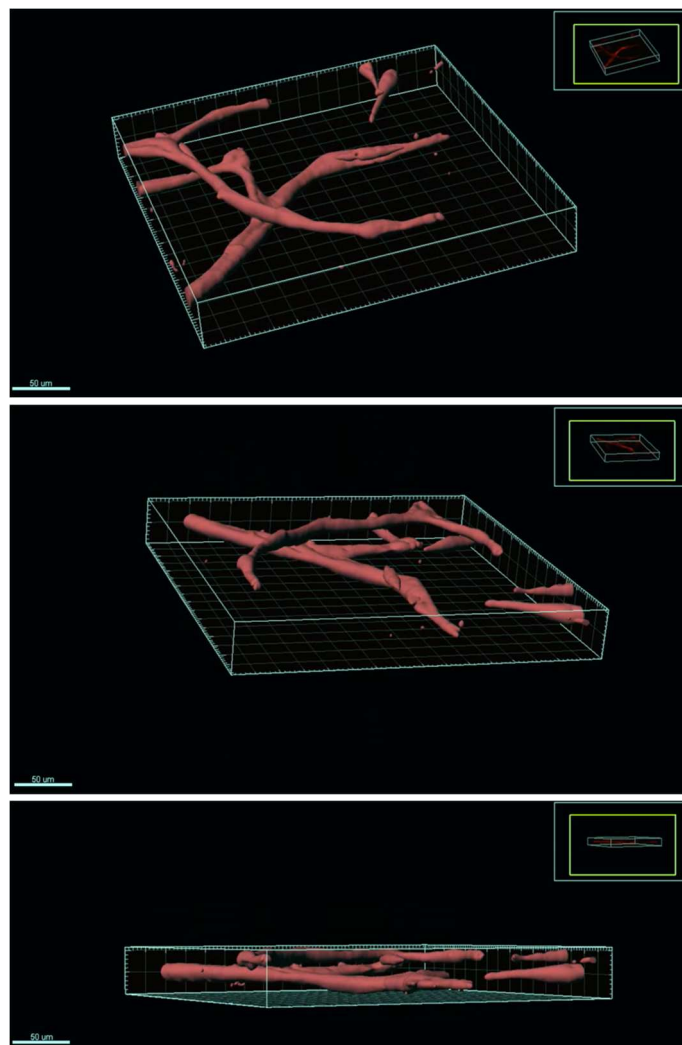


Figure III.3.10 – 3D dimensional reconstruction of self-assembled endothelial networks *in vitro*. Z-stack images of 3 mg/mL collagen gels containing RFP-expressing HUVEC and dermal fibroblasts at 15 days. Scale bar: 50 μm . Grids define the 3D space.

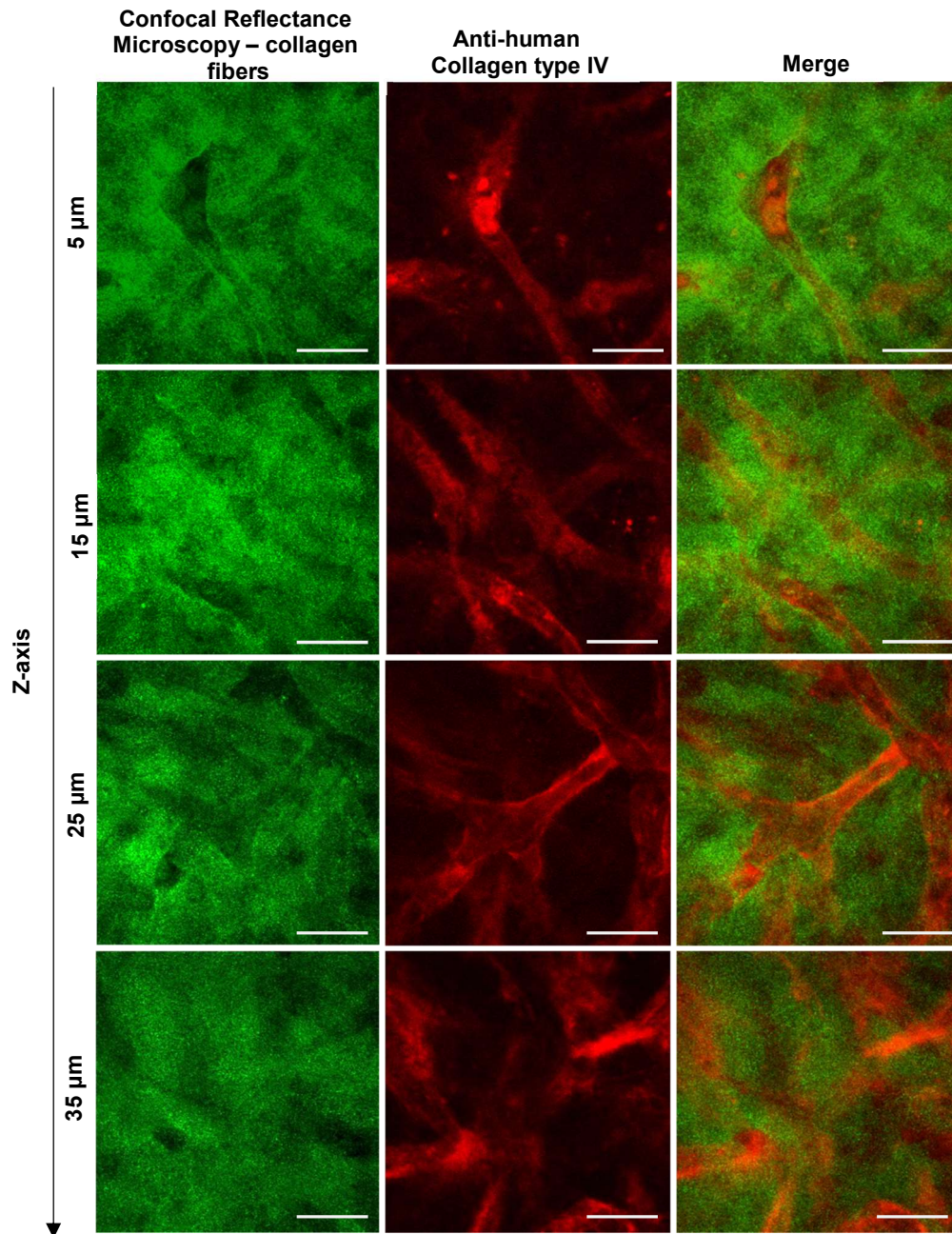


Figure III.3.11 – Confocal reflectance and fluorescence microscopy of 3 mg/mL collagen gels seeded with 5 EC: 10 FB ($\times 10^5$). Unlabeled HUVEC and dermal fibroblasts were co-cultured in 3 mg/mL collagen for 15 days. Confocal reflectance microscopy of collagen matrix is shown in green and immunostaining for secreted collagen type IV is shown in red. Scale bar: 50 μm .

III.4 Discussion

Here, we have shown successful self-assembly of endothelial networks in collagen type I gels, an important step towards incorporation of a functional microvasculature system in 3D bioprinted skin equivalents. Besides endothelial self-assembly, methods to generate capillary-like networks involving pre-patterning of channels lined with EC within a scaffold have been extensively explored (Chaturvedi et al., 2015; Hoch, Tovar, & Borchers, 2014). This strategy offers the advantage of an easy connection to a flow system, which might be of great interest particularly in the development of *in vitro* models of disease and for drug development. However, vessel patterning is often achieved with non-realistic designs and small vessel diameters are often difficult to generate and perfuse (Hasenberg et al., 2015). In contrast, when endothelial cells are allowed to self-assemble into vessel-like structures, they form complex morphologies with patterns that resemble the *in vivo* situation with lumen sizes of the same order of magnitude as native capillaries (Montaño et al., 2010). Moreover, the mechanisms of angiogenesis and lumen formation can only be studied by the latter models. For these reasons, self-assembly of endothelial networks was preferred.

In this chapter, we first evaluated the effect of collagen concentration and cell seeding density in endothelial network formation *in vitro*. Results showed that 2 mg/mL collagen gels contracted significantly more than 3 mg/mL collagen gels. In agreement with this finding, Zhu *et al.* have reported that gels prepared with an initial concentration of 0.75 mg/ml contracted more rapidly and to a smaller final size than gels prepared from 2 mg/ml initial collagen concentration (Zhu et al., 2001). In addition, increasing cell densities improved vessel formation *in vitro*, however increasing cell-induced gel contraction was also observed at the highest cell density tested. In an attempt to reduce contraction, collagen gels were deposited on top of a Transwell-insert membrane. We hypothesized that the Transwell-insert containing a porous PET membrane of 4 μm in diameter could act as an anchor and counteract cell contractile forces. Contraction was reduced by 96% when collagen gels were directly deposited on top of the Transwell-insert porous membrane.

Furthermore, we evaluated the effect of the source and extraction method of fibrillar collagen in endothelial network formation. Telo-collagen type I solution extracted from rat tail tendon and atelo-collagen type I solution extracted from bovine hide were compared. Due to its low immunogenicity, atelo-collagen is often a preferred biomaterial for tissue engineering and clinical applications (Wysocki, Sacewicz, Wiktorska, & Niewiarowska, 2007). However, here we show that atelo-collagen did not induce endothelial network formation *in vitro*. It has been reported that the removal of telo-peptides by pepsin-treatments in atelo-collagen often results in loss of the collagen fibril pattern due to the roles of the C- and N-terminus telo-peptides in

cross-linking and fibril formation (Holmes, Kirk, Tronci, Yang, & Wood, 2017). The presence of intact telopeptides in telo-collagen has been reported to facilitate rapid assembly of collagen into fibrils. More specifically, telo-peptides form intermolecular crosslinks that stabilizes collagen fibrils and significantly increase tensile strength (Shayegan, Altindal, Kiefl, & Forde, 2016). Pepsin-treated collagen lack telo-peptides and form less constrained fibrils. In addition, C-terminal telo-peptides are adjacent to MMP cleavage sites, suggesting a role in regulating fibril degradation. Our results suggest an important role of telo-peptides domains in angiogenesis which appears to be directly linked to a dynamic and tightly controlled relationship between collagen fibrils assembly, stabilization and degradation.

We have also evaluated the effect of VEGF supplementation in the absence of dermal fibroblasts in endothelial network formation. Results showed that VEGF alone was not able to rescue the pro-angiogenic effect of dermal fibroblasts in collagen gels. This result seems to suggest that fibroblasts have an important stabilization role on vessel formation through direct interaction with endothelial cells and/or through secretion of other pro-angiogenic factors besides VEGF. In agreement with our data, Whisler *et al.* have shown in a microfluidic system that in a non-contact co-culture system of endothelial cells and lung fibroblasts, endothelial networks quickly regressed (Whisler, Chen, & Kamm, 2014). However, when fibroblasts were in contact with ECs, networks acquired a stable morphology and high perfusability. Moreover, it has been shown that fibroblasts enhance gel stiffness and lumen formation by adapting the ECM thorough secretion of matrix proteins (Newman, Nakatsu, Chou, Gershon, & Hughes, 2011). In future work, the individual effects of specific growth factors known to be involved in angiogenesis is worth exploring in more depth.

Fetal bovine serum is widely used as a supplement to the culture of several cell types due to its high levels of growth stimulatory factors (Hornsby, Sturek, Harris, & Simonian, 1983; Jayme & Blackman, 1985). We investigated the effect of FBS in angiogenesis *in vitro* by supplementing egm2 medium with 10% FBS. Results showed that angiogenesis was significantly enhanced at day 3 under high FBS concentration culture conditions. These results suggest the contribution of other pro-angiogenic and mitogenic factors in endothelial network formation besides heparin, EGF, IGF, VEGF and hydrocortisone, present in the EGM2 medium. In addition, a possible higher content of these components in the serum might also have an impact on angiogenesis acceleration *in vitro*. In addition, we have shown that at a later stage of angiogenesis, non-supplemented EGM2 medium quickly recovered and no significant differences in vessel morphology were observed between the two conditions. Acceleration of *in vitro* angiogenesis is particularly important in successful engraftment of skin equivalents as the presence of newly formed vessels that can quickly anastomose with the

host vessels can significantly accelerate graft “take” and improve graft survival upon transplantation.

III.5 Conclusions

The present chapter explores the development of a 3D vascularized collagen type I gel, the second step towards the development of full-thickness 3D bioprinted vascularized skin equivalent. Results have shown that increasing collagen concentration and cell densities can significantly increase vessel formation in collagen gels. Cell-induced gel contraction was observed at high endothelial and fibroblast cell densities which can limit the number of cells that can be incorporated in collagen gels. However, gel contraction was reduced by 96% when gels were seeded on top of a porous Transwell-insert membrane.

Moreover, we have shown that bovine atelo-collagen type I gels did not support endothelial network formation *in vitro*. Our results suggest an important role of telo-peptides domains in vessel formation, particularly in collagen fibrils assembly, stabilization and degradation in early-stage angiogenesis. In addition, the inclusion of fibroblasts was found to be essential to promote angiogenesis and VEGF alone did not support vessel formation *in vitro*. Interestingly, supplementation of FBS to the EGM2 medium accelerated angiogenesis *in vitro*, without significant effects in overall vessel morphology. At day 15, interconnected vessel structures with open lumens were observed, as well secretion of endothelium basement membrane collagen IV, indicative of normal vessel maturation.

Together, these results demonstrate the successful generation of a vascularized collagen gel that will be incorporated into a skin equivalent via 3D bioprinting, explored in detail in chapter IV.

III.6 References

- Auger, F. a, Gibot, L., & Lacroix, D. (2013). The pivotal role of vascularization in tissue engineering. *Annual Review of Biomedical Engineering*, 15, 177–200. <https://doi.org/10.1146/annurev-bioeng-071812-152428>
- Chaturvedi, R. R., Stevens, K. R., Solorzano, R. D., Schwartz, R. E., Eyckmans, J., Baranski, J. D., Stapleton, S. C., Bhatia, S. N., & Chen, C. S. (2015). Patterning vascular networks in vivo for tissue engineering applications. *Tissue Engineering. Part C, Methods*, 21(5), 509–517. <https://doi.org/10.1089/ten.TEC.2014.0258>
- Converse, J. M., Smahel, J., Ballantyne, D. L. ., & Harper, A. D. (1975). Inosculation of vessels of skin graft and host bed: a fortuitous encounter. *British Journal of Plastic Surgery*, 28(1955), 274–282.
- E. Saik, J., K. McHale, M., & L. West, J. (2012). Biofunctional Materials for Directing Vascular Development. *Current Vascular Pharmacology*, 10(3), 331–341. <https://doi.org/10.2174/157016112799959314>
- Hasenberg, T., M??hleder, S., Dotzler, A., Bauer, S., Labuda, K., Holnthoner, W., Redl, H., Lauster, R., & Marx, U. (2015). Emulating human microcapillaries in a multi-organ-chip platform. *Journal of Biotechnology*, 216, 1–10. <https://doi.org/10.1016/j.jbiotec.2015.09.038>
- Hoch, E., Tovar, G. E. M. G. E. M., & Borchers, K. (2014). Bioprinting of artificial blood vessels: Current approaches towards a demanding goal. *European Journal of Cardio-Thoracic Surgery*, 46(5), 767–778. <https://doi.org/10.1093/ejcts/ezu242>
- Holmes, R., Kirk, S., Tronci, G., Yang, X., & Wood, D. (2017). Influence of telopeptides on the structural and physical properties of polymeric and monomeric acid-soluble type I collagen. *Materials Science and Engineering: C*, 77, 823–827. <https://doi.org/https://doi.org/10.1016/j.msec.2017.03.267>
- Hornsby, P. J., Sturek, M., Harris, S. E., & Simonian, M. H. (1983). Serum and growth factor requirements for proliferation of human adrenocortical cells in culture: comparison with bovine adrenocortical cells. *In Vitro*, 19(11), 863–869.
- Jayme, D. W., & Blackman, K. E. (1985). Culture media for propagation of mammalian cells, viruses, and other biologicals. *Advances in Biotechnological Processes*, 5, 1–30.
- Laschke, M. W., & Menger, M. D. (2012). Vascularization in tissue engineering: Angiogenesis versus inosculation. *European Surgical Research*, 48(2), 85–92. <https://doi.org/10.1159/000336876>
- Lovett, M., Lee, K., Edwards, A., & Kaplan, D. L. (2009). Vascularization Strategies for Tissue Engineering. *Tissue Engineering Part B: Reviews*, 15(3), 353–370. <https://doi.org/10.1089/ten.teb.2009.0085>
- Matkar, P. N., Ariyagunarajah, R., Leong-Poi, H., & Singh, K. K. (2017). Friends Turned Foes: Angiogenic Growth Factors beyond Angiogenesis. *Biomolecules*, 7(4), 74.

<https://doi.org/10.3390/biom7040074>

- Montaño, I., Schiestl, C., Schneider, J., Pontiggia, L., Luginbühl, J., Biedermann, T., Böttcher-Haberzeth, S., Braziulis, E., Meuli, M., & Reichmann, E. (2010). Formation of human capillaries in vitro: the engineering of prevascularized matrices. *Tissue Engineering. Part A*, *16*(1), 269–282. <https://doi.org/10.1089/ten.tea.2008.0550>
- Mooney, D. J., & Mikos, A. G. (1999). Growing new organs. *Scientific American*, *280*(4), 60–65.
- Newman, A. C., Nakatsu, M. N., Chou, W., Gershon, P. D., & Hughes, C. C. W. (2011). The requirement for fibroblasts in angiogenesis: fibroblast-derived matrix proteins are essential for endothelial cell lumen formation. *Molecular Biology of the Cell*, *22*(20), 3791–3800. <https://doi.org/10.1091/mbc.E11-05-0393>
- Rouwkema, J., & Khademhosseini, A. (2016). Vascularization and Angiogenesis in Tissue Engineering: Beyond Creating Static Networks. *Trends in Biotechnology*, *34*(9), 733–745. <https://doi.org/10.1016/j.tibtech.2016.03.002>
- Shayegan, M., Altindal, T., Kiefl, E., & Forde, N. R. (2016). Intact Telopeptides Enhance Interactions between Collagens. *Biophysical Journal*, *111*(11), 2404–2416. <https://doi.org/10.1016/j.bpj.2016.10.039>
- Staton, C. A., Stribbling, S. M., Tazzyman, S., Hughes, R., Brown, N. J., & Lewis, C. E. (2004). Current methods for assaying angiogenesis in vitro and in vivo. *International Journal of Experimental Pathology*, *85*(5), 233–248. <https://doi.org/10.1111/j.0959-9673.2004.00396.x>
- van Hinsbergh, V. W., Collen, a, & Koolwijk, P. (2001). Role of fibrin matrix in angiogenesis. *Annals of the New York Academy of Sciences*, *936*, 426–437. <https://doi.org/10.1111/j.1749-6632.2001.tb03526.x>
- Whisler, J. A., Chen, M. B., & Kamm, R. D. (2014). Control of perfusable microvascular network morphology using a multiculture microfluidic system. *Tissue Engineering. Part C, Methods*, *20*(7), 543–552. <https://doi.org/10.1089/ten.TEC.2013.0370>
- Wong, K. H. K., Chan, J. M., Kamm, R. D., & Tien, J. (2012). Microfluidic Models of Vascular Functions. *Annu. Rev. Biomed. Eng.*, *14*, 205–230. <https://doi.org/10.1146/annurev-bioeng-071811-150052>
- Wysocki, T., Sacewicz, I., Wiktorska, M., & Niewiarowska, J. (2007). [Atelocollagen as a potential carrier of therapeutics]. *Postepy higieny i medycyny doswiadczalnej (Online)*, *61*, 646–654.
- Zhu, Y. K., Umino, T., Liu, X. D., Wang, H. J., Romberger, D. J., Spurzem, J. R., & Rennard, S. I. (2001). Contraction of fibroblast-containing collagen gels: initial collagen concentration regulates the degree of contraction and cell survival. *In Vitro Cellular & Developmental Biology. Animal*, *37*(1), 10–16. [https://doi.org/10.1290/1071-2690\(2001\)037<0010:COFCCG>2.0.CO;2](https://doi.org/10.1290/1071-2690(2001)037<0010:COFCCG>2.0.CO;2)
- Zudaire, E., Gambardella, L., Kurcz, C., & Vermeren, S. (2011). A Computational Tool for Quantitative Analysis of Vascular Networks. *PLOS ONE*, *6*(11), e27385. Retrieved from <https://doi.org/10.1371/journal.pone.0027385>

CHAPTER IV: 3D Bioprinting of vascularized human skin

IV.1 Introduction

The creation of more complex skin models containing vasculature is significant for different applications. In regenerative medicine, there is a critical need for skin grafts that present better aesthetic and functional recapitulation of native skin aiming at complete integration of the graft onto, and into, the wounded tissue. One of the reasons cultured allografts cannot integrate with the host skin is the lack of a functional vasculature. Skin microvasculature not only promotes graft survival by supplying skin cells with oxygen and nutrients but also modulates inflammation and immune cell migration to the wound site (Pasparakis, Haase, & Nestle, 2014). Moreover, the presence of a vascularized bed has been shown to promote skin engraftment through microvascular connections between graft and recipient capillaries that surround the wound region (Gibot, Galbraith, Huot, & Auger, 2010; Tremblay, Hudon, Berthod, Germain, & Auger, 2005).

Despite many years of research to understand the origin of skin graft revascularization, it was not until recently that it became possible to answer some of the most controversial questions on the mechanisms of graft acceptance. The development of improved imaging techniques and animal models provided researchers with new tools to understand these mechanisms. Capla *et al.* demonstrated that skin graft revascularization occurs through recipient vascular ingrowth and simultaneous donor vascular regression (Capla et al., 2006). Recipient-derived endothelial cells use the donor vascular framework as a guiding conduit for vascular ingrowth. This dynamic process of regression and ingrowth events results in quick connection between the capillaries of the host and the graft. These findings suggest that successful skin revascularization is greatly dependent on a critical short window of time in which anastomosis needs to occur to reestablish blood flow and oxygenation to the wound site. The presence of a pre-existing vascular network accelerates this process facilitating the successful acceptance of the graft. In contrast, non-pre-vascularized grafts rely on a neovascularization process which can take 3 weeks until blood flow is restored (Tsur, Daniller, & Strauch, 1980). Failure in the reestablishment of the supply of oxygen and nutrients to the wound site often leads to graft rejection.

The development of new strategies to promote the graft-host angiogenic cross-talk that allows anastomosis and vascular integration of skin grafts is crucial to overcome the current limitations of skin graft acceptance. Approaches such as the *in vitro* generation of capillary-like networks embedded in engineered skin constructs before transplantation can not only yield faster integration within the host tissue but can also promote long-term skin homeostasis *in vivo*. Multiple approaches using 3D bioprinting technology have shown to successfully generate perfusable capillary-like structures *in vitro* (please see reviews by Hoch, Tovar, and

Borchers 2014 and Frueh et al. 2016 for further details). However, after gel contraction the final size of printed vessels usually ranges from 100–250 μm . This size is significantly larger than the capillaries in the skin microvasculature: < 26 μm at the superficial horizontal plexus and < 50 μm at the dermal-subcutaneous plexus. In addition, these studies have not yet shown integration of the vascularized constructs in the skin context.

The aim of this chapter is the development of a full-thickness vascularized 3D printed skin equivalent. Different printing protocols and culture conditions will be tested for optimal co-culture of endothelial cells, dermal fibroblasts and keratinocytes in a single bioprinted construct. Bioprinted skin grafts with and without ECFC will be characterized following engraftment in a SCID/bg mouse model. To further improve vessel function *in vivo*, we will assess the inclusion of human pericytes in bioprinted vascularized skin constructs. Successful incorporation of a functional microvascular network in a full-thickness 3D printed skin construct will not only be important for the success of permanent engraftment but also for the development of more complex skin models that better represent human skin.

IV.2 Materials and methods

IV.2.1. Cell culture

Keratinocytes were cultured in KGM Gold medium (Lonza), fibroblasts were cultured in Dulbecco's Modified Eagle Medium (DMEM; Gibco) supplemented with 10% fetal bovine serum (Atlanta Biologics) and 1% Pen/Strep (Gibco), and endothelial colony forming cells (ECFC) were cultured in EGM2 medium (Lonza). To visualize endothelial cells by real time imaging, fluorescent-labeled ECs were generated by transfecting lentivirus expressing RFP (Genecopoeia), according to the manufacturer's instructions. Fibroblasts, keratinocytes and ECFC-RFP were maintained in a humidified incubator at 37°C containing 5% CO₂. At approximately 80% confluency, cells were routinely passaged by treatment with 0.1% trypsin-EDTA.

IV.2.2. Microvasculature and epidermal bioinks

The microvasculature bioink was generated by resuspension of 8.0×10^5 human dermal fibroblasts and endothelial colony forming cells, in a 1:1 ratio, in a collagen mixture consisting of 750 $\mu\text{L}/\text{mL}$ of 2.5 mg/mL of type I collagen (Corning), 50 $\mu\text{L}/\text{mL}$ of FBS (Atlanta Biologics), 100 $\mu\text{L}/\text{mL}$ of Reconstitution Buffer 10X (0.05 M NaOH, 2.2% NaHCO₃, and 200 mM HEPES), and 100 $\mu\text{L}/\text{mL}$ of HAM-F12 medium 10X (Gibco). To avoid gelation before printing, the microvasculature bioink was kept on ice. The epidermal bioink was generated by resuspension of 1.6×10^6 human keratinocytes per mL of culture medium composed of 50% KGM medium and 50% **skin differentiation medium**: DMEM/HAM's F-12 (3:1) supplemented with 10% FBS, 0.1 nM cholera toxin (Sigma), 5 $\mu\text{g}/\text{ml}$ insulin (Sigma), 5 $\mu\text{g}/\text{ml}$ apo-transferrin (Sigma), 0.4 $\mu\text{g}/\text{ml}$ hydrocortisone-21 (Sigma) and 0.5 ng/ml epidermal growth factor (Peprotech).

IV.2.3. 3D bioprinting of vascularized skin – Protocol 1

The vascularized printed skin construct was generated by printing 17 layers (300 μm , 2.5 psi) of cold microvasculature bioink on top of a Transwell insert PET membrane (Figure IV.2.1). Upon complete gelation of dermal layers at 37°C for 40 minutes, 3 layers of epidermal bioink (300 μm , 2.5 psi) were printed on top of the 3D construct. To avoid keratinocyte aggregation in the printer's syringe and tubing, volumes of 100 μL of epidermal bioink were repeatedly pipetted directly into the tubing connecting the microvalve dispenser to the syringe. After

printing, 1 mL of epidermal bioink without keratinocytes was added to the bottom compartment of the 12-well Transwell insert. Twenty-four hours later, the medium on top and bottom of the Transwell insert was removed and changed to 100% skin differentiation medium. After 4 days under medium submersion, the Transwell insert containing the vascularized skin equivalent was carefully transferred to air-liquid interface on top of a 100 μm pore cell strainer placed in a Falcon® 6-well Deep Well Plate (Corning). The medium on top of the vascularized skin construct was removed and 9 mL of skin differentiation medium were slowly added to the bottom of the cell strainer. The medium below the cell strainer was replaced every 3 days until the end of the experiment.

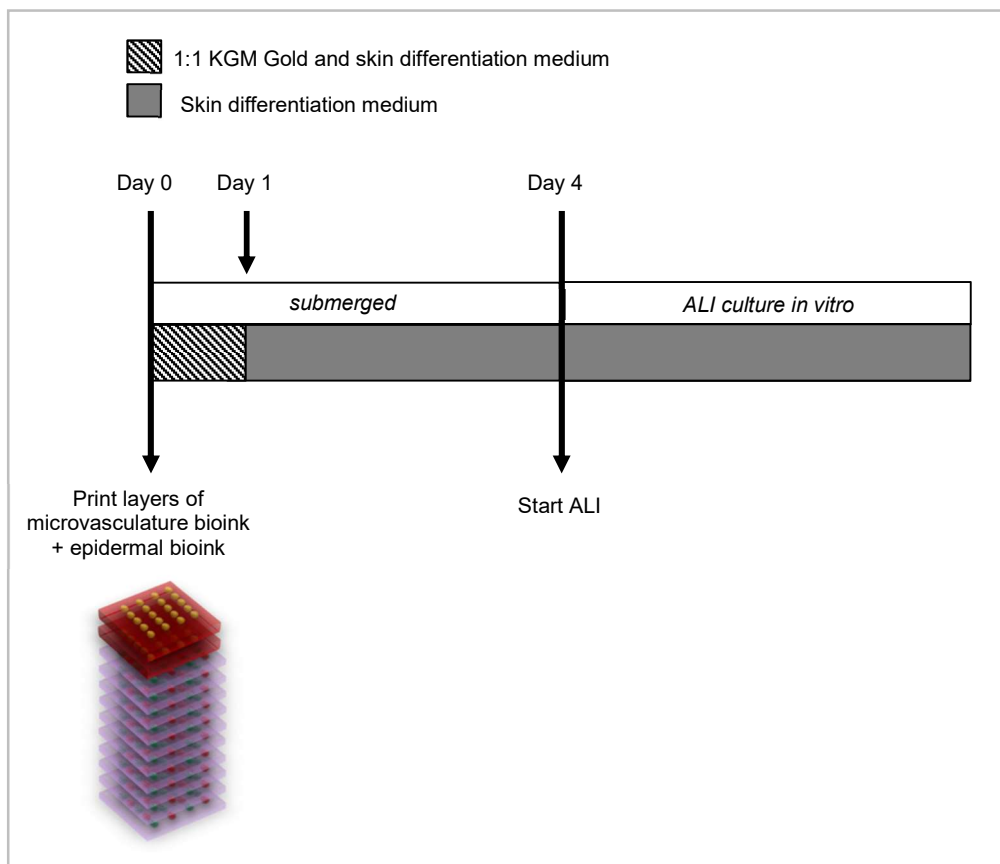


Figure IV.2.1 – *Protocol 1* for bioprinting and maturation of vascularized human skin equivalents. Bioprinted constructs were submerged in skin differentiation medium from day 1 until day 4, and then lifted to air-liquid interface.

IV.2.4. 3D bioprinting of vascularized skin – Protocol 2

The vascularized printed skin construct was generated by printing 17 layers (300 μm , 2.5 psi) of cold microvasculature bioink on top of a Transwell insert PET membrane (Figure IV.2.2). Upon complete gelation of dermal layers at 37°C for 40 minutes, 1 mL and 0.5 mL of EGM2 were added to the bottom and top compartment of the 12-well Transwell insert, respectively, and incubated at 37°C. The medium was changed daily until day 6. At day 6 of submerged culture, the medium on top and bottom of the Transwell insert was removed and washed twice with PBS. Three layers of epidermal bioink (300 μm , 2.5 psi) were then printed on top of the vascularized printed dermis and the medium on the bottom of the Transwell insert was changed to 100% skin differentiation medium. The next day, the medium on top of the construct was replaced to 100% skin differentiation medium. After 4 days under medium submersion, the vascularized skin equivalent was analyzed and characterized. Further epidermal maturation was performed *in vivo*, upon engraftment in the dorsal part of SCID/beige mouse model.

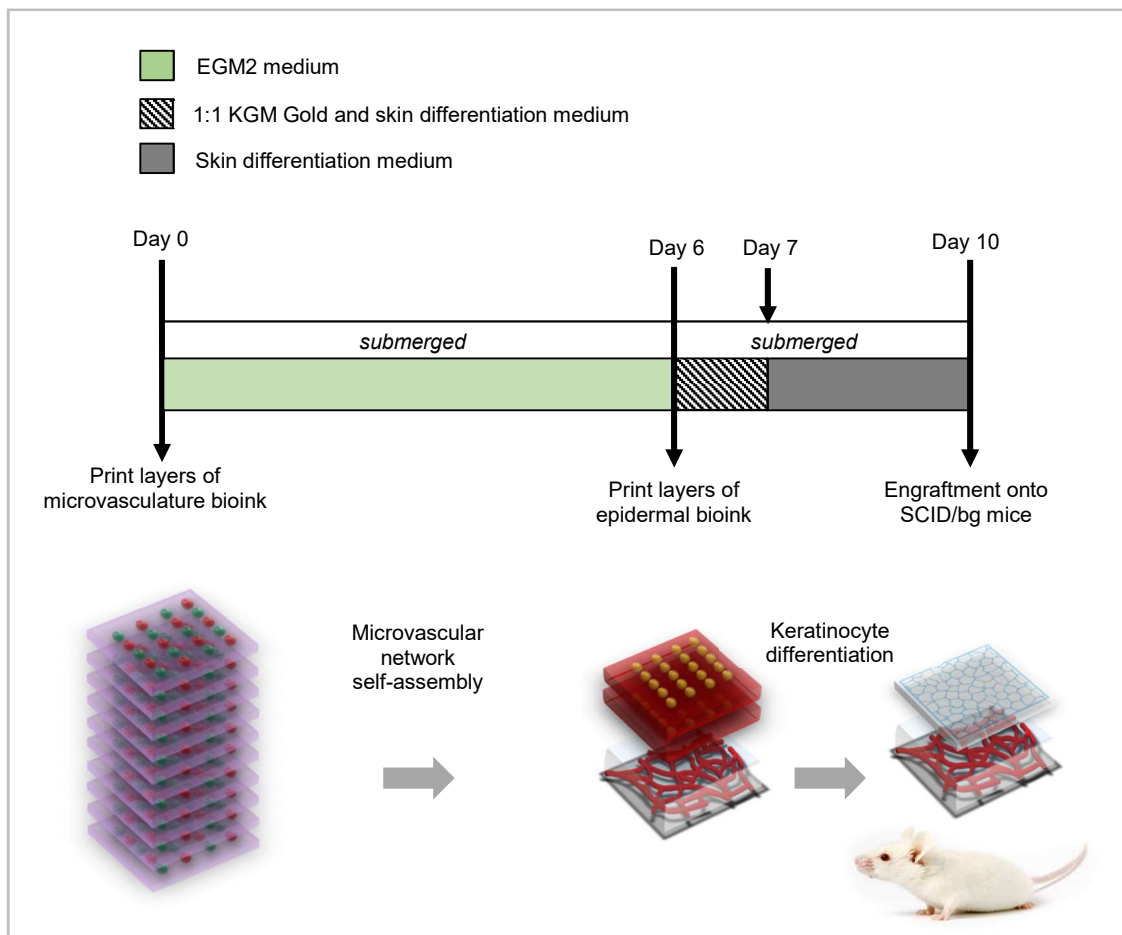


Figure IV.2.2 - Protocol 2 for bioprinting and maturation of vascularized human skin equivalents.

Bioprinted constructs were submerged in EGM2 medium until day 6 to induce endothelial network formation. Epidermal layers were then printed on top of the pre-vascularized dermis and submerged in skin differentiation medium until engraftment.

IV.2.5. Histological and immunofluorescence analysis of skin constructs

Skin samples were placed in an aluminum foil mold (10mm x 20mm x 15mm) containing Optimum Cutting Temperature compound (O.C.T., Tissue-Tek®). The molds were placed on a bath of dry-ice and 100% ethanol until snap-frozen and kept at -80°C until sectioning. O.C.T. blocks were cut into 10 µm sections in a cryostat chamber set to -25°C, collected in Superfrost Plus charges slides and stored at -20°C until use. Epidermal differentiation was evaluated with Hematoxylin & Eosin staining. Hematoxylin dye (Millipore®) was added for 7 min followed by rinsing with running tap water for 1 min. Then eosin dye (Millipore®) was added for 2 min followed by washing with water and dehydration through ethanol graded series. The slides were then immersed in xylene (Sigma) for 10 minutes and mounted with Distyrene Plasticizer Xylene (DPX; Sigma) mounting medium. All histological images were captured on Olympus IX-71 microscope with a couple-charge device (CCD) camera (Olympus, USA).

For immunofluorescence analysis, tissue sections were immersed in cold acetone for 10 minutes and blocked for 1 hour with 10% Normal Goat Serum in PBS. Slides were then incubated overnight at 4°C, in humid chamber, with primary monoclonal antibodies anti-cytokeratin 14 (mouse, 1:200, clone LL002; Abcam) and anti-collagen IV (mouse; 1:200, clone COL-94; Abcam). The next day, the slides were washed three times with PBS and incubated for 1 hour at room temperature with anti-mouse IgG H&L secondary antibodies Alexa Fluor™ 488 or Alexa Fluor™ 568 (goat, 1:500; Abcam). Slides were mounted with VECTASHIELD antifade mounting medium containing DAPI (Vector Labs) for nuclear staining and imaged on Nikon Eclipse Ti-E inverted fluorescence microscope (Nikon Instruments, USA).

IV.2.6. Engraftment of bioprinted vascularized skin in SCID/bg mice

All procedures and animal breeding were performed under protocols approved by the Yale Institutional Animal Care and Use Committee. C.B.57-SCID/bg mice were purchased from Taconic Farms, Germantown, NY. Synthetic skin equivalents were engrafted under sterile conditions onto the side of SCID/bg mice anesthetized by intraperitoneal injection of ketamine/xylazine. Mouse skin (approximately 2 x 2 cm maximum size) was excised from the dorsal side of the animal and a comparable sized piece of synthetic skin was placed on the defect and sutured in place using 6-0 Prolene suture. The graft was then covered with two layers of Vaseline gauze, pre-coated with Bacitracin cream, a layer of Tegaderm, two bandages covering the size of the wound and finally wrapped with Coban 3 M tape. As a control, human skin from deceased donors was obtained through the Yale University Skin

Bank under a protocol approved by the Yale Human Investigation Committee and grafted to SCID/bg mice.

IV.2.7. Two-Photon Laser Scanning Microscopy

After period of skin engraftment on SCID/bg mice, we imaged 2-3 grafts: human skin, synthetic skin with vessels and synthetic skin without vessels, using 2 photon imaging to visualize vessel formation. We injected 10mg/mL Rhodamine Dextran intravenously into each mouse minutes prior to harvesting the skin graft. We removed the underlying layer of connective tissue, mounted the skin grafts onto the slides and imaged using an upright multiphoton laser scanning microscope (Olympus BX61WI). The microscope was equipped with an auto-tunable Titanium-Sapphire two-photon laser (Chameleon Vision II, Coherent) pumped by a Verdi laser source was used for the excitation light source. Volocity® software (Improvision) was used to create sequences of image stacks. Each xy plane spanned 500 µm in each dimension.

IV.2.8. Histochemical analysis of bioprinted skin tissues

Grafts were fixed in formalin and embedded in paraffin for hematoxylin and eosin staining or immunohistochemistry. Sections of 5 µm were used for analysis of the harvested tissues. Primary antibodies reactive with mouse CD31 and human CD31 were used for characterization of vessel origin (mouse CD31, 1:100; human CD31 1:100; BD Pharmingen). Primary antibody reactive with human involucrin was used to assess the origin of the epidermis in bioprinted grafts (1:100: Abcam). Biotinylated secondary Ab (1:100 JacksonImmuno) was used to detect the primary Ab and an avidin binding complex, and a 3-amino-9-ethyl carbazole detection kit was used for color development (Vector Laboratories).

IV.2.9. Statistical analysis

Statistical analyses were performed using Prism 7 software (GraphPad, USA). Data are expressed as mean standard deviation. When the means of 2 variables of more than 2 groups were compared, a two-way ANOVA analysis was performed. Results were considered significant when the P-value (P) < 0.05: * = P < 0.05, ** = P < 0.01, *** = P < 0.001, **** = P < 0.0001, ns = non-significant.

IV.3 Results

IV.3.1. Part A: Fabrication of bioprinted vascularized skin constructs with Protocol 1

IV.3.1.1. Evaluation of endothelial network formation under skin differentiation medium culture

To assess the optimal conditions to co-culture endothelial cells, dermal fibroblasts and keratinocytes in a bioprinted skin construct, we first evaluated the ability of skin differentiation medium to induce endothelial network formation. Live imaging analysis of bioprinted constructs cultured in skin differentiation medium did not show endothelial network formation. On the contrary, culture in EGM2 induced endothelial cell sprouting 1 day after printing and

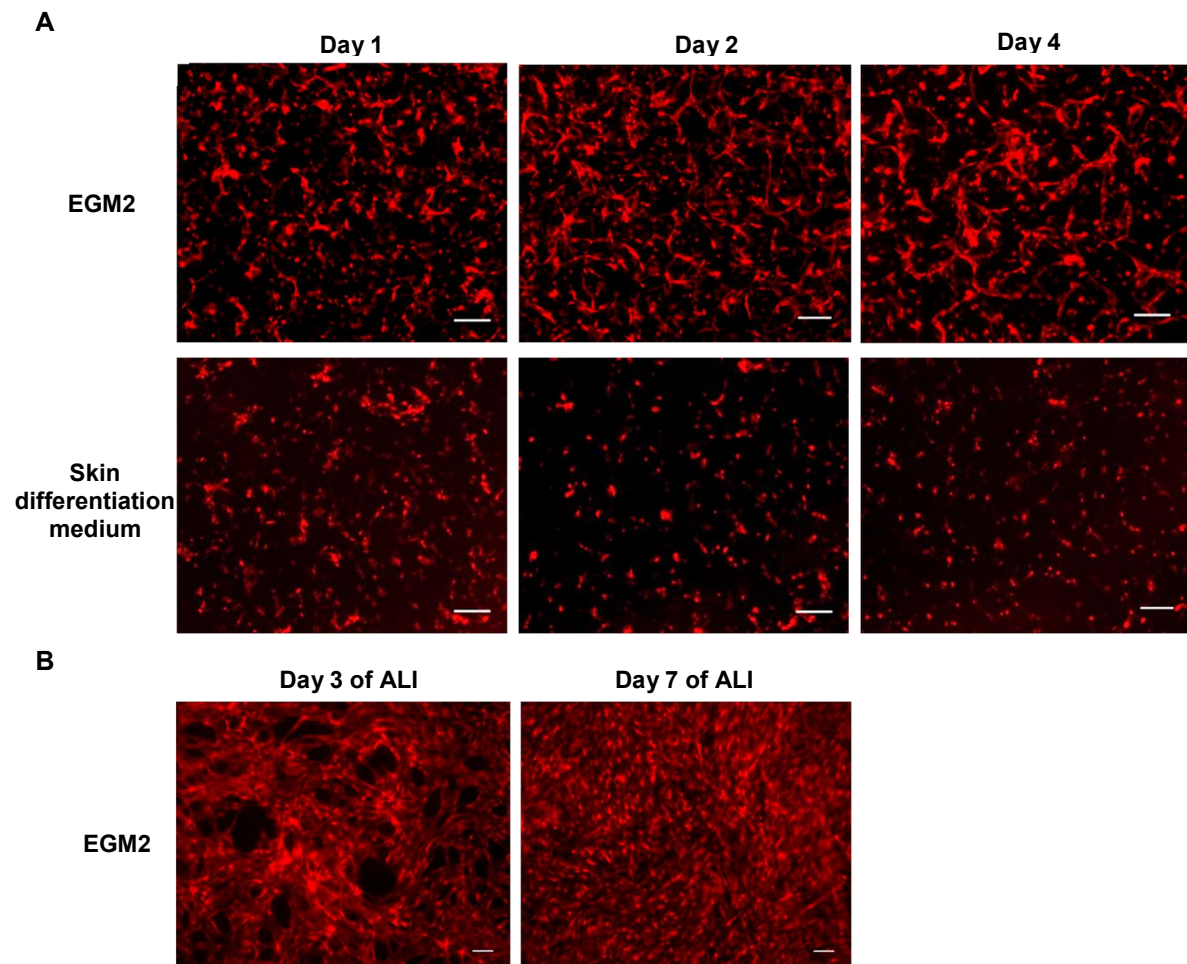


Figure IV.3.1 - Live cell fluorescence microscopy of RFP-expressing ECFC co-cultured with dermal fibroblast in bioprinted constructs. **(A)** RFP-expressing ECFC were co-cultured with dermal fibroblast in EGM2 or skin differentiation medium until day 4. **(B)** Self-assembled endothelial networks cultured in EGM2 were lifted to air-liquid interface from day 4 of *in vitro* culture until day 11 (day 7 of ALI).

Scale bar 100 μm .

self-assembly of capillary-like networks at day 4 (Figure IV.3.1A). However, under ALI culture, bioprinted constructs in EGM2 showed endothelial network regression. The 3-dimensional and luminal organization of the capillary-like network quickly collapsed and formed a monolayer of endothelial cells (Figure IV.3.1B).

IV.3.1.2. Evaluation of endothelial network stability under skin differentiation medium culture

In order to assess if EGM2 medium was required for both induction and maintenance of endothelial networks *in vitro*, human dermal fibroblasts and endothelial cells were co-cultured for 6 days in EGM2 medium and subsequently, cultured in skin differentiation medium for 31 days. Results showed that endothelial networks self-assembled under EGM2 culture but did not regress or collapse when the constructs were submerged in skin differentiation medium from day 6 onwards. Endothelial cells formed lumens and branched structures that closely resembled capillary networks. No significant differences on overall endothelial network morphology were observed between EGM2 and skin differentiation medium. Moreover, no signs of vessel regression were observed in both culture conditions up to 37 days of *in vitro* culture (Figure IV.3.2).

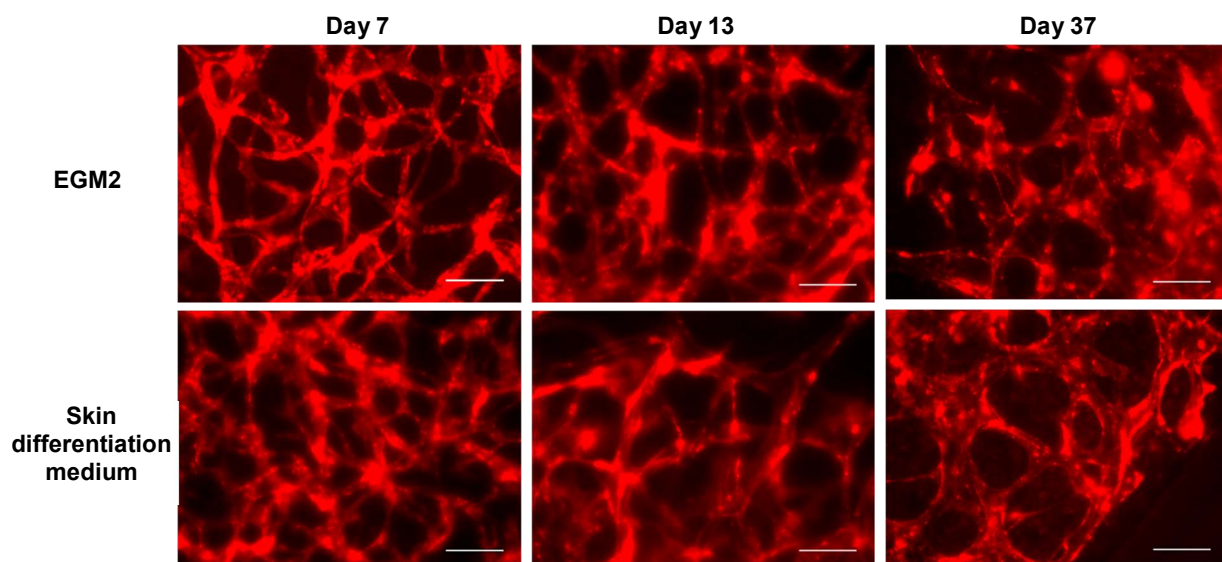


Figure IV.3.2 - Live cell fluorescence microscopy of RFP-expressing ECFC co-cultured with dermal fibroblast in bioprinted constructs. Self-assembled endothelial networks culture in EGM2 for 7 days were cultured in either EGM2 or skin differentiation medium from day 4 until day 37 of *in vitro* culture.

Scale bar: 100 μm .

IV.3.2. Part B: Generation of bioprinted vascularized skin constructs with Protocol 2

Based on the previous results, we adapted protocol 1 and attempted a new printing strategy by bioprinting vascularized skin constructs at 2 different stages. First, bioprinting of a vascularized dermal compartment to allow self-assembly of capillary-like networks for 6 days under EGM2 culture; second, bioprinting of the epidermal compartment at day 6, since skin differentiation medium has shown to support the maintenance of self-assembled endothelial networks and to induce normal epidermal stratification *in vitro*. Histological and immunofluorescence analysis of bioprinted constructs at day 10 showed the generation of a still immature skin tissue (Figure IV.3.3). However, bioprinted vascularized skin constructs showed positive staining for cytokeratin 14, indicative of early-stage differentiation of basal layer keratinocytes. Moreover, immunofluorescence staining for collagen type IV showed the presence of the basement membrane surrounding multiple capillary-like structures with open lumens within the dermis, confirming the preservation of endothelial networks in bioprinted skin constructs under skin differentiation medium culture.

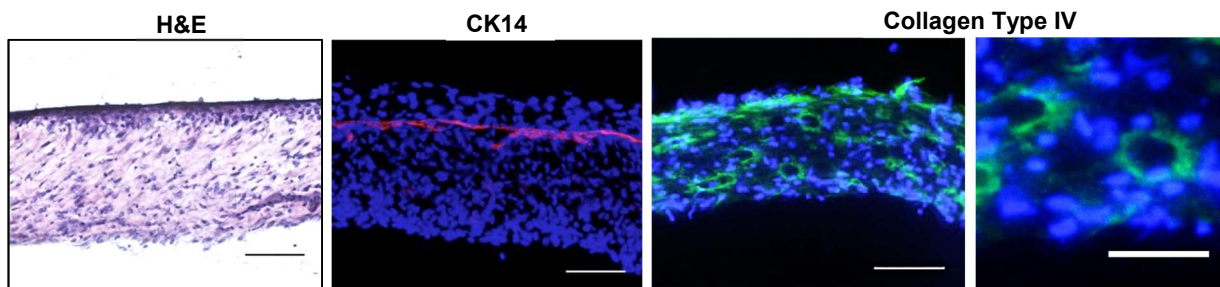


Figure IV.3.3 - Characterization of 3D bioprinted vascularized skin equivalents before engraftment. H&E and immunofluorescence analysis of cytokeratin 14 and collagen type IV at day 10 of *in vitro* culture.

Scale bar: 100 μm (higher magnification: 50 μm).

IV.3.3. Part C: Characterization of 3D bioprinted skin transplanted to immunodeficient mice.

Bioprinted skin substitutes with and without incorporation of human ECFC were implanted on the dorsal part of immunodeficient mice after 10 days of *in vitro* culture. As shown in Figure 6A, significant contraction was observed on bioprinted skin grafts without ECFC 4 weeks post-engraftment. This finding was confirmed by histological analysis of bioprinted skin tissues 6 weeks post-engraftment. The graft border between the bioprinted graft and mouse skin was identified by thin epidermis, presence of hair follicles and a deep dermis with adipose tissue. Bioprinted skin grafts without ECFC were nearly non-detectable 6 weeks post-engraftment and a significant larger area was occupied by the mouse skin in comparison to bioprinted vascularized skin (Figure IV.3.4B).

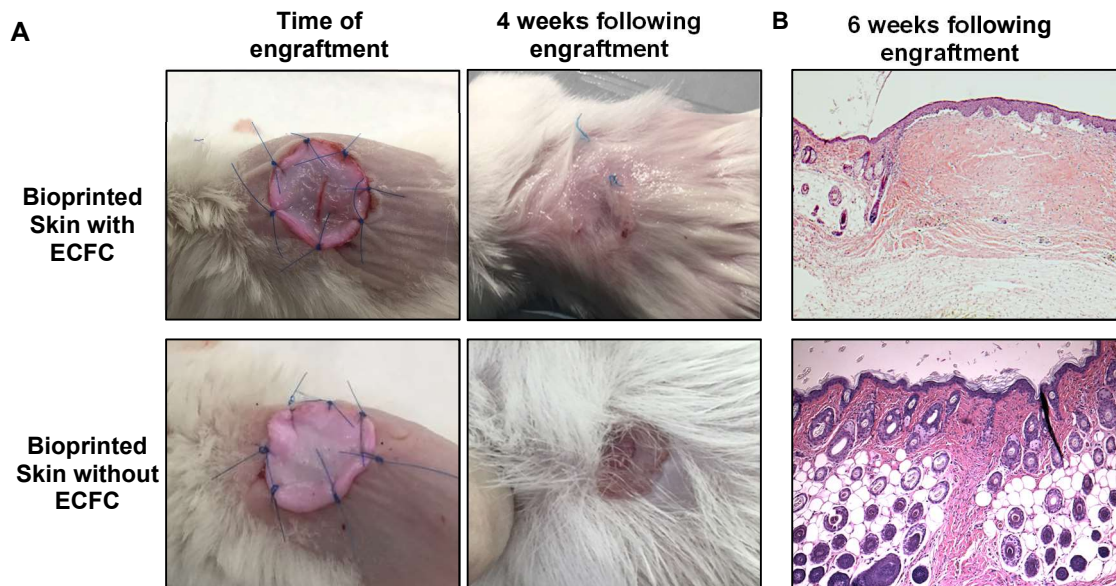


Figure IV.3.4 - Characterization of 3D bioprinted skin equivalents after engraftment. **(A)** Photographs of bioprinted grafts with and without incorporation of ECFCs at the time of engraftment and 4 weeks after engraftment. **(B)** H&E staining of bioprinted grafts with and without incorporation of ECFC at the edge of the mouse tissue, 6 weeks after engraftment. Mice photographs were captured by J. Merola at Yale University.

Moreover, the presence of a mature stratified epidermis was observed in bioprinted vascularized skin grafts. The human origin of the epidermis was assessed by involucrin staining, a marker of human keratinocyte terminal differentiation (Figure IV.3.5). Immunohistochemical analysis confirmed that the epidermis of bioprinted vascularized skin

grafts was of human origin and did not originate from re-epithelization of neighboring mouse keratinocytes.

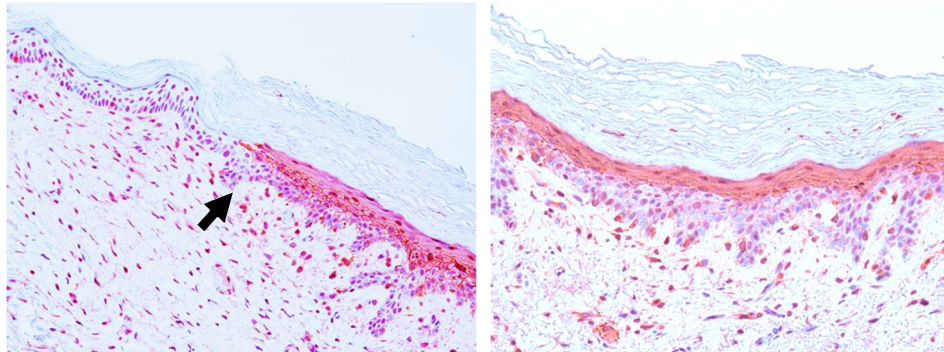


Figure IV.3.5 – Stratified epidermis in 3D bioprinted vascularized skin equivalents after engraftment is of human origin. Immunohistochemical staining of human involucrin, at the border with mouse skin tissue, 6 weeks following engraftment on SCID/bg mouse.

Furthermore, substitutes formulated with human ECFC contained vascular structures 6 weeks post-engraftment. Histological sections confirmed the presence of perfused human CD31-positive vessels that contained red blood cells (Figure IV.3.6A,B). No human ECFC were

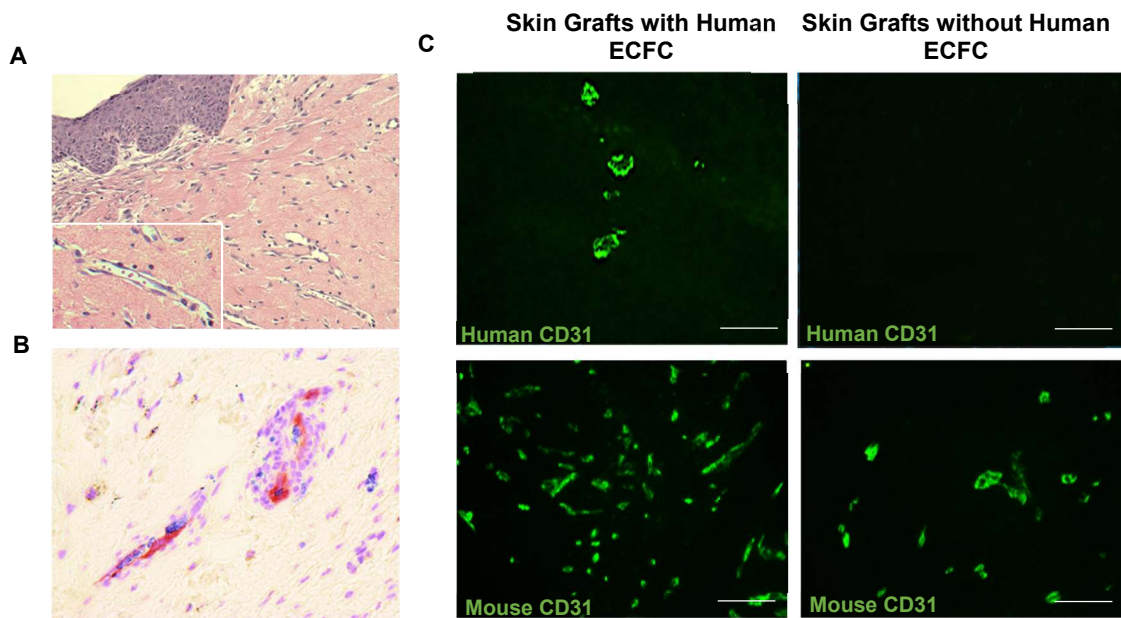


Figure IV.3.6 - 3D bioprinted human skin substitutes support perfusable micro vessels *in vivo*. **(A)** H&E staining of grafted skin substitute containing perfused microvessels. **(B)** IHC staining of vascularized grafts showing perfused microvessels containing human EC. **(C)** Harvested grafts were then co-stained with either antibody to human CD31 or mouse CD31 (IF images were captured by J. Merola at Yale University). Scale bar: 100 μ m.

detected in grafts that did not include human EC. Both grafts also contained mouse CD31 expressing cells, suggesting a limited degree of recipient angiogenesis, which appears to be greater in grafts containing human ECFC (Figure IV.3.6C). The occurrence of anastomosis events between mouse and human vessels was examined via dextran rhodamine dye and anti-human CD31 antibody injection into the mouse circulation for epifluorescence visualization of perfused mouse and human vessels, respectively. As shown in Figure IV.3.7, examination of the intact harvested specimen as a whole mount showed that human vessels formed anastomoses with mouse vessels, similarly to human skin grafts.

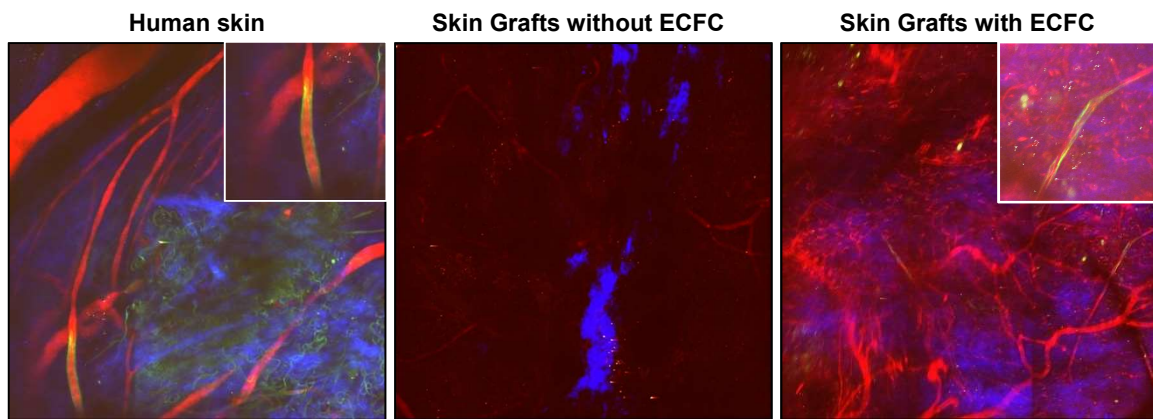


Figure IV.3.7 – Vascularized bioprinted human skin substitutes form anastomoses with mouse vessels. Whole-mount epifluorescence imaging of human skin and bioprinted grafts with and without ECFC, 6 weeks following engraftment on SCID/beige mouse. Pre-harvesting of tissues, mouse and human vessels were stained with rhodamine dextran dye (red) and anti-human CD31 antibody (green), respectively. Images were captured by J. Merola at Yale University.

IV.3.4. Part D: Incorporation of human pericytes in bioprinted endothelial networks

To further improve vessel stability and function of bioprinted grafts *in vivo*, human pericytes were mixed and printed with ECFC and dermal fibroblasts in collagen type I. The optimal ratio of HECFC: dermal fibroblasts: pericytes was evaluated *in vitro*. Live imaging over the period of 15 days revealed significant gel contraction of 1 ECFC :1 FB : 1/9 PC and 1 ECFC: 1/2 FB: 1/9 conditions (Table IV.3.1). Particularly, significant reduction of vessel area and branching points was observed for the 1 ECFC : 1/2 FB : 1/15 PC condition compared to the gels without pericytes (Figure IV.3.8B). Moreover, human pericytes directly associated with cultured endothelial cells, while dermal fibroblasts distributed homogeneously within the gel (Figure IV.3.8C).

Table IV.3.1 - Summary of observations on gel contraction of the co-culture of human dermal fibroblasts, endothelial cells and human pericytes *in vitro* at different ratios in collagen type I gels for 15 days.

RATIO (ECFC: FB: PC)	OBSERVATIONS
1:1:0	No gel contraction
1:1:1/15	No gel contraction
1: 1/2 :1/15	No gel contraction
1:1:1/12	No gel contraction
1: 1/2 :1/12	No gel contraction
1:1:1/9	Gel contraction
1: 1/2 :1/9	Gel contraction

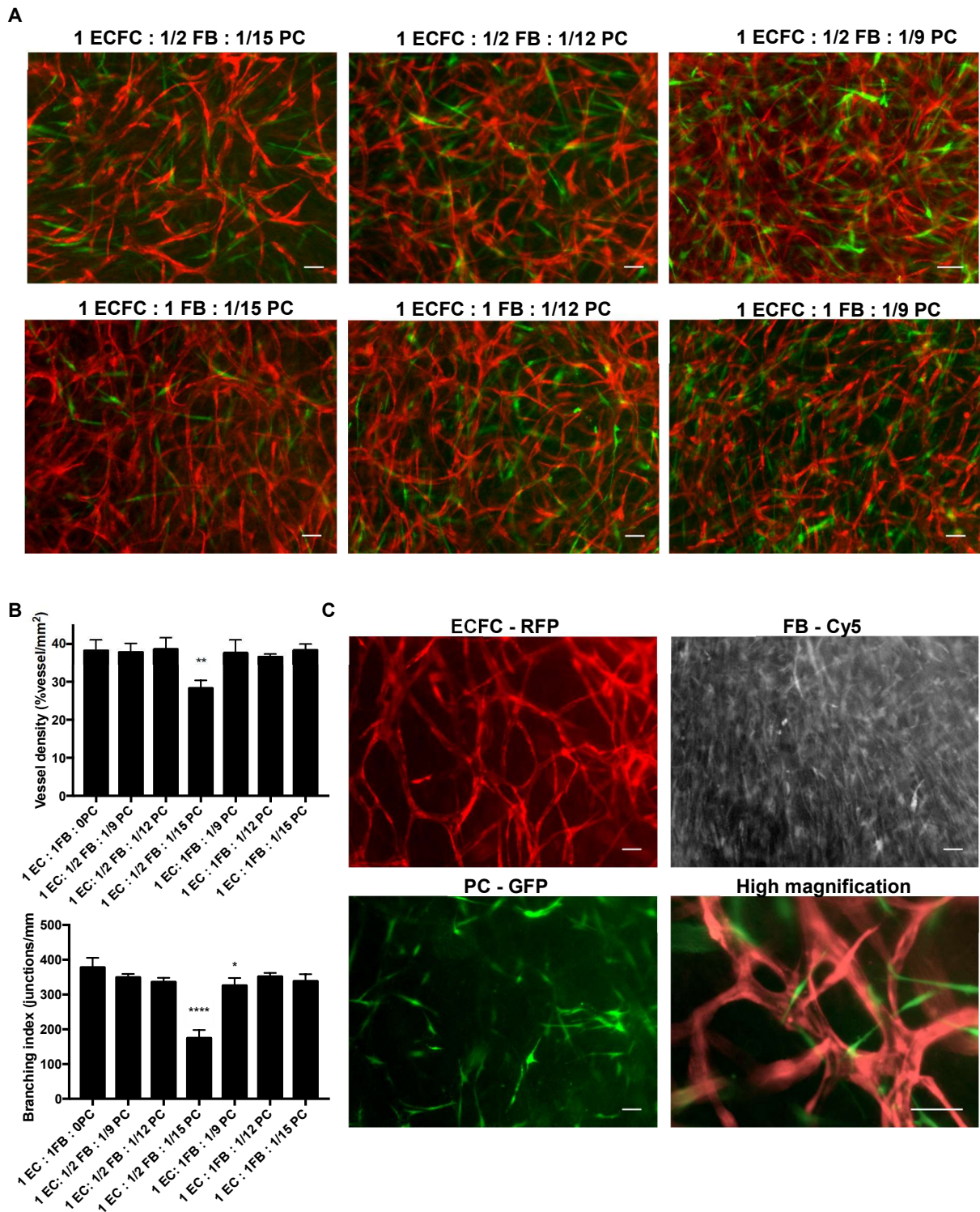


Figure IV.3.8 – Characterization of bioprinted endothelial networks with Incorporated human placental pericytes *in vitro*. **(A)** Representative live images of co-cultures of RFP-expressing ECFC, dermal fibroblasts and GFP-expressing pericytes 7 days after printing. **(B)** Analysis of vessel density and branching index of endothelial networks. **(C)** Live imaging of co-cultures of RFP-expressing ECFC, Cy5-dermal fibroblasts and GFP-expressing pericytes 7 days after printing. Scale bar: 100 μm .

IV.3.4.1. Generation and engraftment of vascularized skin constructs containing human pericytes

Bioprinted skin constructs containing ECFC and pericytes were generated based on protocol 2, with some minor changes. Microvascular bioink was developed by combination of ECFC, dermal fibroblast and pericytes at 1: 1 :1/12 ratio. Constructs were then cultured under submersion conditions for 10 days before engraftment. Similar to bioprinted construct without pericytes, bioprinted constructs containing pericytes revealed early-stage differentiation of basal layer keratinocytes and preservation of self-assembled endothelial networks with open lumens (Figure IV.3.9A). Engraftment of bioprinted skin grafts containing pericytes contracted significantly *in vivo* and the developed necrotic regions 3 weeks after engraftment (Figure IV.3.9B). Six weeks post-engraftment, grafts slough off and could not be harvested for further analysis.

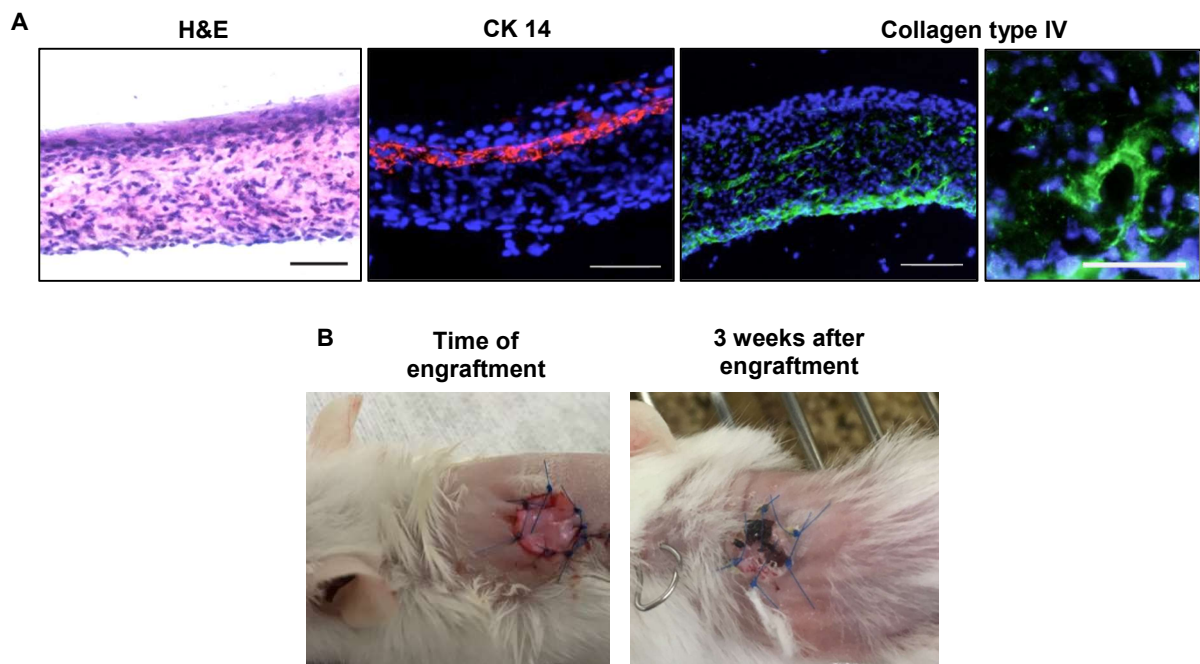


Figure IV.3.9 - Characterization of 3D bioprinted vascularized skin equivalents with human placental pericytes. **(A)** H&E and immunofluorescence analysis of cytochrome 14 and collagen type IV at day 10 of in vitro culture. Scale bar: 100 μm (higher magnification: 50 μm). **(B)** Photographs of vascularized bioprinted grafts with incorporation of human placental pericytes at the time of engraftment and 3 weeks following engraftment. Photographs of mice were captured by J. Merola at Yale University.

IV.4 Discussion

In the present study we examined the effects of medium composition on the co-culture of endothelial cells, dermal fibroblasts and keratinocytes to generate a full-thickness vascularized bioprinted skin construct morphologically similar to human skin. Here, we show that although skin differentiation medium did not support endothelial cell sprouting and angiogenesis *in vitro*, it allowed long-term culture of pre-assembled endothelial networks, similarly to EGM2 medium. Once new vessels assembled, the endothelial cells became resistant to regression. This effect on the initial assembly of endothelial networks by skin differentiation medium may be explained by the lack of growth factors in its composition required to induce vessel formation, such as VEGF, heparin, ascorbic acid, and IGF, which are present in EGM2 medium. The contribution of each of these growth factors on angiogenesis has been extensively reported in the literature. For example, IGF1 strongly controls vascular growth by stimulating endothelial cell migration and tube formation through activation of PI3 kinase pathway and by activating endothelial cell metabolism by significantly upregulating amino acid and glucose uptake (Bach, 2015; Jacobo & Kazlauskas, 2015). Depletion of ascorbic acid has also been shown to restrict angiogenesis both *in vitro* and *in vivo* as it is necessary for the stabilization of the collagen type IV triple helix produced by endothelial cells to form new vessels (Telang, Clem, Eaton, & Chesney, 2007). However, the molecular mechanisms of vascular quiescence after endothelial cell self-assembly remain largely unknown.

Moreover, we have shown that culture of vascularized skin constructs under ALI culture caused vessel regression and collapsing of self-assembled endothelial networks. As previously described in chapter II, ALI culture reduced initial construct thickness by 5- to 20-fold overtime. Our data suggest that this significant reduction of the dermis thickness has a detrimental effect on the 3D dimensional stability of microvascular structures.

To overcome these obstacles, we adopted a new approach by bioprinting vascularized skin constructs in 2 stages. First, printing of vascularized dermal layers and culture in EGM2 medium for 6 days, and second, printing of epidermal bioink layers and culture in skin differentiation medium for 4 days. This 2-step approach allowed successful self-assembly of endothelial networks in the dermis during the period of EGM2 culture and subsequent epidermal keratinization in skin differentiation medium with no visible effects on the organization of the pre-assembled microvasculature. To avoid ALI-induced regression and collapsing of self-assembled endothelial networks, bioprinted constructs were cultured under submersion. Under these conditions, multiple vessels with open lumens were observed in the dermis as well early-stage differentiation of basal keratinocytes in the epidermis.

A potential concern of this new printing approach is the resulting poor epidermal stratification, as ALI culture is an important factor for the maturation of skin equivalents *in vitro*. Previous work has demonstrated that dehydration and osmotic stress acts as a signal on human keratinocytes grown at air-liquid interface to induce the expression of markers of terminal differentiation (Mammone, Ingrassia, & Goyarts, 2008; Prunieras, Regnier, & Woodley, 1983). For this reason, this printing approach might limit the use of vascularized bioprinted constructs *in vitro* in disease modeling or transdermal delivery studies. However, a potential solution to the collapsing effect on endothelial networks under ALI culture, is to limit ALI-induced dehydration by incorporating components that help retain water in the dermis compartment, such as glycosaminoglycans and proteoglycans. In tissues such cartilage and skin, GAGs act as shock absorbers by resisting compressive forces (Ayerst, Merry, & Day, 2017; Smith & Melrose, 2015). Due to their repeating disaccharide units and hydrophilic groups, GAGs increase water uptake and influence the tissue elasticity. Several groups have investigated the incorporation of GAGs into synthetic and natural polymers (Gupta, Werdenberg, Blevins, & Grande-Allen, 2007; Saddiq, Barbenel, & Grant, 2009; Wang et al., 2015). Lungu *et al.* have studied the effect of hyaluronic acid or chondroitin sulfate incorporation on collagen gels and found that the addition of hyaluronic acid or chondroitin sulfate improved water uptake by 3-fold compared to collagen alone. In addition, scaffolds with GAGs were less prone to enzymatic degradation by collagenase (Lungu et al., 2011). Therefore, investigation of how GAGs control water retention and vascularization in the context of bioprinted skin constructs is worth exploring.

For tissue replacement, we hypothesized that ALI-induced maturation of vascularized bioprinted grafts could be completed *in vivo* upon engraftment. Here, we showed that bioprinted vascularized constructs engrafted onto a SCID/bg mouse model formed a well-stratified epidermis *in vivo* and human vascular structures were preserved and perfused six weeks post-engraftment, similarly to human skin. In addition, connections between human and mouse vessels to re-established perfusion within the graft were observed in vascularized bioprinted grafts. Interestingly, bioprinted grafts that did not contain ECFC showed a lower degree of engraftment and host angiogenesis compared to vascularized grafts. We speculate that the presence of pre-existing vessels in bioprinted grafts stimulated ingrowth of mouse vessels into bioprinted grafts through secretion of angiogenic factors. However, further clarification is required on whether successful early engraftment and reperfusion of vascularized grafts were established through anastomoses between host and human vessels or through host's neovascularization into the graft. Investigation of anastomoses occurrence and mouse vessels ingrowth into the graft at earlier times might be useful to help answering this question.

It has been proposed that inclusion of pericytes in newly formed capillary tubes is necessary to maintain their integrity and contractile function. In addition to promoting vessel maturation and stabilization, pericytes play a role in regulation of vessel guidance in angiogenesis through secretion of matrix metalloproteinases allowing endothelial cell migration. Therefore, to improve the clinical utility of bioprinted grafts, we investigated the incorporation of placental pericytes in vascular beds. Here, we showed that the number of pericytes in bioprinted vascularized grafts not only had an effect on the morphology of capillary-like structures but significantly increased gel contraction *in vitro*. Furthermore, this effect was significantly augmented upon engraftment in SCID/bg mouse model, resulting in poor healing and engraftment of bioprinted skin tissues. It has been reported that injured epithelia can activate pericyte proliferation and differentiation into myofibroblasts that contribute to scarring and delayed healing (Chang, Chou, Chen, & Lin, 2012; Humphreys, 2012; Thomas, Cowin, & Mills, 2017). Therapeutic approaches that can potential block pericyte–myofibroblast transition offer a promising solution to prevent fibrosis. It has been reported that blocking VEGFR signaling can lead to significant attenuation of inflammation and downregulation of profibrotic cytokines, such as PDGF and TGF β 1 (Lin et al., 2011).

Moreover, a potential bottleneck in skin tissue replacement is the large number of cells required to generate skin equivalents since they can be harvested only in small quantities directly from human biopsies. In addition, it may be impractical to obtain such cells from the recipient's own skin specially in patients with compromised recipient beds (e.g., in diabetes, thermal burns, or venous leg ulcers) or in hosts with impaired angiogenesis (e.g., the elderly) (Alzahrani, Ammar, Alzahrani, & Shoaib, 2013; Tahergorabi & Khazaei, 2012; Zhang et al., 2011). A potential approach to this obstacle is to isolate ECFC from either umbilical cord blood, adult bone marrow, or adult peripheral blood (Asahara et al., 1997). As we shown in this chapter, ECFC isolated from umbilical cord blood can actively participate in angiogenesis and improve skin engraftment in immunocompromise mice. However, unlike keratinocytes or fibroblasts, human EC can initiate an immune response by resting allogeneic T-cells (Morhenn & Nickoloff, 1987; Pober et al., 1983). Human ECs initiate rejection by direct presentation of non-self class I and class II MHC proteins to circulating alloreactive effector memory T cells which are highly abundant in the adult human population. Abrahimi *et al.*, have recently found that elimination of MHC molecule expression on human ECFCs using CRISPR/Cas 9 technology can diminish recognition of human ECs by T cells *in vitro* (Abrahimi et al., 2015). ECFC ablated for MHC molecules eliminated rejection of self-assembled perfusable networks implanted into immunodeficient mouse hosts subsequently inoculated with peripheral blood mononuclear cells from a donor allogeneic to the EC donor. Successful engraftment of a 3-D

printed human skin graft by incorporating allogeneic ECFC without triggering rejection in the host would be of great clinical utility.

IV.5 Conclusions

In this chapter, we adopted a new approach to bioprinting vascularized skin constructs by printing of dermal and epidermal compartments at 2 different stages. This 2-step approach allowed successful self-assembly of endothelial networks in the dermis during the period of EGM2 culture and subsequent epidermal keratinization in skin differentiation medium with no visible effects on the organization of the pre-assembled microvasculature. To avoid ALI-induced regression and collapsing of self-assembled endothelial networks, bioprinted constructs were cultured under submersion *in vitro*. Under these conditions, multiple vessels with open lumens were observed in the dermis as well early-stage differentiation of basal keratinocytes in the epidermis. Upon engraftment in a SCID/bg mouse model, epidermal maturation of vascularized bioprinted grafts was completed as observed by the presence of a well-stratified epidermis 6 weeks post-engraftment. In addition, connections between preserved human vascular structures and mouse vessels to re-established perfusion within the graft were observed in vascularized bioprinted grafts. Bioprinted grafts that did not contain ECFC showed a lower degree of engraftment and host angiogenesis compared to vascularized grafts. Inclusion of pericytes in the vascular bed of bioprinted grafts did not show improvement in graft integration with the host tissue. We hypothesize that ALI-induced dehydration and pericyte-induced contraction can be reduced by incorporation of glycosaminoglycans and inhibitors of pericyte-myofibroblast transition, respectively. In addition, to avoid rejection of bioprinted grafts in patients, the inclusion of ECFC that do not trigger an immune response might significantly increase its utility in skin tissue replacement.

IV.6 References

- Abrahimi, P., Chang, W. G., Kluger, M. S., Qyang, Y., Tellides, G., Saltzman, W. M., & Pober, J. S. (2015). Efficient gene disruption in cultured primary human endothelial cells by CRISPR/Cas9. *Circulation Research*, *117*(2), 121–128. <https://doi.org/10.1161/CIRCRESAHA.117.306290>
- Alzahrani, H., Ammar, H., Alzahrani, A., & Shoaib, H. (2013). Healing of chronic diabetic foot ulcers with a skin substitute: Patient selection is the key to success. *Open Journal of Regenerative Medicine*, *2*(2), 15–19. <https://doi.org/10.4236/ojrm.2013.22003>
- Asahara, T., Murohara, T., Sullivan, A., Silver, M., van der Zee, R., Li, T., Witzenbichler, B., Schatteman, G., & Isner, J. M. (1997). Isolation of Putative Progenitor Endothelial Cells for Angiogenesis. *Science*, *275*(5302), 964–966. <https://doi.org/10.1126/science.275.5302.964>
- Ayerst, B. I., Merry, C. L. R., & Day, A. J. (2017). The Good the Bad and the Ugly of Glycosaminoglycans in Tissue Engineering Applications. *Pharmaceuticals (Basel, Switzerland)*, *10*(2), 54. <https://doi.org/10.3390/ph10020054>
- Bach, L. A. (2015). Endothelial cells and the IGF system. *Journal of Molecular Endocrinology*, *54*(1), R1–R13. <https://doi.org/10.1530/JME-14-0215>
- Capla, J. M., Ceradini, D. J., Tepper, O. M., Callaghan, M. J., Bhatt, K. a, Galiano, R. D., Levine, J. P., & Gurtner, G. C. (2006). Skin graft vascularization involves precisely regulated regression and replacement of endothelial cells through both angiogenesis and vasculogenesis. *Plastic and Reconstructive Surgery*, *117*(3), 836–844. <https://doi.org/10.1097/01.prs.0000201459.91559.7f>
- Chang, F.-C., Chou, Y.-H., Chen, Y.-T., & Lin, S.-L. (2012). Novel insights into pericyte–myofibroblast transition and therapeutic targets in renal fibrosis. *Journal of the Formosan Medical Association*, *111*(11), 589–598. <https://doi.org/https://doi.org/10.1016/j.jfma.2012.09.008>
- Frueh, F. S., Menger, M. D., Lindenblatt, N., Giovanoli, P., & Laschke, M. W. (2016). Current and emerging vascularization strategies in skin tissue engineering. *Critical Reviews in Biotechnology*, *8551*(July), 1–13. <https://doi.org/10.1080/07388551.2016.1209157>
- Gibot, L., Galbraith, T., Huot, J., & Auger, F. A. (2010). A Preexisting Microvascular Network Benefits *In Vivo* Revascularization of a Microvascularized Tissue-Engineered Skin Substitute. *Tissue Engineering Part A*, *16*(10), 3199–3206. <https://doi.org/10.1089/ten.tea.2010.0189>
- Gupta, V., Werdenberg, J. A., Blevins, T. L., & Grande-Allen, K. J. (2007). Synthesis of glycosaminoglycans in differently loaded regions of collagen gels seeded with valvular interstitial cells. *Tissue Engineering*, *13*(1), 41–49. <https://doi.org/10.1089/ten.2006.0091>
- Hoch, E., Tovar, G. E. M. G. E. M., & Borchers, K. (2014). Bioprinting of artificial blood vessels: Current approaches towards a demanding goal. *European Journal of Cardio-Thoracic Surgery*, *46*(5), 767–778. <https://doi.org/10.1093/ejcts/ezu242>
- Humphreys, B. D. (2012). Targeting pericyte differentiation as a strategy to modulate kidney fibrosis in

- diabetic nephropathy. *Seminars in Nephrology*, 32(5), 463–470. <https://doi.org/10.1016/j.semnephrol.2012.07.009>
- Jacobo, S. M. P., & Kazlauskas, A. (2015). Insulin-like growth factor 1 (IGF-1) stabilizes nascent blood vessels. *The Journal of Biological Chemistry*, 290(10), 6349–6360. <https://doi.org/10.1074/jbc.M114.634154>
- Lin, S.-L., Chang, F.-C., Schrimpf, C., Chen, Y.-T., Wu, C.-F., Wu, V.-C., Chiang, W.-C., Kuhnert, F., Kuo, C. J., Chen, Y.-M., Wu, K.-D., Tsai, T.-J., & Duffield, J. S. (2011). Targeting Endothelium-Pericyte Cross Talk by Inhibiting VEGF Receptor Signaling Attenuates Kidney Microvascular Rarefaction and Fibrosis. *The American Journal of Pathology*, 178(2), 911–923. <https://doi.org/https://doi.org/10.1016/j.ajpath.2010.10.012>
- Lungu, A., Albu, M. G., Florea, N. M., Stancu, I. C., Vasile, E., & Iovu, H. (2011). The influence of glycosaminoglycan type on the collagen-glycosaminoglycan porous scaffolds. *Digest Journal of Nanomaterials and Biostructures*, 6(4), 1867–1875.
- Mammone, T., Ingrassia, M., & Goyarts, E. (2008). Osmotic stress induces terminal differentiation in cultured normal human epidermal keratinocytes. *In Vitro Cellular & Developmental Biology - Animal*, 44(5), 135–139. <https://doi.org/10.1007/s11626-008-9087-z>
- Morhenn, V. B., & Nickoloff, B. J. (1987). Interleukin-2 stimulates resting human T lymphocytes' response to allogeneic, gamma interferon-treated keratinocytes. *The Journal of Investigative Dermatology*, 89(5), 464–468.
- Pasparakis, M., Haase, I., & Nestle, F. O. (2014). Mechanisms regulating skin immunity and inflammation. *Nature Reviews. Immunology*, 14(5), 289–301. <https://doi.org/10.1038/nri3646>
- Pober, J. S., Collins, T., Gimbrone, M. A., Cotran, R. S., Gitlin, J. D., Fiers, W., Clayberger, C., Krensky, A. M., Burakoff, S. J., & Reiss, C. S. (1983). Lymphocytes recognize human vascular endothelial and dermal fibroblast Ia antigens induced by recombinant immune interferon. *Nature*, 305(5936), 726–729. <https://doi.org/10.1038/305726a0>
- Prunieras, M., Regnier, M., & Woodley, D. (1983). Methods for cultivation of keratinocytes with an air-liquid interface. *The Journal of Investigative Dermatology*, 81(1 Suppl), 28s–33s.
- Saddiq, Z. A., Barbenel, J. C., & Grant, M. H. (2009). The mechanical strength of collagen gels containing glycosaminoglycans and populated with fibroblasts. *Journal of Biomedical Materials Research. Part A*, 89(3), 697–706. <https://doi.org/10.1002/jbm.a.32007>
- Smith, M. M., & Melrose, J. (2015). Proteoglycans in Normal and Healing Skin. *Advances in Wound Care*, 4(3), 152–173. <https://doi.org/10.1089/wound.2013.0464>
- Tahergorabi, Z., & Khazaei, M. (2012). Imbalance of angiogenesis in diabetic complications: the mechanisms. *International Journal of Preventive Medicine*, 3(12), 827–838. Retrieved from <https://www.ncbi.nlm.nih.gov/pubmed/23272281>
- Telang, S., Clem, A. L., Eaton, J. W., & Chesney, J. (2007). Depletion of ascorbic acid restricts

angiogenesis and retards tumor growth in a mouse model. *Neoplasia (New York, N.Y.)*, 9(1), 47–56. Retrieved from <https://www.ncbi.nlm.nih.gov/pubmed/17325743>

Thomas, H., Cowin, A. J., & Mills, S. J. (2017). The Importance of Pericytes in Healing: Wounds and other Pathologies. *International Journal of Molecular Sciences*, 18(6), 1129. <https://doi.org/10.3390/ijms18061129>

Tremblay, P. L., Hudon, V., Berthod, F., Germain, L., & Auger, F. (2005). Inosculation of tissue-engineered capillaries with the host's vasculature in a reconstructed skin transplanted on mice. *American Journal of Transplantation*, 5(5), 1002–1010. <https://doi.org/10.1111/j.1600-6143.2005.00790.x>

Tsur, H., Daniller, A., & Strauch, B. (1980). Neovascularization of Skin Flaps: Route and Timing. *Plastic and Reconstructive Surgery*, 66(1), 85–90.

Wang, M., Lyu, Z., Chen, G., Wang, H., Yuan, Y., Ding, K., Yu, Q., Yuan, L., & Chen, H. (2015). A new avenue to the synthesis of GAG-mimicking polymers highly promoting neural differentiation of embryonic stem cells. *Chemical Communications*, 51(84), 15434–15437. <https://doi.org/10.1039/C5CC06944K>

Zhang, X., Sarkar, K., Rey, S., Sebastian, R., Andrikopoulou, E., Marti, G. P., Fox-Talbot, K., Semenza, G. L., & Harmon, J. W. (2011). Aging impairs the mobilization and homing of bone marrow-derived angiogenic cells to burn wounds. *Journal of Molecular Medicine*, 89(10), 985–995. <https://doi.org/10.1007/s00109-011-0754-2>

NEW DIRECTIONS AND FUTURE ADVANCES

Over the past four decades, there has been significant progress in the design and engineering of human skin grafts for wounds (Alrubaiy & Kathem K. Al-Rubaiy, 2009; Debels, Hamdi, Abberton, & Morrison, 2015) . Although these have facilitated the development of the first few generations of skin grafts, there remains much room for improvement in skin tissue engineering. For instance, contemporary approaches to skin engineering do not take into account the precise positioning of the cells within the individual strata. This positioning, however, is critical for faithfully reproducing the cell-cell and cell-matrix interactions within the skin, and can greatly influence the *in vivo* performance of the graft. 3D bioprinters are capable of dispensing live cells, soluble factors, and phase-changing hydrogels in a desired pattern while maintaining very high cell viability, offering tremendous potential in the fabrication of 3D skin substitutes (Derakhshanfar et al., 2018; Munoz-Abraham et al., 2016; Murphy & Atala, 2014; Ozbolat, Moncal, & Gudapati, 2016). By precisely locating multiple types of matrix materials and cells in a layer-by-layer assembly, various functional tissues can be fabricated with appropriate structures and cell compositions in a wide range of sizes, in a high-throughput, and highly reproducible fashion. The multi-layered and highly stratified structure of skin makes it a prototypical tissue to be fabricated using 3D bioprinting while overcoming some of the limitations of traditional tissue engineering schemes. Here, we demonstrated that 3D bioprinting can be used to fabricate human skin *in vitro* from skin cells and the printed skin is morphologically and biologically similar to human skin. The innovative 3D bioprinting technology will allow us to generate more precisely controlled skin structure with higher throughput in a rapid and reproducible manner. The proof-of-concept work proposed in this thesis is a critical first-step for translating such advances to the clinic under GMP. However, for clinical use further improvements to the protocol are still needed.

- Incorporation of adnexa in bioprinted human skin

Scientists have been studying hair follicle development for more than 3 decades. Several of the successful studies in hair follicle neogenesis have employed mouse cells or a coculture of human and mouse cells (Kang, Kwack, Kim, Kim, & Sung, 2012; Takagi et al., 2016; Toyoshima et al., 2012). In contrast to mouse cells, human dermal papilla cells lose their inductive potential to form hair follicles during initial expansion phase in 2D culture (Higgins, Chen, Cerise, Jahoda, & Christiano, 2013; Lin et al., 2016; Ng, Wang, Yeong, & Naing, 2016). Recent studies on hair follicle neogenesis have shown that a key step for successfully bioengineering human hair *in vitro* is the spatial distribution and compartmentalization of the

epithelial and mesenchymal cells (Balana, Charreau, & Leiros, 2015; Mahjour, Ghaffarpasand, & Wang, 2012; Ohyama & Veraitch, 2013). Higgins et al. demonstrated that human dermal papilla cells cultured as 3D spheroids restore part of their inductive capacity (Higgins et al., 2013). Additionally, following transplantation into intact human skin grafted on the back of mice models hair follicle fibers were successfully generated.

The recent advances in 3D bioprinting technology have now made possible to reproduce the three-dimensional microenvironment of the hair with high precision: different cells types can be precisely placed at defined positions within the scaffold/matrix. Moreover, 3D bioprinting has the potential to allow the production of human hair follicle units in a large scale and in a reproducible manner. The optimization of printing and culture protocols in order to accomplish this goal is currently be explored in Dr. Karande's laboratory.

- Development of bio-inks specific for tissue engineering of human skin

The 3D bioprinted skin equivalent that we report in this work lacks matrix components and cell types found in natural skin. Many bioinks used in 3D bioprinting are predominantly based on collagen alone and are incapable of reproducing the compositional and biomechanical complexity of native tissues (Vijayavenkataraman, Lu, & Fuh, 2016). While this approach has led to significant accomplishments, the development of bioinks appropriate for clinical translation is under-explored. Because of the versatility of 3D printing, the macromolecular composition of the matrix can be varied at different depths, allowing mimicry of reticular dermis, papillary dermis and epidermal basement membrane. Different cell types can be combined with different matrix molecules to be deposited at different tissue depths by incorporating them into specific bioinks. The development of complex bioinks formulated from individual matrix components, sourced from human tissue or via recombinant technology, might be structurally and functionally superior to bioinks currently used for printing as these are less likely to trigger an immune response after transplantation. The feasibility and benefits of such an approach, however, remain to be demonstrated. Recombinant DNA technology has revolutionized medicine by facilitating the production of therapeutic human proteins and factors in non-human sources with increasing ease and efficiency. The field is now sufficiently mature, and can contribute, with similar impact, towards the development of human ECM molecules. We have initiated efforts using recombinant human ECM molecules that are now commercially available to formulate improved bioinks for scaled production of human skin tissues. We argue that the combination of appropriate human cells and human matrix materials can lead to the development of superior transplantation solutions.

- Isolation and culture of cell types free of animal proteins for 3D printing

Much of the experience to date in the development of human skin equivalents uses non-human matrix molecules and human cells exposed to animal proteins during isolation and culture. In other words, neither the cell populations nor the matrix molecules used in the various bio-inks have been optimized with constituents that can be incorporated into an animal protein-free Good Manufacturing Practice (GMP) protocol. Although we were able to isolate all cell types required for the structural components of a tri-layered skin substitute (epidermis, papillary dermis and reticular dermis) from de-identified human tissues, I have initiated efforts in collaboration with Yale University, to modify culture protocols and procedures for each cell type to be free of animal proteins.

Smooth muscle cells (VSMC) and pericytes (PC), can be routinely isolated and cultured from umbilical artery or placental microvessels, respectively, by methods previously described. VSMC have been cultured under serum free conditions (Dartsch, Weiss, & Betz, 1990), but serum-free culture conditions for Pericytes have not as yet been described.

Moreover, our methodology for isolation and culture of KC follows a published approach in which isolated KC can be induced to differentiate into a keratinizing stratified squamous epithelium (i.e. an epidermis) (Brohem et al., 2011). In this work, we have cultured isolated keratinocytes in medium supplemented with fetal bovine serum (FBS). However, conditions have been described to isolate and culture human KC from foreskin under conditions using defined media in the absence of FBS (Boyce & Ham, 1985; Lamb & Ambler, 2013; Richards, Leavesley, Topping, & Upton, 2008). It is possible that FBS might be required for successful keratinization of bioprinted constructs. In such case, AB serum or cord blood derived serum (both sources lacking anti-ABO antibodies) can be used in its place (Kocaoemer, Kern, Klüter, & Bieback, 2007). If successful, human platelet-deficient plasma-derived serum or human platelet lysate might be sufficient (Schallmoser & Strunk, 2009). Depending on these results, fractionation of human serum to identify essential components to induce complete keratinization might be worth exploring.

Additionally, dermal FB were one of the very first cell types to be cultured in completely defined medium using growth factors (PDGF or EFG) to replace serum (Betsholtz & Westermark, 1984; Lembach, 1976). More recently, xeno- and serum-free culture media have become commercially available. Isolation and expansion of fibroblasts in such media conditions should also be explored in the future.

I expect that we will be able to culture all the relevant cell types and maintain appropriate differentiated features by substituting human serum or cord blood plasma for FBS,

supplementing the medium as needed with recombinant human growth factors. However, it is still uncertain if replacement of serum with an entirely defined medium will be possible.

- **Fabrication of “immunoevasive” human skin graft**

Organ transplantation is the most effective therapy for end stage organ failure, including heart failure, and the greatest challenge facing the field of organ transplantation is the shortage of suitable organs. According to the Organ Procurement and Transplantation Network (OPTN), 14,780 transplants were performed this past year, but 114,779 people are awaiting a lifesaving organ transplant and, on average, 20 persons on the waiting list will die each day (UNOS, 2018). Tissue engineering, which combines multidisciplinary approaches to repair, replace or regenerate tissues and organs, has the potential to solve this problem. If replacement organs are to be generated in a timely fashion, the cell sources used for tissue engineering are likely to be derived from sources allogeneic to the recipient patient. Experience from organ transplantation has indicated that rejection processes can be initiated by an only limited number of cell types. The target of rejection appears to be the blood vessels, and more specifically EC, since cultured human dermal microvascular EC (HDMEC) can activate allogeneic effector memory T cells (Al-Lamki, Bradley, & Pober, 2008). Other cells in human skin could contribute to T cell activation, but experiments with synthetic microvessels in protein hydrogels, in which the only human cell type has been HECFC-derived EC, showed that EC alone are sufficient to trigger rejection (Shiao et al., 2007). This problem might be avoided by use of the patient’s own EC (and other cell types), but these would not likely be available in advance and would delay fabrication compared to off-the-shelf products made from allogeneic cells, such as Apligraf. Interestingly, there is a growing consensus that even hiPS cells used for tissue engineering are likely to be derived from allogeneic sources to permit rapid manufacture (Martin, 2017).

Human ECs initiate rejection by direct presentation of non-self class I and class II MHC proteins to circulating alloreactive effector memory T cells which arise from prior infections and are highly abundant in human adults (Pober, Merola, Liu, & Manes, 2017). Furthermore, donor specific antibodies (DSA), present in a significant percentage of the human adult population, may lead to complement activation on the EC, thereby activating pro-inflammatory signaling cascades that promote recruitment and proliferation of alloreactive T cells and underlies cardiac allograft vasculopathy, the major cause of late heart graft loss (Jane-Wit et al., 2013; Pober, Jane-Wit, Qin, & Tellides, 2014). Abrahimi et al have found that elimination of MHC molecule expression on human ECs, achieved using CRISPR/Cas 9 technology, can diminish recognition of human ECs by both T cells and DSA *in vitro* and eliminate rejection of

self-assembled perfusable EC networks implanted into immunodeficient mouse hosts subsequently inoculated with peripheral blood mononuclear cells from a donor allogeneic to the EC donor (Abrahimi et al., 2015). I have recently initiated efforts in collaboration with Dr. Pober's laboratory to establish perfusion of a 3-D printed tissue engineered human skin graft by incorporating endothelial cells without triggering rejection. If successful, future work could include development of techniques to create "immuno-evasive" vascularized skin graft under conditions suitable for conversion to GMP.

References

- Abrahimi, P., Chang, W. G., Kluger, M. S., Qyang, Y., Tellides, G., Saltzman, W. M., & Pober, J. S. (2015). Efficient gene disruption in cultured primary human endothelial cells by CRISPR/Cas9. *Circulation Research*, *117*(2), 121–128. <https://doi.org/10.1161/CIRCRESAHA.117.306290>
- Al-Lamki, R. S., Bradley, J. R., & Pober, J. S. (2008). Endothelial cells in allograft rejection. *Transplantation*. <https://doi.org/10.1097/TP.0b013e3181891d8b>
- Alrubaiy, L., & Kathem K. Al-Rubaiy. (2009). Skin Substitutes: A Brief Review of Types and Clinical Applications. *Oman Medical Journal*, *24*(1), 6–8. <https://doi.org/10.5001/omj.2009.2>
- Balana, M. E., Charreau, H. E., & Leiros, G. J. (2015). Epidermal stem cells and skin tissue engineering in hair follicle regeneration. *World Journal of Stem Cells*, *7*(4), 711–727. <https://doi.org/10.4252/wjsc.v7.i4.711>
- Betsholtz, C., & Westermark, B. (1984). Growth factor-induced proliferation of human fibroblasts in serum-free culture depends on cell density and extracellular calcium concentration. *Journal of Cellular Physiology*, *118*(2), 203–210. <https://doi.org/10.1002/jcp.1041180213>
- Boyce, S. T., & Ham, R. G. (1985). Cultivation, frozen storage, and clonal growth of normal human epidermal keratinocytes in serum-free media. *Journal of Tissue Culture Methods*, *9*(2), 83–93. <https://doi.org/10.1007/BF01797779>
- Brohem, C. A., da Silva Cardeal, L. B., Tiago, M., Soengas, M. S. M. S., de Moraes Barros, S. B., & Maria-Engler, S. S. (2011). Artificial skin in perspective: concepts and applications. *Pigment Cell {&} Melanoma Research*, *24*(1), 35–50. <https://doi.org/10.1111/j.1755-148X.2010.00786.x>
- Dartsch, P. C., Weiss, H. D., & Betz, E. (1990). Human vascular smooth muscle cells in culture: growth characteristics and protein pattern by use of serum-free media supplements. *European Journal of Cell Biology*, *51*(2), 285–294.
- Debels, H., Hamdi, M., Abberton, K., & Morrison, W. (2015). Dermal matrices and bioengineered skin substitutes: a critical review of current options. *Plastic and Reconstructive Surgery. Global Open*, *3*(1), e284. <https://doi.org/10.1097/GOX.0000000000000219>
- Derakhshanfar, S., Mbeleck, R., Xu, K., Zhang, X., Zhong, W., & Xing, M. (2018). 3D bioprinting for biomedical devices and tissue engineering: A review of recent trends and advances. *Bioactive Materials*, *3*(2), 144–156. <https://doi.org/https://doi.org/10.1016/j.bioactmat.2017.11.008>
- Higgins, C. A., Chen, J. C., Cerise, J. E., Jahoda, C. A. B., & Christiano, A. M. (2013). Microenvironmental reprogramming by three-dimensional culture enables dermal papilla cells to induce de novo human hair-follicle growth. *Proceedings of the National Academy of Sciences of the United States of America*, *110*(49), 19679–19688. <https://doi.org/10.1073/pnas.1309970110>
- Jane-Wit, D., Manes, T. D., Yi, T., Qin, L., Clark, P., Kirkiles-Smith, N. C., Abrahimi, P., Devalliere, J., Moeckel, G., Kulkarni, S., Tellides, G., & Pober, J. S. (2013). Alloantibody and complement

- promote T cell-mediated cardiac allograft vasculopathy through noncanonical nuclear factor- κ B signaling in endothelial Cells. *Circulation*, 128(23), 2504–2516. <https://doi.org/10.1161/CIRCULATIONAHA.113.002972>
- Kang, B. M., Kwack, M. H., Kim, M. K., Kim, J. C., & Sung, Y. K. (2012, January). Sphere formation increases the ability of cultured human dermal papilla cells to induce hair follicles from mouse epidermal cells in a reconstitution assay. *The Journal of Investigative Dermatology*. United States. <https://doi.org/10.1038/jid.2011.250>
- Kocaoemer, A., Kern, S., Klüter, H., & Bieback, K. (2007). Human AB Serum and Thrombin-Activated Platelet-Rich Plasma Are Suitable Alternatives to Fetal Calf Serum for the Expansion of Mesenchymal Stem Cells from Adipose Tissue. *STEM CELLS*, 25(5), 1270–1278. <https://doi.org/10.1634/stemcells.2006-0627>
- Lamb, R., & Ambler, C. A. (2013). Keratinocytes Propagated in Serum-Free, Feeder-Free Culture Conditions Fail to Form Stratified Epidermis in a Reconstituted Skin Model. *PLoS ONE*, 8(1), 1–8. <https://doi.org/10.1371/journal.pone.0052494>
- Lembach, K. J. (1976). Enhanced synthesis and extracellular accumulation of hyaluronic acid during stimulation of quiescent human fibroblasts by mouse epidermal growth factor. *Journal of Cellular Physiology*, 89(2), 277–288. <https://doi.org/10.1002/jcp.1040890211>
- Lin, B., Miao, Y., Wang, J., Fan, Z., Du, L., Su, Y., Liu, B., Hu, Z., & Xing, M. (2016). Surface Tension Guided Hanging-Drop: Producing Controllable 3D Spheroid of High-Passaged Human Dermal Papilla Cells and Forming Inductive Microtissues for Hair-Follicle Regeneration. *ACS Applied Materials & Interfaces*, 8(9), 5906–5916. <https://doi.org/10.1021/acsami.6b00202>
- Mahjour, S. B., Ghaffarpasand, F., & Wang, H. (2012). Hair Follicle Regeneration in Skin Grafts: Current Concepts and Future Perspectives. *Tissue Engineering. Part B, Reviews*, 18(1), 15–23. <https://doi.org/10.1089/ten.teb.2011.0064>
- Martin, U. (2017). Therapeutic Application of Pluripotent Stem Cells: Challenges and Risks. *Frontiers in Medicine*, 4, 229. <https://doi.org/10.3389/fmed.2017.00229>
- Munoz-Abraham, A. S., Rodriguez-Davalos, M. I., Bertacco, A., Wengerter, B., Geibel, J. P., & Mulligan, D. C. (2016). 3D Printing of Organs for Transplantation: Where Are We and Where Are We Heading? *Current Transplantation Reports*, 3(1), 93–99. <https://doi.org/10.1007/s40472-016-0089-6>
- Murphy, S. V., & Atala, A. (2014). 3D bioprinting of tissues and organs. *Nature Biotechnology*, 32(8), 773–785. <https://doi.org/10.1038/nbt.2958>
- Ng, W. L., Wang, S., Yeong, W. Y., & Naing, M. W. (2016). Skin Bioprinting: Impending Reality or Fantasy? *Trends in Biotechnology*, 34(3), 689–699. <https://doi.org/10.1016/j.tibtech.2016.04.006>
- Ohyama, M., & Veraitch, O. (2013). Strategies to enhance epithelial–mesenchymal interactions for human hair follicle bioengineering. *Journal of Dermatological Science*, 70(2), 78–87.

<https://doi.org/10.1016/j.jdermsci.2013.02.004>

- Ozbolat, I. T., Moncal, K. K., & Gudapati, H. (2016). Evaluation of bioprinter technologies. *Additive Manufacturing*. <https://doi.org/10.1016/j.addma.2016.10.003>
- Pober, J. S., Jane-Wit, D., Qin, L., & Tellides, G. (2014). Interacting mechanisms in the pathogenesis of cardiac allograft vasculopathy. *Arteriosclerosis, Thrombosis, and Vascular Biology*, 34(8), 1609–1614. <https://doi.org/10.1161/ATVBAHA.114.302818>
- Pober, J. S., Merola, J., Liu, R., & Manes, T. D. (2017). Antigen Presentation by Vascular Cells. *Frontiers in Immunology*, 8, 1907. <https://doi.org/10.3389/fimmu.2017.01907>
- Richards, S., Leavesley, D., Topping, G., & Upton, Z. (2008). Development of defined media for the serum-free expansion of primary keratinocytes and human embryonic stem cells. *Tissue Engineering. Part C, Methods*, 14(3), 221–232. <https://doi.org/10.1089/ten.tec.2007.0428>
- Schallmoser, K., & Strunk, D. (2009). Preparation of pooled human platelet lysate (pHPL) as an efficient supplement for animal serum-free human stem cell cultures. *Journal of Visualized Experiments : JoVE*, (32), 1523. <https://doi.org/10.3791/1523>
- Shiao, S. L., Kirkiles-Smith, N. C., Shepherd, B. R., McNiff, J. M., Carr, E. J., & Pober, J. S. (2007). Human effector memory CD4⁺ T cells directly recognize allogeneic endothelial cells in vitro and in vivo. *Journal of Immunology (Baltimore, Md. : 1950)*, 179(7), 4397–4404. <https://doi.org/https://doi.org/10.4049/jimmunol.179.7.4397>
- Takagi, R., Ishimaru, J., Sugawara, A., Toyoshima, K. K. -e., Ishida, K., Ogawa, M., Sakakibara, K., Asakawa, K., Kashiwakura, A., Oshima, M., Minamide, R., Sato, A., Yoshitake, T., ... Tsuji, T. (2016). Bioengineering a 3D integumentary organ system from iPS cells using an in vivo transplantation model. *Science Advances*, 2(4), e1500887–e1500887. <https://doi.org/10.1126/sciadv.1500887>
- Toyoshima, K., Asakawa, K., Ishibashi, N., Toki, H., Ogawa, M., Hasegawa, T., Irié, T., Tachikawa, T., Sato, A., Takeda, A., & Tsuji, T. (2012). Fully functional hair follicle regeneration through the rearrangement of stem cells and their niches. *Nature Communications*, 3, 784.
- UNOS. (2018). Data. Retrieved June 30, 2018, from <https://unos.org/data/>
- Vijayavenkataraman, S., Lu, W. F., & Fuh, J. Y. H. (2016). 3D bioprinting of skin: a state-of-the-art review on modelling, materials, and processes. *Biofabrication*, 8(3), 32001. <https://doi.org/10.1088/1758-5090/8/3/032001>

LIST OF PUBLICATIONS

Oral communications

Dec 2017 - "Fabrication of Vascularized Skin Tissue Grafts using 3D Bioprinting Technology" – presented at **2017 TERMIS-AM Annual Conference and Exhibition** (Charlotte, NC).

Aug 2017 - "A 3D Bioprinting Platform for the Fabrication of Human Vascularized Skin Grafts for Regenerative Medicine" presented at the **Gordon Research Seminar (GRS) – Barrier Function of Mammalian Skin** (Waterville Valley, NH).

Jan 2017: "Design and Fabrication of Vascularized Human Skin" presented at **Averill Park High School** (Averill Park, NY).

Poster communications

Mar 2017 - "Design and Fabrication of Vascularized Full-Thickness Human skin via 3D Bioprinting" – presented at the **Rensselaer Polytechnic Institute's Graduate Research Symposium** (Troy, NY).

Oct 2016 - "Design and Fabrication of Vascularized Full-Thickness Human skin via 3D Bioprinting" – presented at the **1st International Bioprinting & 3D Printing in the Life Sciences Conference** (Cambridge, United Kingdom).

List of publications

Baltazar T.*, Motter Catarino C.*, Karande, P. (2018). Bioprinting of human skin: Gaps, opportunities, and future directions In *3D Bioprinting in Regenerative Engineering: Principles and Applications*. (pp. 175-196) CRC Press.

Baltazar T. et al. (2018). "A 3D Bioprinting Platform for the Fabrication of Human Vascularized Skin Grafts for Regenerative Medicine Applications". Manuscript in preparation.

Baltazar T., Fei L., Totsingan F., Gross R., Karande P. (2018). "*In vitro* toxicity and inflammatory response evaluation of antimicrobial Sophorolipids on human epidermal keratinocytes". Manuscript in preparation.

Awards

Oct 2016 - **Best Poster Award** – 1st International Bioprinting & 3D Printing in the Life Sciences Conference, Cambridge, UK.

Mar 2017- **Finalist of the “Three Minutes’ Thesis” Competition** (Rensselaer Polytechnic Institute, NY).

Mar 2017 - **Best Poster Award** – Graduate Research Symposium (Rensselaer Polytechnic Institute, NY).

Dec 2017 - **Wake Forest Institute for Regenerative Medicine Young Investigator Award 2017**, TERMIS-AM Conference, Charlotte, NC.